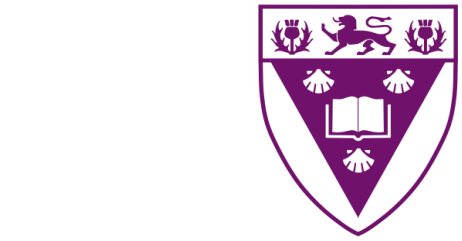

RHODES UNIVERSITY

Where leaders learn

ELECTROSPUN FIBRE BASED COLORIMETRIC PROBES FOR BIOLOGICAL MOLECULES

A thesis submitted to Rhodes University in fulfilment of the requirements for the Degree of **Doctor of Philosophy (Science)**

BY

BOITUMELO MUDABUKA

SUPERVISOR: NELSON TORTO

Co-SUPERVISOR: SIBULELO VILAKAZI

DEDICATION

This thesis is dedicated to the two most important men in my life, my husband Innocent Noto Mudabuka and our son Kgosi Mudabuka.

ACKNOWLEDGEMENTS

I would like to express my gratitude to my supervisor Professor Nelson Torto, for the kind invitation to work in his research group and for allowing me to work on an interesting topic and for his guidance and financial support throughout the course of my graduate program. I have learnt so much from you especially how to be a free thinker and an independent scientist. I am also grateful to Professor Zenixole Tshentu for his guidance and input in my work. I am grateful for the fruitful scientific discussions we have had concerning my work.

I would also like to acknowledge my group members Dr Sylvestre Degni, Dr Samuel Chogome, Dr Shima Batlokwa, Dr Janes Mokgadi, Dr Godfred Darko, Dr Andrew Andayi, Dr Dezzline adhiambo Oding, Bella Pule, Phumelele Kleyi, Yolanda Tancu, Awokoya Kehinde, Bridget Moronkola, Kediemetse Mothibedi, Noor Gulamussen, Kwanele Mgolozeli, Nokuthula Ngomane and Mamello Mohale for their cooperation and support in my work. I would like to extend my gratitude to the faculty and staff of the Chemistry Department during my graduate studies, I enjoyed working with you and learning from all of you.

I am deeply indebted to my friend, Mmapula Van Zeijl who supported me along these three years with her love and support. She has been a great listener and encouraged me whenever I felt disappointed. I am deeply indebted to my family for all their love and support.

Most importantly, I would like to thank my husband and true love, Noto. Thank you for your unconditional love, constant patience, and great deal of understanding. I am extremely grateful for your devotion to my life so that I could finish my post graduate studies. Many thanks to my son kgosi Mudabuka for your understanding and sacrifices for me to pursue my studies, I am looking forward to spending more time with you.

Last but not the least I am thankful to the Almighty in helping me to accomplish the task.

ABSTRACT

The thesis reports the use of electrospun nanofibres as a platform for the development of colorimetric probes. Three colorimetric probes in the form of electrospun nanofibre test strips were developed for the selective detection of ascorbic acid and dopamine because they are crucial biomolecules for physiological processes in human metabolism and usually coexist in biological samples. The simultaneous detection of the biomolecules is very important as their abnormal concentration levels would lead to diseases such as Parkinson's and schizophrenia. Different methods of incorporating detector agents into the nanofibre were exploited for the detection of the biomolecules. The methods included physical incorporation of nanoparticles, covalent bonding of ligand/dyes through surface modification of the fibres. The first colorimetric test strip for ascorbic acid was based on copper-gold alloy nanoparticles prepared *in-situ* and hosted in nylon6. The test strip showed selectivity in detecting ascorbic acid in the pH range 2 – 7. The suitability of fibres in hosting copper-gold alloy nanoparticles for the colorimetric detection of ascorbic acid was investigated using nylon6, poly(vinyl benzyl chloride)-styrene and cellulose acetate based test strips. All the test strips exhibited leaching and the nylon6 based test strip was found to be thermally stable up to 60 ˚C. The colorimetric performance of the test strips was maintained and neither was colour decay exhibited after 10 months of storage in a shelf. The test strip achieved an eye-ball limit of detection of 1.76 $x10^{-2}$ mg L^{-1} and its suitability was demonstrated by the determination of ascorbic acid in fruit juices, urine, serum, and vitamin C tablets. The second colorimetric test strip for ascorbic acid and dopamine employed prussian blue synthesised *in-situ* in nylon6. Ascorbic acid turned the deep blue test strip to light blue at pH 3, and a faded navy blue colour at a pH range of 6 - 7 while dopamine changed the strip to purple at the same pH range. The versatility of the test strip was demonstrated by detecting ascorbic acid in commercial fruit juices as well as by detecting ascorbic acid as well as dopamine in fortified

urine. The eye-ball detection limit of the Prussian blue test strip for ascorbic acid and dopamine was 17.6 mg L^{-1} and 18.9 mg L^{-1}, respectively. The third method involved a covalent approach, where poly(vinylbenzyl chloride) nanofibers were post functionalised with 2-(2′-pyridyl)-imidazole and iron(III) for the selective detection of ascorbic acid and dopamine. The eye-ball detection limit for ascorbic acid and dopamine was 17.6 mg L^{-1} and 18.9 mg L^{-1}, respectively. The test strip was selective for dopamine, but the detection of ascorbic acid suffered from interference by glutathione. The application of the test strips was nevertheless demonstrated by the detection of ascorbic acid in fruit juices and dopamine in fortified urine. The developed test strips employing the three approaches were applied without sample pre-treatment and use of supporting equipment.

TABLE OF CONTENTS

ABBREVIATIONS AND SYMBOLS

AA	Ascorbic acid
AgNPs	Silver nanoparticles
Ag	Silver
AIBN	Azoisobutyronitrile
ATRP	Atom transfer radical polymerization
AuNPs	Gold nanoparticles
Au	Gold
Cu-Au	Copper-gold
CuNPs	Copper nanoparticles
Cu	Copper
$CuSO_4.5H_20$	Copper sulphate
DA	Dopamine
DCPIP	Dichlorophenol indophenol
EPR	Electron paramagnetic resonance
Fe(III)-PMIH	Iron(III) - 2-(2′- pyridyl)-imidazole
FTIR	Fourier transform infrared spectroscopy
$HAuCl_4.4H_2O$	Chloride trihydrate
hCG	Human chronic gonadotropin
HPLC-ECD	High performance liquid chromatography electrochemical detection
$K_3[Fe\ (CN)_6]$	Potassium ferricyanide

LFIA	Lateral flow immunoassays
NMR	Nuclear magnetic resonance
MUA	11-mercaptoundecanoic acid
MBA	4-Mercaptophenyl-boronic acid
NPs	Nanoparticles
$NaBH_4$	Sodium borohydride
PIMH	2-(2′-pyridyl)-imidazole
POC	Point of care
POU	Point of use
PVBC-styrene	Poly(vinylbenzyl chloride)-styrene
PVBC	Poly(vinylbenzyl chloride)
SPR	Surface plasmon resonance
SEM	Scanning electron microscopy
TEM	Transmission electron microscope
μPADs	paper based microfluidic devices
WHO	World health organisation
XPS	X-ray photoelectron spectroscopy

LIST OF FIGURES

LIST OF SCHEMES

LIST OF TABLES

Chapter 1 INTRODUCTION

1.1 OVERVIEW

Chapter 1 motivates the need for point of care and point of use devices. The chapter also provides literature review on the existing paper based POC and POU devices which are: (1) lateral flow formats (2) dipsticks and (3) microfluidic devices. Literature review for the detection techniques for the existing POC and POU devices is also presented. Commonly used detector agents are also discussed in detail. Finally the characteristics of paper, its advantages and disadvantages as a support for POC and POU devices are discussed.

1.2 BACKGROUND

While there are numerous technologies for the detection of target analytes, there is still a need for the development of inexpensive, sensitive, and rapid alternatives. Many diagnostic tests are still performed at centralised laboratories and utilise expensive as well as complicated instrumentation. However, in developing countries the majority of the population lives in rural areas where testing facilities are not readily available. Even in urban areas where facilities are available, there are challenges associated with shortage of expertise necessary to operate and maintain instrumentation. There are also cost implications associated with equipment maintenance. The time required for samples to be sent to the central laboratory for testing especially in rural areas where such facilities are not available cause delays that affect the turnaround time. The delays may be attributed to the fact that transportation of samples to the centralised laboratories depends on the availability of a good road system. Sample transport and storage conditions can also have an important effect on the quality of test results as samples not properly stored before testing may deteriorate. The detection methods

in a laboratory set up also depend on a time-consuming sample preparation step(s) that directly influences the turnaround time. Therefore there is a general need for the development of affordable detection methods in order to improve the capacity to monitor in health care, food quality, environmental health, and animal health.

Lack of infrastructure, shortage of expertise and increase in health care associated infections has made it necessary to develop on-site diagnostic tests. Colorimetric probes or 'Point of care' (POC) in medical diagnosis and 'Point-of-use' (POU) in food quality control and environmental monitoring are an emerging technology that promises giant leaps in diagnostics.

Although the majority of POC and POU applications have been in health care, there have been some reports on food safety, environmental monitoring and veterinary diagnostics. Advancements made in the development of POC and POU diagnostic probes is in the miniaturisation of devices used for testing that has resulted in low sample volumes, fewer complications, reduction in the need for experts to run the samples and also maintain facilities, consequently reducing the costs.

Paper based lateral flow test devices and dipsticks based on colorimetric detection are the established configurations used in POU and POC testing. The two formats have gained popularity in the market because they are portable and interpretation of results does not require instrumentation.

1.3 EXISTING TECHNOLOGIES FOR POINT OF CARE AND POINT OF USE DEVICES

1.3.1 Lateral flow assays

The lateral flow format is based on the migration of a fluid by capillary action along a strip of polymeric material or membrane incorporating antibodies and a visible-signalling system. At one end of the strip is a sample application pad. In close contact with the strip material and the sample application pad is the conjugate release pad impregnated with dried recognition elements. The test process starts with the introduction of a sample at the sample application pad which treats the sample and releases it. The treated sample is then wicked by capillary action to the conjugate pad where specific interactions will take place and will continue with the chromatographic process. The strip consists of two bands; the test line and the control line immobilised with antibodies. Recognition of the sample analyte at the test line and the reporter will result in the required response. An absorbent pad attached at the distal side of the strip will wick the liquid to the end of the strip to maintain the flow as shown in Fig 1.1 [1]. The components of a lateral flow device are normally enclosed in a housing to achieve robustness. Only the sample application and the reading windows are exposed.

When antibodies are exclusively used as recognition elements, the tests are called "lateral flow immunoassays" (LFIA). Antibodies have been applied in LFIA because they recognise specific substances with antigen binding sites. Although nitrocellulose was historically used for filtration, it has since been adapted as a substrate for the strip in lateral flow devices.

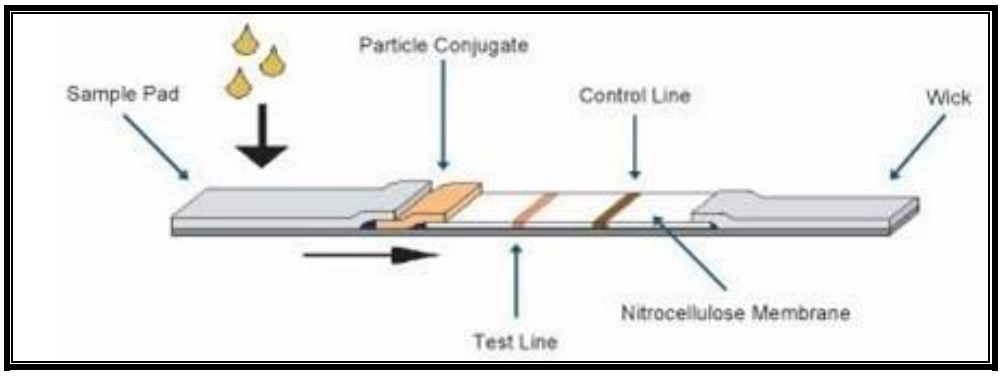

Figure 1.1: Schematic view of a typical lateral flow assay

LFIA can be divided into two categories; direct immunoassay, (i.e. double sandwich assays) and competitive assays. In the direct assays, the response is directly proportional to the analyte concentration. Two lines are indicative of positive results, otherwise conjugated particles bypass the test line and are captured at the control line to give negative results.

In a competitive assay, the response is negatively correlated to the analyte concentration. Positive results are therefore indicated by the absence of a test line while a single control line is an indication of negative results. The competitive assay is mainly used to test small molecules.

The general procedures applied in lateral flow assay are depicted in Fig.1.2. Flow through or vertical through are more complex than lateral flow formats as their use requires multiple steps; sample placement on the device, washing and addition of analyte-colloidal gold conjugates. Because the flows through devices require skilled personnel for operation they are less popular.

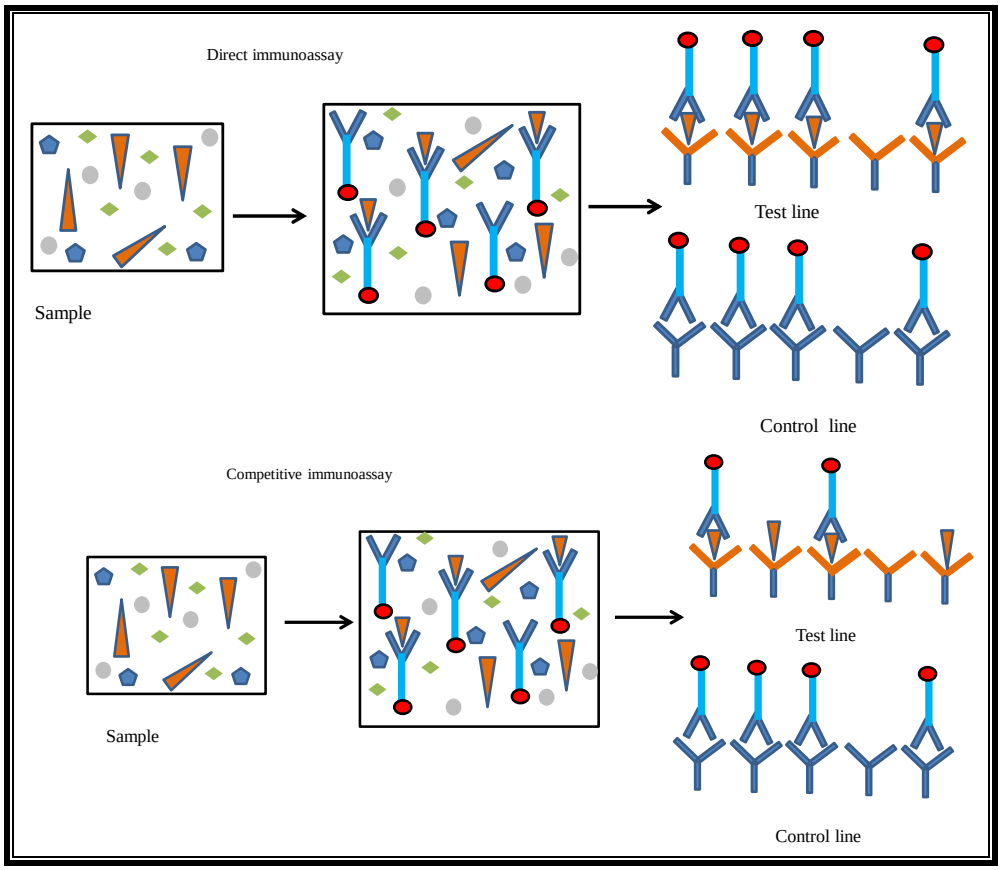

Figure 1.2: Common immunoassay procedures in lateral flow assay: Direct immunoassay and competitive immunoassay

1.3.2 Dipstick assays

Lateral flow assays are often incorrectly referred to as “dipsticks". Real dipstick assays are based on the immunoblotting principle and do not rely on lateral fluid flow through a membrane. Commercial dipsticks for a specific reaction for example, for pH measurements, where reagents are absorbed directly on the paper strip are available. The first dipstick test for semi-quantification of glucose in urine was proposed in the 1950s followed by its commercialisation in the 1960’s [2]. Colour change compared to a colour-coded chart to determine glucose concentration. Today urinalysis dipsticks for multiple detections of glucose, bilirubin, ketone (acetoacetic acid), blood, pH, protein, urobilinogen, nitrite, and leukocytes are commercially available. Multistick [3] and *uricheck 10* [3] are few examples of the available brands. The urinalysis device consists of a narrow strip of plastic affixed with

paper reagents pads for different analytes. To use the device, the test area of the dipstick is dipped into the sample colours generated on each pad and are dependent on the concentration of the analyte. The colours are then compared against a colorimetric chart that comes with the dipstick kit as illustrated in Fig. 1.3 [4].

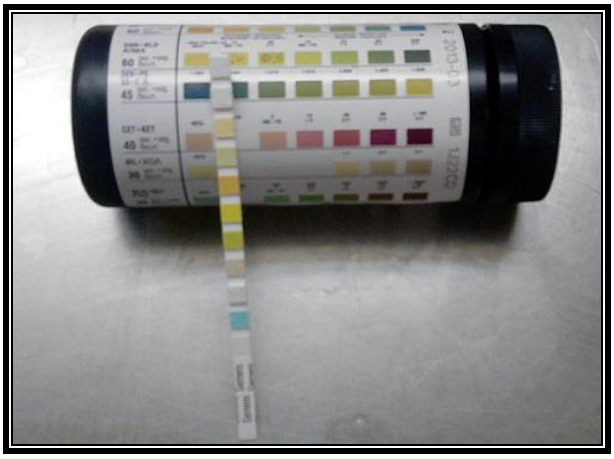

Figure 1.3: The Multistix urine test strip (Siemens Medial Solutions Diagnocstics) showing the manufacturer's coloured scale

The last few years have seen a shift from a basic design concept of dipsticks and lateral flow to paper based microfluidic devices (μPADs).

1.3.3 Paper based microfluidic devices

Whitesides and co-workers [5] showed that paper can be patterned into microfluidic channels separated by hydrophobic walls for multiple analyte detection. As in the case of urinalysis test strips the detection zones of μPADs contain reagents required to generate colour in the presence of the analyte of interest. First hydrophobic patterns are fabricated, followed by formation of detection zones where reagents are deposited into different reservoirs. The hydrophobic walls/barriers direct the analyte to detection zones where specific reactions take

place. The proposed barriers comprises of hydrophobic materials such as ethyl cellulose, silicones, polystyrene, rosin, waxes, paraffin, printer vanish and cellulose esters. Other designs comprise of adsorbent under layers as an alternative to hydrophobic barriers. Photolithography [6,7], analogue plotting [8], inkjet printing [9] and etching [10,11], plasma treatment [12], paper cutting [13], wax printing [14], flexography printing [15], screen printing [16], and laser treatment [5] have been reported in literature for producing microfluidic multiplex paper devices. Figure 1.4 [17], depicts a method employing lithographic technique to create microfluidic channel using hydrophobic photoresist, SU-8 polymer. The concept is demonstrated for the colorimetric detection of glucose and protein [17]. The reported paper based microfluidic devices were generally fabricated in paper such as filter and chromatography paper made from pure cellulose. The choice of the technique depends on the type of material used and modification required.

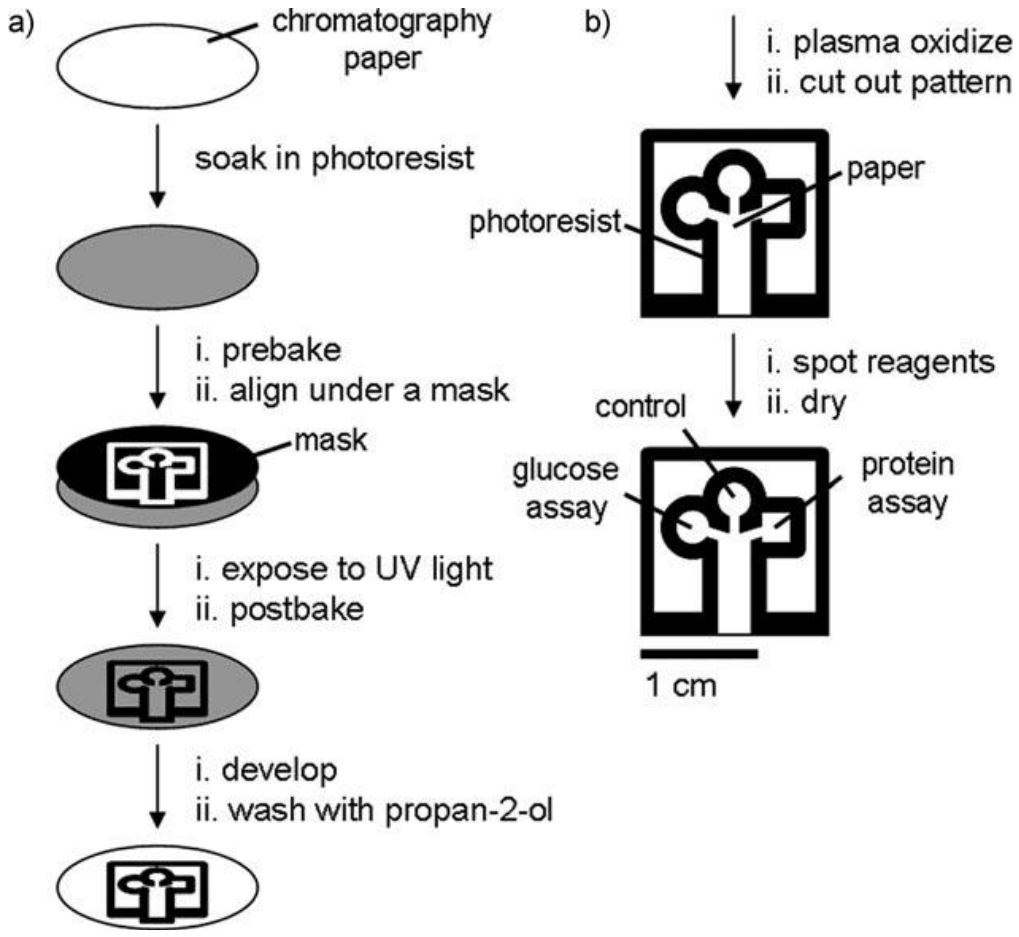

Figure 1.4: Diagram depicting the method employing photolithography to pattern for SU-8 photoresist into paper to create millimeter-sized channels

According to Li *et al* [18] patterning paper principles can be divided into three categories; (1) physical blocking of the pores in paper using agents such as photoresist SU-8 and Poly(dimethylsiloxane (PDMS), (2) physical deposition of a hydrophobic reagent (polystyrene or wax) on the cellulose fibre surfaces and (3) chemical modification of fibre surfaces using cellulose reactive agents. The solid wax procedure, first described by Lu *et al* [19] is the most suitable for manufacturing large volume microfluidic paper devices. The method requires a solid ink printer and a hot plate or oven. First a computer program is used to design patterns of channels and reservoirs, and then a wax printer is employed to print the

computer's design on paper. The paper will then be placed in an oven or hot plate to melt the wax so that it penetrates the paper to generate hydrophobic barriers that extend through its full thickness. Microfluidic devices fabricated in nitrocellulose membrane have also been reported [20]. Fig. 1.5 [20] shows schematic diagram of printing wax on a nitrocelluloce membrane.

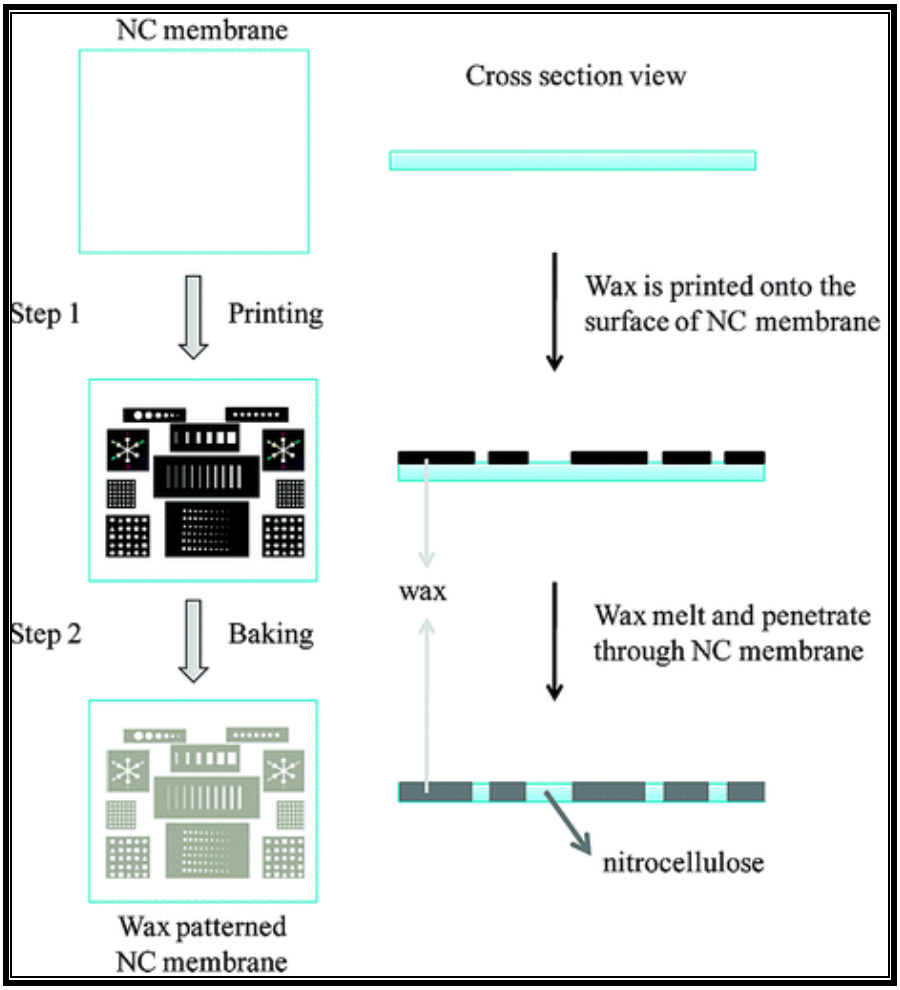

Figure 1. 5: **Schematic diagram of printing wax onto a nitrocellulose membrane**

Some paper-based microfluidic designs do not require the formation of a hydrophilic channel within a hydrophobic barrier. Wang *et al*. [21] cut paper into a tree-shaped design with seven

branches and a stem for the semi-quantitative detection of protein. The design allowed uniform microfluidic flow along the multiple branches when the stem was placed into a wicking solution and spotted with the sample at the branch.

Microfluidic paper devices have also shown the potential to achieve sample preparation and detection in a single step for complex biological samples like blood. Whitesides group developed a three dimensional microfluidic paper where each layer was made of different types of paper [5]. The first layer for example could be made of filter paper that serves as a sample preparation step to remove red blood cells from a blood sample. The analyte in the sample would react with the detection reagents in the middle layer before it diffuses to the bottom layer where the results are visually detected.

The detection mode on paper based devices in addition to colorimetry, could also be achieved by electrochemical [22-24], chemiluminescence, [25] and fluorescence for POC and PUC.

1.4 DETECTION TECHNIQUES

1.4.1 Electrochemical detection

Electrochemical lateral flow test strips that incorporate antibodies [26-29], aptamers [30] or complementary DNA [31] to capture or label target molecules have been reported. Traditionally, electrochemical sensors rely on a three-electrode system, counter electrode, a working electrode and a reference electrode. A wide range of inks may be used for the fabrication of electrodes on various substrates including paper. Carbon inks have been widely adopted for the fabrication of counter and working electrodes while silver/silver chloride has been adopted for the fabrication of reference electrodes in microfluidic designs [22,24]. Gold may also be used for the fabrication of working electrodes. Electrodes may be deposited on a paper matrix by sputtering through a shadow mask [32]. Electrochemical detection of glucose, lactate and uric acid on a paper-based device was first demonstrated by Dungchai *et*

al [22]. The conductive electrode pads were screen-printed in the hydrophilic region of the paper where enzymes were subsequently spotted. The electrode design by Dungchai *et al* [22] is shown in Fig 1.6. The analysis was performed using chronoamperometry at the optimal potential for hydrogen peroxide production. Oxidase enzymes catalysed the oxidation of the enzyme substrate such as glucose, uric acid and lactate and reduced oxygen to hydrogen peroxide. Electrochemical analysis has also been demonstrated for the detection of dopamine [33], drugs [32] and tumour markers [34]. The detection of glucose using a hand held glucometer is another excellent example of a successful POC electrochemical device [3,23].

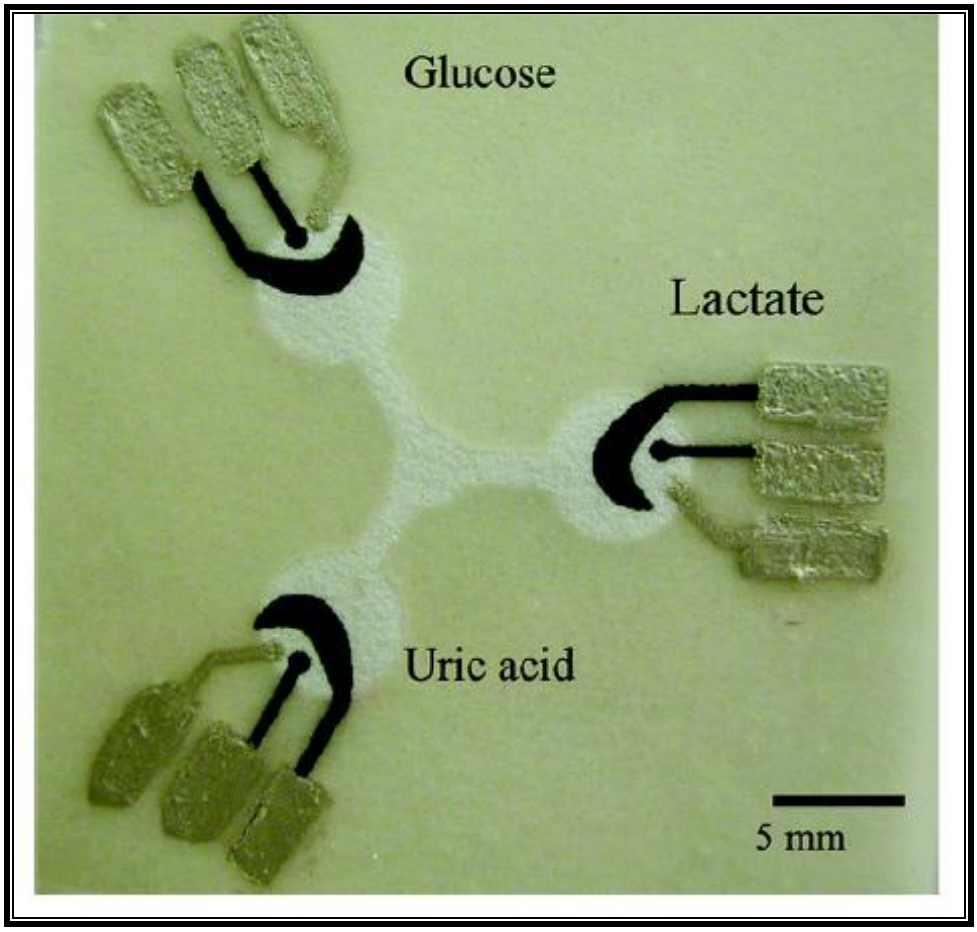

Figure 1.6: Paper based device with three electrode system for the electrochemical detection of glucose, lactate and uric acid

1.4.2 Fluorescence detection

Immunofluoroscence assays employ monoclonal or polyclonal antibodies conjugated to a flourochrome, the response to analyte can only be visualised using a fluorescence microscope, flourometer, or fluorescence scanner. The principle is based on the emission of light by flourophores after excitation at a certain wavelength. The processes that contribute to fluorescence are illustrated by the Jablonski diagram in Fig. 1.7 [35].

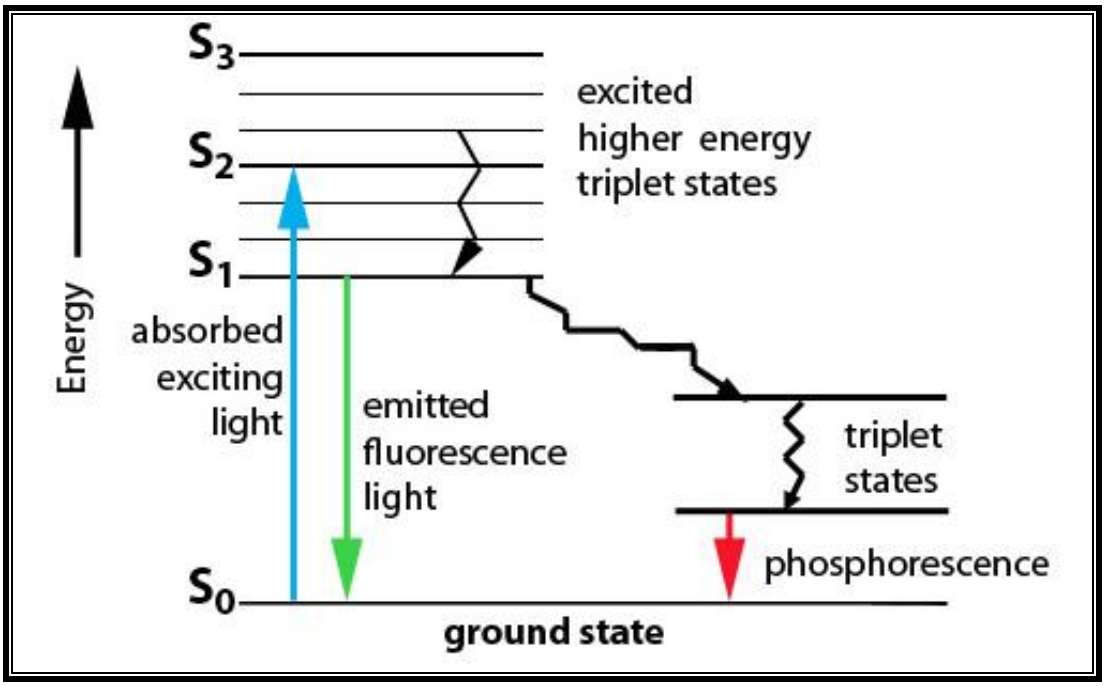

Figure 1.7: Schematic diagram of the Jablonski diagram depicting the relaxation mechanisms for excited state molecules

When a photon of energy, supplied by an external source such as a lamp or a laser, is absorbed by a fluorophore, it creates an excited, unstable electronic singlet state (S1). This process is distinct from chemiluminescence, in which the excited state is created by a chemical reaction. The excited state of a fluorophore is characterized by a very short half-life, usually in the order of a few nanoseconds. During this brief period, the excited molecules

generally relax toward the lowest vibrational energy level within the electronic excited state (Fig 1.7). The energy lost in the relaxation is dissipated as heat. It is from the relaxed singlet excited state (S1) that fluorescence emission originates. Because the emitted photon usually carries less energy and therefore has a longer wavelength than the excitation photon, the emitted fluorescence can be distinguished from the excitation light. The difference between the excitation and emission wavelengths is called the Stokes shift. For analytical applications, it is desirable that a wide Stokes shift be achieved. Fluorescent compounds or fluorophores can be identified and quantified on the basis of their excitation and emission properties [1]. Common fluorophores include dyes, quantum dots and conjugated polymers. Detection mechanism by fluorescence can either be by fluorescence quenching or enhancement.

1.4.3 Chemiluminescent detection

Chemiluminescent detection is based on emission of light generated by a chemical reaction such as oxidation. Chemiluminescence detection of biological analytes and tumour markers has been reported in literature [36]. A chemiluminescence reaction between a rhodanine derivative and hydrogen peroxide based on microfluidic-paper device was developed by Yu *et al* [37] for the detection of glucose and uric acid. Glucose or uric acid in the sample interact with the oxidase enzyme and produce hydrogen peroxide which in turn interacts with rhodanine derivative resulting chemiluminnescence. The peak intensity of the emitted light is proportional to the concentration of the analyte. The use of chemiluminescence as a label for immunoassay was first described in 1976 [38]. To date, the majority of commercially available automated immunoassay analyzers make use of chemiluminescence because of its sensitivity. Sandwich type employing luminal-H_2O_2 chemiluminescence system catalysed by silver nanoparticles (AgNPs) has been reported for tumour detection. However, nowadays

colloidal gold nanoparicles (AuNPs) have been used most as a label material in lateral assays [39].

Electrochemical, chemiluminescence, and fluorescence detection based on paper require the use of instrumentation (hand held readers) for the detection of analytes rendering the technique complex and expensive.

Colorimetric detection on the other hand does not require instrumentation, rendering it cost effective and simple to use. To be useful to low resource settings in emerging economies, POC and PUC devices should meet the World Health Organisation (WHO) ASSURED criteria for ideal rapid tests. In short ASSURED means

A Affordable

S Sensitive

S Specific

U User friendly

R Robust and rapid

E Equipment free

D deliverance to those who need the test

Environmental conditions such as insufficient water, unreliable electricity, high temperatures (35 ˚C - 45 ˚C) and humidity need to be considered when developing POU and POC devices [40]. Unsurprisingly the colorimetric detection has been widely adopted for POC and POU devices as it seems to meet the WHO criteria for rapid testing. Various types of detector agents have been reported for the visualisation of a signal. The most commonly used detector

agents are metal nanoparticles (NPs) and dyes. Other possibilities include enzyme conjugates, dye sacs, fluorescent particles and magnetic particles. Metal NPs and dyes are discussed at length in section 1.3.1 and 1.3.2.

1.5 MOST COMMONLY USED DETECTOR AGENTS/LABELS IN COLORIMETRIC LATERAL FLOW, DIPSTICK AND MICROFLUIDIC DEVICES

1.5.1 Metal nanoparticles

Metal NPs have sizes in the range 1-100 nm; they have different chemical and physical properties derived from their corresponding bulk materials because of quantum effects [41]. The quantum effect of NPs provides an opportunity for the development of advanced materials with designed properties not just by changing the chemical composition but by controlling the size and shape of the components. Properties of nano-sized metal particles such as reactivity, melting temperature, optical and magnetic properties change when particles become smaller than a critical size. The properties are size dependant and are widely believed to be a result of the high ratio of surface to bulk atoms. The smaller the particle becomes, the more the proportion of surface atoms increases. As particles decrease in size the number of surface atoms becomes equal to or even exceeds the number of inner-core atoms. For a typical bulk material, the surface is negligibly small in comparison to the total volume [42]. How colour exhibited by NPs is affected by size is discussed in the following section.

1.5.1.1 Optical properties of nanoparticles

Metals are often silvery white or greyish due to total reflection of light. This is because their electrons are not bound to individual atoms. Instead they form a cloud around the atomic cores therefore the atoms cannot absorb light; consequently photons are reflected back to the

eye producing a sheen associated with metals. Notable exceptions are reddish copper and yellowish gold due to total absorption of light by the large surface area.

However electrons can behave as either a wave or particle. An electron cloud that behaves as a wave has a certain energy value, and may absorb light of the same wavelength, producing resonance. The absorption of the electromagnetic radiation causes oscillation of the surface electron/conduction electrons and the process is known as plasmons. The process is termed surface plasmon resonance (SPR) because it occurs at the surface of the metal.

Generally, the optical properties of metal NPs are dominated by their SPR characteristics. The electric field of the incoming radiation induces an electric dipole in the metal particle by displacing many of the delocalised electrons in one direction away from the rest of the metal particle. The displacement of the electron cloud under the effect of the electric field leads to the formation of surface charges, positive where it is lacking and negative where it is concentrated as illustrated by Fig. 1.8 [43,44]. Since an electromagnetic wave impinging on the metal surface only has a certain penetration depth (50 nm for Ag and Au), only the electrons on the surface are significant [41].

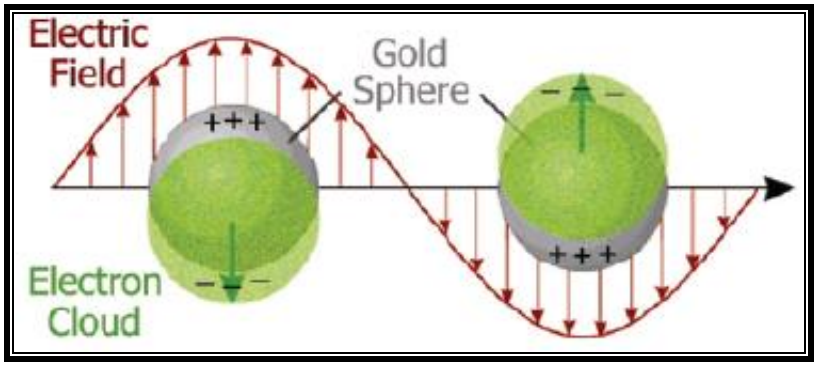

Figure 1.8: Schematic illustration of the collective oscillation of free electrons under the effect of an electromagnetic wave

The oscillation wavelength depends on a number of factors, including particle size, shape and the nature of surrounding medium. For nonspherical particles, such as rods, the resonance wavelength depends on the orientation of the electric field relative to the particle, and thus, oscillations either along (longitudinal) or across (transversal) the rod are possible (Fig. 1.9) [44,45].

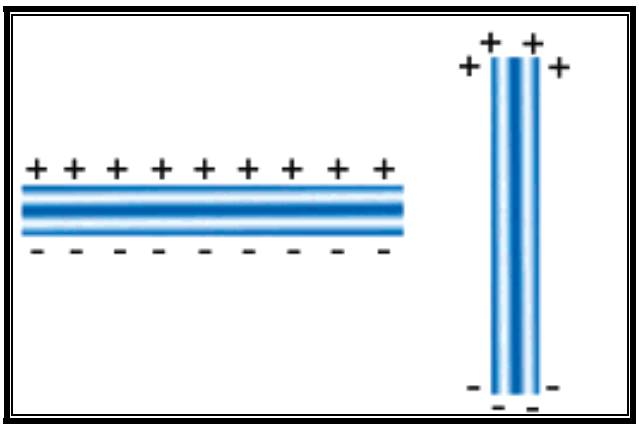

Figure 1.9: Schematic illustration of transversal and longitudinal oscillation of electrons in a metal nanorod

The average distance between neighbouring metal NPs is also important. Aggregation of colloidal metal particles can lower plasmon frequencies and shift the plasmon absorbance to longer wavelength. Only metals with free electrons such as gold (Au), copper (Cu), silver (Ag) and alkali metals have plasmon resonance in the visible spectrum, the property that gives them their distinctive colours. For many metals such as lead, indium, mercury, tin and cadmium the surface plasmon frequency lies in the UV part of the spectrum and NPs do not display colour effects [44]. Au-Ag-Cu series exhibit very intense surface plasmon band making them plasmonic metals of choice for optical applications [43], therefore nanometals of these metals have been used in the development of colorimetric probes.

However several other factors have motivated the use of AuNPs as colorimetric in immune assays. These include compatibility with chemistries needed to perform assays, stability and ease of preparation. Recent development has focused on protecting efficiently copper and silver for improved chemical stabilities. As a consequence nanometals of these metals especially silver have also gained popularity for development of colorimetric probes. Given the outstanding characteristics of metal NPs, their synthesis has found considerable interest in the development of POC and POU devices.

1.5.1.2 Synthesis of metal nanoparticles

Traditionally, NPs were synthesised by chemical and physical means. Physical techniques include proton irradiation [46], laser ablation [88], vacuum vapor deposition [47] and radiation methods [48]. Physical means usually need high temperature, vacuum and expensive equipments.

Examples of chemical approaches include microemulsion (colloidal) techniques [49,50] sonochemical reduction [51] and chemical reduction of metal salts [52,53]. Chemical reduction is the most preferred due to its simplicity. In general chemical reduction reactions involve reduction of metal salts in some type of solvent and separate reducing agents. It can realise better size and size distribution control by optimizing the experimental parameters, such as the molar ratio of reducing agent with precursor salt [54]. There are mainly two approaches to the production of metal NPs that include wet chemical methods and direct synthesis or a seeding growth method. Direct synthesis can be categorized in two ways namely the Turkevitch method [55] and the Brust-Schiffrin method [56].

1.5.1.2.1 Turkevitch method

The first reproducible standard recipe for the preparation of metal colloids was established by Turkevish [55,57]. In this method gold ($AuCl_4^-$) was reduced with sodium citrate. Based on growth of nucleation, growth, and agglomeration he also proposed a mechanism for the stepwise formation of nanoclusters [Fig.1.10].

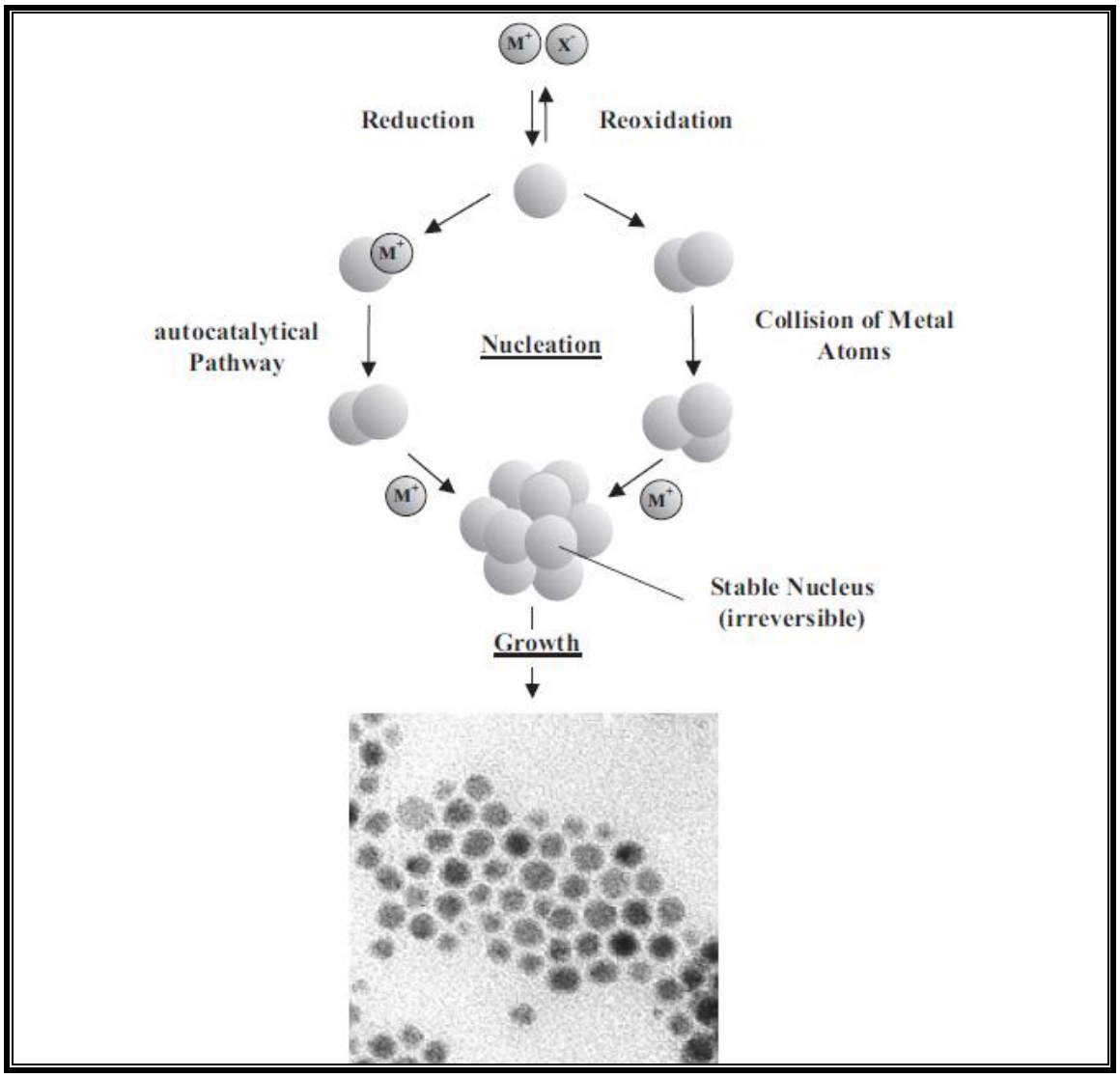

Figure 1.10: Schematic illustration of formation of nanostructured metal colloids via the "salt reduction" method

The metal is reduced to give zerovalent metal atoms in the embroyonic stage of nucleation. Further collision between ions, metal atoms, or clusters forms an irreversible 'seed' of stable metal nuclei. Depending on the difference of the redox potentials between the metal salt and the reducing agent applied, and the strength of the metal-metal salt bonds, the diameter of the seed nuclei can be below 1 nm [58]. The Turkevitch method was later refined by Frens [59] where spherical particles over a tunable range of sizes from 15 to 150 nm could be produced by varying the ratio of gold salt to citrate concentration in the medium. This method is often used when a rather loose shell of ligands is required around the gold core in order to prepare a precursor to valuable AuNPs based materials.

1.5.1.2.2 Brust-Schiffrin method

Brust method is a two phase protocol that utilises organic solvents to produce small nanoparticles (1-5 nm) with narrow dispersity [56]. The method employs borohydride reduction of metal salts in the presence of an alkanethiol capping agent. In synthesis, the salt is first transferred to the organic phase using a suitable surfactant. Then sodium borohydride ($NaBH_4$) is added to the aqueous phase [60,56]. Samples generated with this method are stable for long periods of time when dry and can be repeatedly isolated and re-dissolved in common organic solvents such as hexane or toluene without irreversible aggregation or decomposition. The reason for that is the capping agent is covalently bonded to the surface of the metal nanoparticle. Brust *et al.* extended the synthesis to p-mercaptophenol stabilized AuNPs in a single phase system [60] which opened an avenue to the syntheses of AuNPs stabilized by a variety of functional thiol ligands [61]. Subsequently many publications have since appeared describing the use of the Brust-Schiffrin procedure for the synthesis of other stable AuNPs or monolayer-protected clusters that contained functional thiols [62-64].

1.5.1.2.3 Seed mediated growth method

In seed mediated growth approach, small nanoparticle seeds serve as nucleation centers to grow NPs to a desired size. The size controlled-growth of NPs requires isotropic growth on the surface of nanoparticle nuclei. These result in the increase in the particle size that is spherical in shape [65,66]. However, the anisotropic growth of particles would result in various shapes such as nanorods, triangles and hexagonal nanoplates. Anisotropic growth can be facilitated by addition of surfactants such as cetyltrimethy-ammonium bromide, sodium dodecylsulfonate and poly(vinyl pyrrolidone) [67-71]. In order to prepare particles with the desired size, the experimental conditions are controlled so that all new metal atoms generated by reduction are deposited on the surface of the seed particles without further nucleation. Hydroxylamine and ascorbic acid are common reducing agents used in seeding growth of AuNPs [61,72]. The particle sizes can be easily manipulated by varying the ratio of seed to metal salt. Seed mediated growth presents an option to synthesize metal NPs of other shapes.

Generally metal NPs agglomerate due to high active surface area. This should be avoided through stabilisation because most desirable properties of NPs are destroyed after they become agglomerated.

1.5.1.3 Stabilisation and functionalisation of metal nanoparticles

Stabilisation may be achieved with a large variety of capping agents, which may be recognition elements that interact specifically with analytes of interest. Macromolecules such as proteins or DNA as well as electron donor or ligands including phosphines [73], amines [74] or thiols [75] may be employed as recognition molecules. The recognition elements can be attached to the nanoparticle surface through electrostatic interaction [76], specific recognition (antibody-antigen) [77] and covalent coupling [78]. Physical adsorption is a quick

and simple process with benefits of time saving and does not require complex ligands preparation. It involves the coulombic repulsion between NPs caused by electrical double layer formed by recognition elements such as sodium citrate, $NaBH_4$ adsorbed at the particle surface as shown in Fig. 1.11. Though electrostatic or physical adsorption of ions on NPs is simple, binding of recognition elements is not strong enough to withstand change in experimental conditions such as ionic strength and pH.

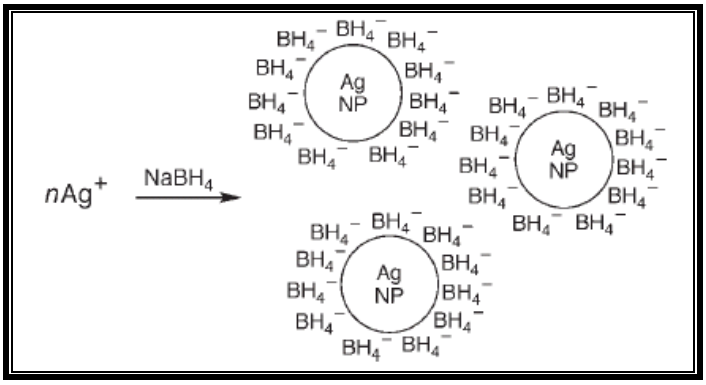

Figure 1.11: Repulsive force that separate Ag nanoparticles (NPs) with adsorbed Borohydride

NPs prepared through steric stabilisation (use of polymers) however are less sensitive towards changes in ionic strength. Polymers may be employed as steric stabilizers and also as a means of controlling nanoparticle growth and interparticle spacing. This is achieved by coordinating sterically demanding organic molecules that act as protective shields on the metallic surface [79,80]. Using a polymer as a protecting agent has been demonstrated to be a good method of producing, NPs/polymer nanocomposites. The resulting composite combine the optical and electrical properties of the particles and the cohesion stability of the polymer [81]. Polymers provide several advantages over small-molecule ligand as stabilising agents for NPs. They may consist of multiple repeating units, each of which can display ligand

functionality. Functional groups, such as carboxyl, hydroxyl, amines and esters play an important role in steric stabilisation. Small molecule ligands typically require very strong affinities for nanoparticle surface sites to ensure nanoparticle stability. Copolymers are usually more effective in steric stabilisation than homopolymers because copolymers consist of more than one type of repeated unit [82].

Sulfur containing recognition elements are predominant as the most functional groups for metal NPs as they offer a strong covalent bond. The approach employs thiols such as alkanethiolates, glutathione, didulfied-modified DNA, and peptides. Immunostrip assays have mostly benefitted from the macromolecule labelling like metallic NPs conjugated to antibodies [83]. Though the approach sometimes requires an intensive work on synthesis of ligands, it offers high stability: they are thermally stable and can withstand high salt concentrations. Since most applications require stability, the covalent approach is most common.

1.5.1.4 Sensing mechanism for colorimetric nanoparticles probes

Nanoparticles probes are operated in the colorimetric mode, mainly because of higher molar extinction coefficients and size dependant optical properties. Analyte induced aggregation of functionalised NPs is the main sensing mechanism on nanoparticle-based diagnostic probes. When NPs aggregate, their fields interact leading to inter-particle Plasmon coupling and consequently to coupling induced SPR shift. Although NPs are stabilised against aggregation by means of anions or polymers adsorbed on their surfaces, changes in the media such as pH and ionic strength can cause nanoparticle destabilisation and aggregation. Nanoparticle SPR is extremely sensitive to changes in local refractive index induced by analyte binding at or near the nanoparticle surface. Analyte binding to nanoparticle surface functionalised with

ligands changes the composition of the medium at the surface and produces an SPR shift. The magnitude of the shift is proportional to the degree of binding that takes place. Refractive index probes are highly interesting for pollutants detection.

1.5.1.5 Common nanoparticles based probes

Colloidal Au is the historical detector for lateral flow devices. A variety of lateral flow assays that employ antigen antibody interaction to provide a rapid detection of analytes have been reported [84,85].

Home pregnancy test is the most familiar and popular example of detection by NPs in lateral flow designs. The test relies on the principle to detect the presence of human chronic gonadotropin (hCG) in maternal urine. NPs (< 50 nm) are bound to antibodies complementary to hCG forming a gold-hCG complex. If the woman is pregnant, hCG in the urine binds to the antibodies and consequently aggregation of NPs giving a positive signal [86].

HIV tests employing AuNPs such as Uni-Gold Recombigen [87] have also been reported and are available in the market. HIV antigens are attached onto a membrane. Antibodies in the specimen combine with the NPs and they will attach to the antigen to give positive results. Few more lateral flow tests employing AuNPs are shown in Table 1.1. In LFIA devices colloidal gold (20-40 nm) can be dispensed in high density at the test line hence it is much more preferred compared to monodisperse particles (100-300).

Table 1.1: Lateral flow tests that employ gold nanoparticles

Analyte	Method	Application	Reference
Aflatoxin B1 in pig feed extracts	Colloidal gold labelled primary Antibody	Contamination with aflatoxin B1	[84]
Sulfadimidine in urine or milk	Colloidal gold labelled primary Antibody	Residue of antibiotic Sulfadimidine	[85]
Generic test on Sulfonamides in eggs and chicken muscle	Colloidal gold labelled antibody	Residue of antibiotics	[88]
Progesterone in bovine milk	Colloidal gold labelled analyte-ovalbumin conjugate	Determination of the reproductive status of dairy animals	[89]
indomethacin (IDM) in water samples	Colloidal gold labelled primary antibody	Indomethacin (IDM), a nonsteroidal anti-inflammatory drug (NSAID	[90]
Antibody to Trichinella in swine serum	Colloidal gold labelled antigen	Trichinellosis	[91]

Other colorimetric nanoparticle assays adapted to enzymatic reactions have also been reported. For example, He [92] *et al* reported an ultrasensitive lateral flow strip device based on a horseradish peroxidase – gold nanoparticle for the detection of nucleic acid. The lateral flow device combined the unique properties of AuNPs and enzymatic catalysis and could detect visually 10 aM target DNA. An enzymatic paper "dipstick" for detection of enzyme inhibitors that incorporated a sol-gel/enzyme/gold nanoparticle composite with colorimetric

detection was reported. The detection mechanism is based on the growth of AuNPs induced by the product of the enzymatic reaction [93].

Paper based microfluidic devices employing NPs have been reported. Ratnarathorn *et al.* [94] fabricated a paper based device the colorimetric detection of copper using AgNPs. AgNPs functionalised with homocysteine and dithiothreitol were immobilised in the test zone. A colour change was observed upon copper-induced aggregation of NPs through binding of copper to the carboxyl and amino functional groups on homocysteine and dithiothreitol. In addition to NPs colorimetric detection also employs enzymatic and molecular dyes most.

1.5.2 Dyes

Unlike most organic compounds, dyes possess colour because they absorb light in the visible spectrum (400–700 nm), have at least one chromophore (colour-bearing group), and have a conjugated system and exhibit resonance of electrons. A chromophore is generally a group of atoms in a molecule responsible for its interaction with radiation at a given wavelength. An example of a common chromophore is conjugated multiple bond rich in electrons, i.e. a structure with alternating double and single bonds, and exhibit resonance of electrons. Electrons in these moieties may be readily promoted by the absorption of UV or visible light. Molecules or atoms absorb visible or UV light only when the energy of the impinging photon corresponds exactly to the energy gap associated with electronic transition. Dyes can be classified based on their source, chemical structure, method of application, colour and chemical properties. The following is a discussion of dyes based on chromophore nature [42].

1.5.2.1 Classification of dyes based on their chromophore

Azo dyes contain at least one or more azo (-N=N-) groups attached to two groups, of which at least one, but more usually both are aromatic. The mono azo dyes are the most important and contain at least an electron donating and electron accepting group.

Some of the important red dyes are based on the anthraquinone structure. Anthraquinone dyes are essentially colourless and are based on 9, 10-anthraquinone depicted in Fig. 1.12. Commercially useful dyes are produced by introducing electron donating groups such as amino, hydroxyl into one or more of α position on the anthraquinone [42].

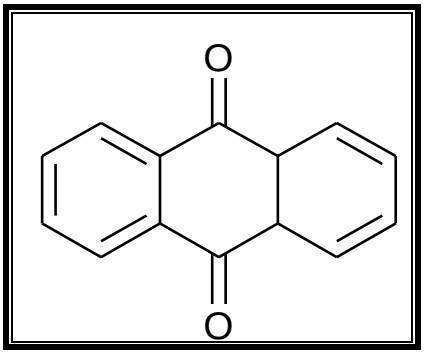

Figure 1.12: Structure of 9, 10-anthraquinone

The indigoid chromophore in Fig.1.13 is one of the most ancient and natural dyes obtained from indigofera tinctoria. It is still one of the most prevalent dyes used to colour denim jeans and jackets. Tyran purple is one of its commonly known derivatives [95].

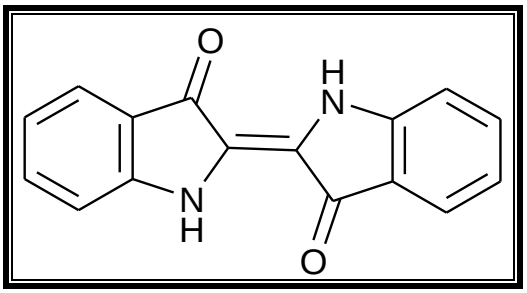

Figure 1.13: Basic indigo structure

Cationic dyes as chromophores are called basic dyes because the chromophores in these dye molecules contain a positive charge. The salt-forming counterion is in most cases the colourless anion of a low molecular mass inorganic or organic acid. They form a coloured cationic salt when dissolved in water. The positive charge of cationic dyes may be either localized or delocalized. Fig. 1.14 depicts the positive charge localized on an ammonium group and delocalized across the dye cation. Cationic dyes exhibit good affinity for negatively charged wood pulp and unbleached pulp grades. Because of their colouring strength, cationic dyes are used in the office supplies industry for the manufacture of ink, typewriter ribbon, and copying paper [42]

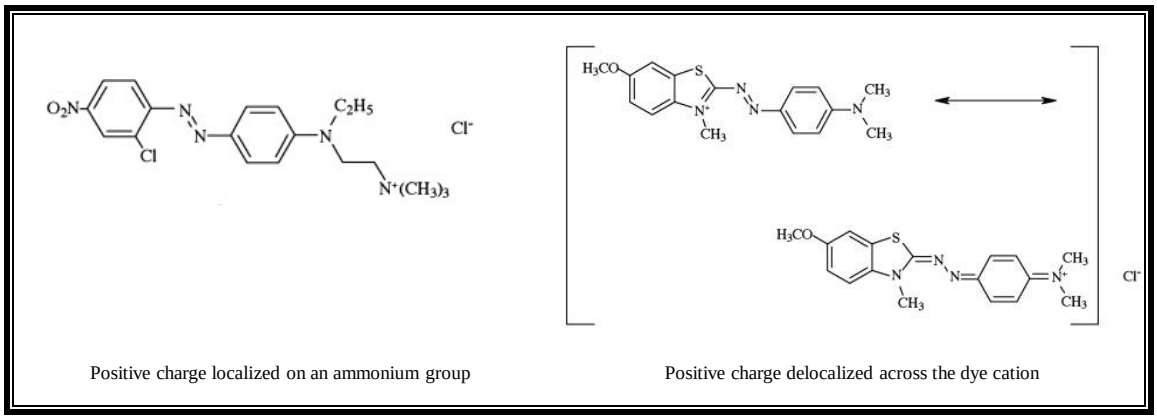

Figure 1.14: Structures depicting cationic dyes chromophores depicting delocalization of positive charge on an ammonium group and delocalisation of positive charge across the dye cation

Polymethine and related Chromophores include dyes of aliphatic molecules with conjugated systems. The most well-known representative of this group is β-Carotene having a straight conjugated system. However, there are also dyes with aromatic structures in this class. Cyanine dyes are the best known polymethine dyes. They find wide applications as sensitizing dyes for silver halide photography and infrared absorbers for optical data storage and other (bio) imaging applications [96].

Di- or Triarylcarbenium and related chromophores can be considered as branched polymethines. The branches are two aryl rings, in which the polymethine chain is incorporated, and by another R group bonded to the central methine carbon atom as illustrated in Fig. 1.15 [5].

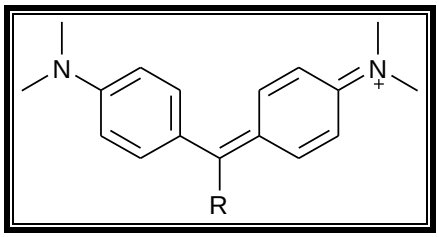

Figure 1.15: Structure of a branched polymethine

The phthalocyanines are constituted by a ring structure of aromatic or benzopyrrole rings (Fig.1.16), usually with a metal ion in the centre, that are slightly reminiscent of chlorophyll and haemoglobin and vitamin B12. Complexes of phthalocyanine have been synthesised with nearly all the metals of the periodic table. Of all the metal complexes copper phthalocyanines gives the best combination of colour and properties, consequently the majority of

phthalocyanine dyes are based on copper phthalocyanine. Their colours range from blue–black to metallic bronze depending on the manufacturing process [97].

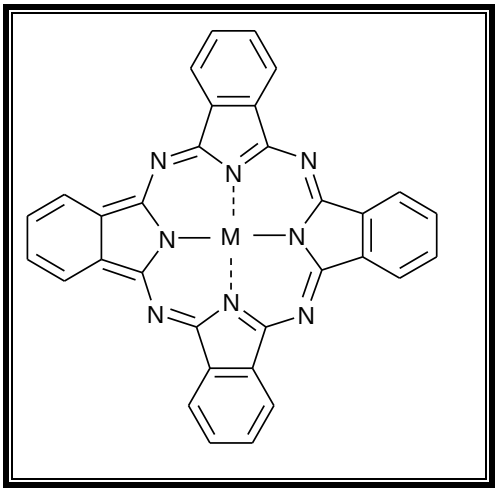

Figure 1.16: structures of a phthalocyanine complex

Based upon their use, some dyes have been classified as indicator dyes.

1.5.2.2 Indicator dyes

Indicators *(probes)* are synthetic dyes that undergo colour changes on interaction with chemical species. The purpose of using so-called *indicator chemistry* in optical sensing is to convert the concentration of a chemical analyte into a measurable optical signal. In general terms, an indicator dye can be characterized as follows: (1) it shows different optical properties when the system it forms part of changes its status, (2) leads to a reversible change. The first characteristic means that the indicator molecule reacts as a part of the system. The second characteristic specifically differentiates indicator dyes from colour forming reagents. The latter are widely used in reactions in which colours are formed by chemical or biochemical (mostly enzymatic) reactions between the analyte and added reagents. The reactions are widely used in analytical and diagnostic test kits but are normally not reversible.

The different optical properties mentioned are clearly linked to structural properties: a change in optical properties also indicates a change of molecular structure. The most important structural changes for indicator dyes are (1) reversible transition between acid and base form of a molecule (pH indicator), (2) reversible transition between reduced and oxidized forms of a molecule (redox indicator), and (3) reversible transition between the free molecule and its complex with a cation (metal indicator) [98,99].

1.5.3 Common dye based probes

Early colorimetric sensing employing dyes was demonstrated in pH detection. The most widely used pH indicators include azo dyes, nitrophenols, phthaleins and sulfophthaleins. Varying the substituent on the chromophores yields pH indicators with different transition ranges. Several chromophores undergo useful colour changes on protonation, including simple, neutral azo dyes, styryl dyes and indophenols. For example, at pH > 8.1 phenolphthalene absorbs light across the broad band of the visible spectrum. In this state it appears red because it is deprotonated (Fig. 1.17).

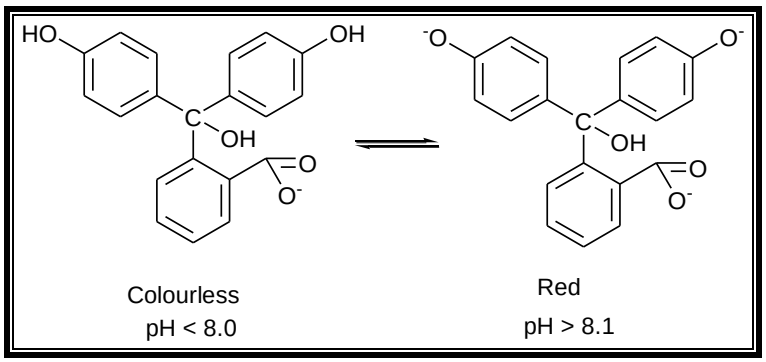

Figure 1.17: Structural and colour-change properties of phenolphalein with pH

Litmus and pH papers are used to characterize the relative acidity or basicity of a substance based on colour change. These are filter papers that have been treated with a mixture of pH sensitive dyes. The dye can turn red in response to acidic conditions (pH<7) and blue under alkaline conditions (pH>7). Litmus paper is generally a light purple in neutral conditions (pH=7).

This wide range between colour changes limits use in determining specific pH values. There are numerous other indicators of pH change with both specific and wide ranges that can be used to determine the exact pH of a solution. General purpose pH paper provides a quick and effective pH determination. The strip or tape containing the pH indicator is first dipped into a liquid, and then the resulting colour change is compared to the colour chart provided to determine pH levels.

Commercial urinalysis tests employing molecular and enzymatic dyes for pH, glucose, ketone, protein, urobilinogen, bilirubin, nitrite, leukocytes and occult blood are common. Typically, the reagent strip for glucose is impregnated with the enzyme glucose oxidase. The enzyme then converts glucose to form gluconic acid and hygrogen peroxide. Peroxide then catalyses the reaction of hydrogen peroxide with a chromogen i.e potassium iodide, resulting in a colour changes from clear to brown. The intensity of the colour depends on the concentration of the glucose in the sample. The reaction is summarised in equations 1 and 2.

$$\text{Glucose} + O_2 \xrightarrow{\text{Glucose Oxidase}} \text{Gluconic acid} + H_2O_2 \quad \text{.....eqn 1}$$

$$H_2O_2 + \text{Chromogen} \longrightarrow \text{Oxidised chromogen} \quad \text{.....eqn 2}$$

The chromogen employed depends on the test strip used. Nitrite test is an indication of the urinary tract infection. Nitrite reacts with *p*-arsanilic acid to form a dizonium compound that

couples with the quinoline to produce a pink colour as summarised in the equations that follows.

Nitrite + *p*-arsanilic acid ⟶ diazonium compound .....eqn 3

3-hydroxyl-1,2,3,4tetrahydrobenz-(h)-quioline + diazonium compound = pink colour .....eqn 4

The summary of urinalysis tests are shown in Table 1.2 [100].

Table1.2: A summary of other dipstick tests for urine based on dyes

Assay	Measurement principle	Reaction
Protein	Based on protein error of indicators. The test strip changes from yellow to green in the presence of protein	tetrabromophenol blue (pH 3, yellow) $\xrightarrow{\text{protein}}$ tetrabromophenol blue (pH>4.6, blue)
Blood	Peroxidise activity of haemoglobin and myglobin which catalyses the oxidation of a chromogen in the presence of organic peroxidase	H_2O_2 + Chromogen $\xrightarrow[\text{peroxide}]{\text{haemoglobin}}$ oxidised chromogen + H_2O_2
urobilinogen	Ehrlich Aldehyde	p-diethylaminobenzadehyde + urobilinogen = azo compound (red)
Ketone	Sodium nitroprusside in alkaline medium react with diacetic acid in urine	Acetoacetic acid + Na nitroprusside + glycine $\xrightarrow{\text{alkaline}}$ Violet to purple colour
Bilirubin	Reaction of a dizonium salt with bilirubin in acidic medium	Bilirubin + diazine $\xrightarrow{\text{acid}}$ Azobilirubin
Leukocyte esterase	Presence of esterase from granulocytes yields a violet colour	Rection A Indoxyl or pyrole carbonic ester $\xrightarrow[\text{esterase}]{\text{granulocytic}}$ Indoxyl or pyrole Rection B Indoxyl or pyrole + diazonium salt dye = purple

In microfluidic design, colorimetric detection was demonstrated using pH, glucose and protein in artificial urine [17]. The enzymatic oxidation of iodide to iodine resulted in a colour change from clear to brown in a glucose assay. Tetrabromophenol showed colour change from yellow to blue for the protein assay. Abe *et al.* [11] developed a multianalyte microfluidic device to quantitatively detect human serum albumin, glucose, and pH. Dungchai *et al*. [101] proposed an alternative design that employs multiple colorimetric indicators to visually discriminate between different analyte concentrations such as glucose, lactate, and uric acid. The assay is based on the oxidation of soluble indicators such as 4-aminoantipyrine, 3,5-dichloro-2-hydroxybenzenesulfonic acid, o-dianisidine dihydrochloride, and potassium iodide by H_2O_2 produced by analyte-specific oxidase enzymes. Lateral flow formats employing dyes are summarised in Table 1.3.

Table 1.3: Lateral flow devices employing dyes

Analyte	Method	Application	Reference
Oestrone sulphate in mares' urine	Uniformly blue dyed polystyrene microsphere labelled primary antibody	Confirmation of pregnancy	[102]
Albumin in urine	Alkaline colour reaction to tetrabromphenol blue	Nephropathy	[103]
Human or animal IgG in mosquito bloodmeal	Dye-labelled anti-IgG antibodies	IgG (human or chicken) to detect different host sources of blood meal in insects	[104]
Antibody to Schistosoma japonicum in serum	Blue colloidal dye labelled egg antigen	Schistosomiasis	[105]

It is clear that paper and its derivatives (nitrocellulose membrane) form a major part of the POC and POU devices. Tests are being designed on paper or nitrocellulose with the intention to cut on the cost associated with instrumentation and to facilitate testing in low resource settings that can be prohibitively expensive in the emerging economies using other technologies.

1.6 PAPER/ NITROCELLULOSE AS A SUPPORT FOR DIAGNOSTIC ASSAYS

Paper has been commonly used as a platform for POC and POU devices because of its low-cost and abundance [106,17,5,107]. It is a thin sheet of material made from pressing together cellulose fibres. It's been considered interesting in the development of POC and PUC devices because it can wick the liquid into its hydrophilic fibres without a pump [5].

Nitrocellulose membrane used as a strip material is the most critical part of the lateral flow devices because it controls the capillary flow of the mobile phase and it irreversibly captures the reagents at the test line and control lines. The membrane also controls the diffusion and the capillary flow of the mobile phase. Table 1.4 [108] shows the typical polymers used for membranes and their binding properties; however nitrocellulose is used the most. Nitrocellulose established its place over the others due to its higher capacity to bind irreversibly and hydophobically to proteins by absorption [109]. Nitrocelluloce membrane has also found applications in microfluidic devices [20] as it was mentioned earlier in section 1.1.3.

Table 1.4: Summary of polymers from which the membrane can be made from

Membrane polymer	**Primary binding mechanism**
Nitrocellulose	Electrostatic
Polyvinylidene fluoride	hydrophobic
Nylon (charge-modified)	electrostatic
Polyethersulfone	Hydrophobic

Although there is a wide variety of paper material to choose from, its choice depends on the steps required to fabricate the device and its application. This is because the performance of the device depends largely on the structural properties of the platform (paper or nitrocellulose membrane) like porosity, pore size and thickness. The structural properties of paper and nitrocellulose membrane and how they affect the performance of the devices are discussed in the following section. Paper and nitrocellulose membrane are discussed here because of their close relationship. Nitrocellulose is a kind of paper substrate made from pure cellulose nitrate by substituting hydroxyl moieties on sugar units.

1.6.1 Physical characteristics of paper/nitrocellulose

Nitrocellulose membrane's binding capacity is determined by the available of polymer surface area for immobilisation. Surface area is equally critical in paper-based microfluidic devices because of its impact on reagent deposition, sensitivity and reproducibility. Surface area in both formats is determined by parameters such as the pore size, porosity (amount of air in the three dimensional structure), thickness and to a minor extend the structural

characteristics unique to a polymer. Keeping all other parameters constant, surface area decreases nonlinearly with pore size, increases linearly with thickness and increases nonlinearly with porosity [108].

Capillary flow rate is also a key factor in the performance of the lateral flow and microfluidic devices. It is the migration speed at which a sample front move along a strip after the liquid is introduced at one end. It is largely determined by the aggregate properties of the porous structure. Flow rate increases with the increase in the aggregate pore size. It is also critical in achieving sensitivity depending on the location of the test line/zone. The further the test line/zone is from the sample inlet, the slower the flow rate the analyte passes through the test line/zone and the higher the effective concentration of the analyte. Measuring capillary flow rate is very difficult as the speed decays as the liquid moves along the membrane. The preferred parameter is therefore the capillary flow time, the time required for the liquid to fill completely a strip of defined length. It is inversely proportional to the flow rate

Porosity expresses how much air is inside the membrane structure and it is an independent from pore size. It is an important parameter due to its influence on the capillary flow rate. When pore size distribution and thickness are kept constant, capillary flow rate increases linearly with increasing porosity of the strip increases. Pore size also has an effect on the binding of the analytes. As pore size decreases, the membrane surface area increases and more analytes can attach to the membrane. However, if the pores are too small, the molecules do not fit in it. The membrane must also be able to withstand short and long term storage and allow the solution phase to interact with the immobilized phase without affecting the chemistry.

Thickness is also one parameter for defining how much liquid the membrane/paper can absorb. The numbers of labelled molecules in lateral flow devices that can reach the detecting

antibodies are specifically determined by the volume after the test line. The width of the test and control lines partly depends on the membrane's thickness. The spread of reagents is greater on a thin membrane/paper than on a thicker membrane/paper because of the restriction of the vertical flow of the reagents [108]. Moreover, thickness also influences the visibility of the signal.

It is very clear that the structural properties of paper and the nitrocellulose membrane determine the performance of POC and PUC devices. However, paper does not readily posses the desired physical properties for its applications.

1.6.2 Disadvantages associated with paper/nitrocellulose as a support for point of care and point of use devices

Paper based devices limitations are mainly related to its material properties, for example, paper is not suited for absorbance measurements because its fibres lead to large amounts of light scattering [18]. Commercial paper grade often differ in porosity, particle retention and flow rate. Due to their wicking properties, filter paper has been widely exploited in the development of paper based microfluidic devices [5,13,110,111]. However, filter paper comes in different degrees of purity, hardness and chemical resistance. Printer paper on the other hand, due to low porosity and surface tension effects has proved unsuitable for fabrication of hydrophilic channels. High porosity may also be disadvantageous, filter paper for example with larger pore size than the standard grade can swell their cellulose fibres and constrain capillary flow.

Most importantly paper is not readily available as it may not be generated in the laboratory. It has to be ordered from manufactures. It is envisaged that extending beyond characteristics of a commercial paper to novel platforms or substrates will play a great role in the realisation of POC and POU devices. There is also a need for improved quality platforms that can

withstand long term storage as paper tends to discolour upon prolonged storage due to exposure to humidity, high temperature and sunlight.

Nitrocellulose is hydrophobic by nature due to its cellulose acetate blends and tends to exhibit a high degree of non-specific binding towards biomolecules. Antibody-coated label molecules can attach to the membrane in the same manner they do to the test line antibodies.

1.7 OBJECTIVES

The objective of the studies in this thesis was to develop colorimetric probes in the form of test strips for AA and DA employing NPs, dyes/ligands as detector agents hosted in a nanofibre platform. The aim was to specifically develop:

1. A colorimetric test strip for ascorbic acid based on copper-gold (Cu-Au) NPs in electrospun nylon6
2. A colorimetric test strip based on prussian blue for the detection of AA and DA
3. A poly(vinylbenzyl chloride) colorimetric test strip based on electrospun nanofibre functionalised with Fe(III) - 2-(2'- pyridyl)-imidazole for the detection of AA and DA

In order to realise the development of these test strips, initial studies were to be carried out in solution to evaluate if reactions of interest and subsequent colour changes would be achieved. The ability of analytes of interest to interact with detector agents on a solid substrate would then be examined. The solid substrate, a polymer electrospun fibre was to be fabricated through electrospinning. The role of fibres in hosting nanoparticles that were employed for the colorimetric detection of ascorbic acid would be investigated using nylon6, poly(vinylbenzyl chloride)-styrene and cellulose acetate based fibres. Further investigations on the stability and effects of long-term storage of polymer electrospun supported colorimetric probes would then be carried out.

The next chapter will discuss the incorporation of metal NPs and dyes into polymers and subsequently polymer electrospun nanofibres.

Chapter 2 ELECTROSPINNING

2.1 OVERVIEW

The chapter discusses the use of electrospun polymeric nanofibers as a support for colorimetric probes and electrospinning as the versatile process of fabricating electrospun nanofibres. Ways of incorporating colour signalling reagents into polymers and subsequently electroospun nanofibres are also discussed in this chapter.

2.2 ELECTROSPUN POLYMER NANOFIBER AS SUPPORT FOR DYES AND NANOPARTICLES

Bringing materials to the nanometer scale has an advantage of improving their properties, while it affords them new advanced characteristics beyond bulk materials. Some of the unusual properties exhibited by nano structures include high surface area to volume ratio, which can be exploited for various applications. Some nano sized structures like nanotubes, nanowires, nanocomposites and nanofibres have received great interest for various applications. The interest of this thesis is in the application of polymer electrospun nanofibres as a support for colorimetric probes for biological molecules.

Recently there has been great interest in the unique mechanical, chemical and optical properties that can be achieved by combining the advantages of metal NPs, dyes and polymer nanofibres. Incorporation of metal NPs into nanofibres affords them other characteristics such as catalytic and optical properties. Colorimetric probes in form of test strips based on nanometals incorporated in electrospun nanofibres present an opportunity for the development of simple low cost sensing platforms for the detection of analytes of interest.

2.3 TECHNIQUES FOR PRODUCTION OF POLYMER ELECTROSPUN NANOFIBRE

The most common techniques available for the production of polymer fibres include electrospinning, drawing [112], template synthesis [113], phase separation [114], and self assembly [115]. Even though each method has its own advantage(s), electrospinning has a leading edge over all of them due to the fact that nanofibre orientation is easily controllable [116]. Fibre arrangement has a significant effect on the performance of the subsequent analytical device. Controlling the fibre orientation is especially desirable for their application as support for POC and POU devices. Electrospinning is simple, reproducible, is applicable to many polymers and scalable. Table 2.1 [116] shows a comparison of different nanofibre techniques.

Table 2.1: Comparison of different nanofibre fabrication technique

Fabrication technique	Advantages	Disadvantages
Drawing	Simple equipment	Discontinuous process Not scalable Fibre dimension not controllable
Template synthesis	Continuous process Templates can be used to vary fibre dimensions	Not scalable
Temperature induced phase separation.	Simple equipment Convenient to process Mechanical properties of the fibre can be varied by changing the polymer composition	Limited to specific polymers Not scalable Fibre dimension not controllable
Molecular self-assembly	For fabrication of fibres of diameter of few nm, and few microns in length	Complex process Not scalable Fibre dimension not controllable
Electrospinning	Continuous process Simple instrument Cost effective Scalable	Jet instability Toxic solvents

2.4 ELECTROSPINNING: FABRICATION OF NANOFIBRE

Electrospinning is a technique that relies on repulsive electrostatic forces to draw a viscoelastic solution into nanofibres [117,116]. A standard laboratory electrospinning set-up generally consists of three major components; (1) a spinneret (typically a syringe needle) connected to a high voltage supply used to generate potential differences, (2) a pump connected to the syringe employed to control the flow rate of the polymer and (3) a collector as depicted in Fig. 2.1. Spinneret could also be a wire or rolling drum in a pool of polymer for needleless electrospinning.

Figure 2.1: Schematic illustration of an electrospinning set-up

The basic principles of electrospinning are concerned with application of high voltage (electric field) to a polymer solution. When voltage is applied to a polymer drop emanating from the metallic needle, the charged particles start to concentrate on the surface of the

polymer drop, thus resulting in the excess build-up of charged particles at the tip of the drop. When the applied electric field overcomes surface tension a liquid jet is induced which undergoes stretching into continuous nanofibres and accelerates towards a grounded collector [118,116,117]. Shortly after the jet of polymer flows away from the tip in a nearly straight line, it undergoes an electrically induced bending instability that causes the stretching of the bent sections of the jet. In needless electrospinning, the rotation of the spinneret loads a thin layer of polymer solution onto its surface. Its rotation and perturbance create conical spikes on the surface of the solution layer. When a high voltage is applied to the spinneret, these spikes tend to concentrate charges and amplify the perturbance and the fluid around the spikes is drawn to these spikes under high electric force. Taylor cones are thus formed. When applied electric field is enough, fine solution jets are then ejected from the tips of the Taylor cones. The geometry of the spinneret could also be cylindrical, coil, disc and beaded chain.

Various parameters potentially affect electrospinning. Solution properties (surface tension, solution concentration & viscosity, conductivity) and operation parameters (voltage, flow rate, distance from tip to collector) particularly affect the morphology of the obtained fibres.

2.4.1 Polymer solution parameters

The polymer solution properties play a significant role in controlling the fibre diameter and the structural morphology. During electrospinning the electrical property of the solution, surface tension and viscosity will determine the degree of stretching.

The charges on the polymer must be high enough to overcome surface tension of the solution. As the solution jet is from the surface of a charged polymer towards the collection plate, surface tension may cause the solution to breakup into droplets. It has been also attributed to formation of beads during electrospinning. A higher viscosity will mean that there is greater

interaction between the solvent and polymer molecules thus when the solution is stretched under the influence of the charges, the solvent molecules will tend to spread over the entangled polymer molecules thus reducing the tendency for the solvent molecules to come together under the influence of surface tension [119,120].

Solution concentration and viscosity are closely correlated, as an increase in solution concentration always results in solution viscosity. If the solution is too dilute, surface tension will break up the solution into droplets before reaching the collector, therefore electrospraying may occur and particles may form instead of fibers (Fig. 2.2). Alternatively when the polymer concentration is low, chain entanglement may be insufficient resulting in beaded fibres (Fig. 2.2). However, when the concentration is very high, the polymer solution becomes too thick to be stretched into jets. Electrospinnable optimal concentration range is therefore polymer dependant. In needle electrospinning, the increase in concentration and viscosity favours the increase in fibres diameter [121]. However in needleless electrospinning, as long as polymer solutions can be electrospun into nanofibers successfully, the polymer concentration doesn't affect the fibre diameter significantly [122].

Another polymer solution parameter that affects the fibre morphology is its conductivity.

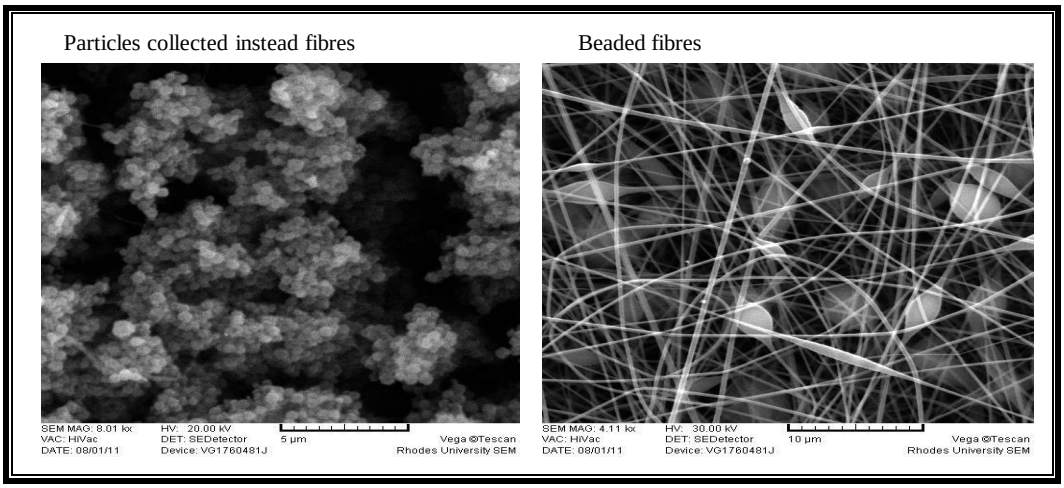

Figure 2.2: Scanning electron micrograph of particles and fibres with beaded morphologies

For a polymer solution to be electrospun, it must carry sufficient charges that are able to overcome the surface tension of the solution. Subsequent stretching of the electrospinning jet is also dependent on the solution's ability to carry charges. The functional groups on the polymer backbone, solvents used and ionic species present in the solution determines its conductivity. Mineral salts, mineral acids, carboxylic acids, some complexes of acids with amines, stannous chloride and some tetraalkylammonium salts may be added to the solvents to increase its conductivity [119]. The conductivity of the solution determines the fibre morphology and the diameter distribution. Highly conductive solutions will be extremely unstable in the presence of strong electric fields, leading to dramatic bending instabilities and broad diameter distribution. Processing conditions also affects electrospinning although less significant than solution parameters.

2.4.2 Processing conditions

The processing parameters include voltage applied, flow rate of the polymer solution and the distance between the needle tip and the collector.

Voltage is necessary in the electrospinning process to induce charges on the solution. Electrospinning will then be initiated when electrostatic field overcomes surface tension which induces the formation of a liquid jet that undergoes stretching into continuous nanofibres and accelerates towards the collector [123,124]. During electrospinning applied electrical potential translate into spinning current and results in different mode of jet initiation and instabilities. Keeping other variables constant, (solution conductivity and flow rate) an increase in applied electrical potential causes an increase in spinning current and subsequently an increase in mass flow from the needle tip to the collector. Smaller and less stable tailor cone may result. Generally higher voltage in both needleless and needle electrospinning induces higher repulsive forces on the jet which favours the formation of uniform fibres with smaller thinner fibres [124].

Flow rate my significantly affect fibre morphology in needle electrospinning. High flow rates cause fibres to be collected without sufficient solvent evaporation leading to flattened web-like appearance as demonstrated in Fig. 2.3 [125,118]. Optimised lower solution flow rate which maintains the Taylor cone is more ideal since it permits time for solvent evaporation and produces better fibres. However, a solution flow rate below the threshold for a given voltage causes evaporation at the needle tip, thus preventing electrospinning. The diameter and pore size increase accordingly, with higher flow rates, however fibres may not dry completely before reaching the collector resulting in beaded morphologies [126]. Flow rate in needless can't be precisely controlled but could be adjusted just in a very limited range through changing the spinneret speed. Adjusting flow rate has shown to affect productivity with less effect on the fibre morphology.

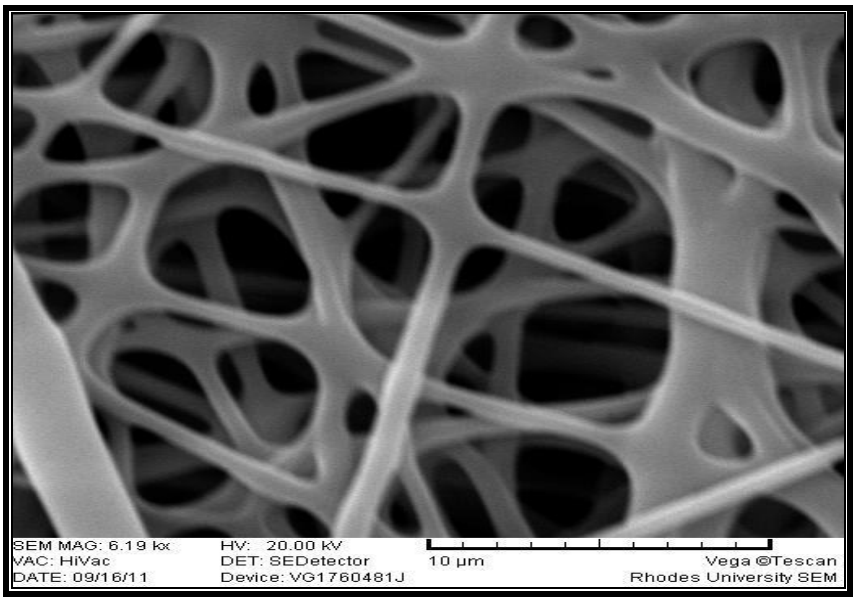

Figure 2.3: Scanning electron micrograph of web like morphology fibres resulting from insufficient solvent evaporation

The collecting distance must be large enough to ensure sufficient solvent evaporation from the jet before deposition in both needle and needless electrospinning. Tip-collector distance has a direct influence on jet flight time and electric field strength. A decrease in this distance shortens flight times and solvent evaporation time, and increases the electric field strength, which results in increase of bead formation. The wider gap allows more time for the fluid jet to stretch fully and for the solvent to evaporate completely. When the gap is increased more, the collected fibres are dried and fully stretched, and the fibre diameter is reduced. However, the collecting distance should not be too large either, since a larger distance would require a higher applied voltage to initiate electrospinning, which may cause corona discharge.

In addition nanofibre alignment may be modified by altering electrospinning equipment. Strong external field, collector type and charges exerted by adjacent fibres, mainly control the motion of fibres during electrospinning. Nanofibres deposition can either be on stationery or rotating targets. Randomly oriented fibres may be achieved on a stationery target due to non-

preferential direction for electrostatic forces [127-129]. However stationery collectors are not suitable for needless electrospinning because the deposition of numerous nanofibres accumulates a large amount of charges on the collector, which can finally disturb or even stop the electrospinning process. With a rotating target such as a rotating drum, if the rotating speed matches the evaporated jet depositions, the fibres are collected on a cylindrical surface in a circumferential manner resulting in a fair alignment [130,131]. Fibre alignment has been shown to improve mechanical strength of the nanofibre matrices. Mechanical strength of fibres is critical for any application.

2.4.3 Mechanical properties of polymer electrospun fibre

Electrospun nanofibres posses a wide range of mechanical properties due to their high surface area and tiny pores. Varying fibre diameter, aligning fibres, choice of polymer, and nanofibre cross-linking are currently some of the strategies used to alter mechanical strength of nanofibres. Nanofibres are a representation of a dynamic structure where pore size and shape can change. These properties make them ideal for diverse applications, such as in drug delivery [132,133], tissue engineering [134] and wound healing [135,136] and even as support for POU and POC devices [137-139].

Because electrospinning relies on repulsive electrostatic forces to draw a viscoelastic solution into nanofibers [117,116], detection agent may be incorporated into the polymer solution prior to electrospinning.

2.5 INCORPORATION/ IMMOBILIZATION OF DETECTION AGENTS INTO POLYMERS

Polymers are expected to be optically inert and they function as 1) a solid support onto which detection agents are being immobilized and 2) a material possessing certain permeation

selectivity for the analytes of interest while rejecting others. The polymeric matrix is limited to retaining the colour-signalling reagent in place and to favour the diffusion of analyte molecules to the sensing molecules. However, the polymer properties have a pronounced effect on the performances of the colour signalling reagent as well as the resulting optical probe [197]. Polymers are convenient due to the fact that they can easily be processed into small particles and thin films that can be deposited onto optical fibres [140], and waveguides [141,142] for fabrication of optical probes. The choice of the polymer is determined by its compatibility with the sample. Following the choice of the colour signalling reagent and polymeric support, the next step in the diagnostic probe design is the immobilization of the dye in-or on-a support.

Several methods exist for incorporation of NPs into polymeric nanocomposites resulting in improved mechanical, electrical and optical properties. Polymer matrix containing metal NPs may be prepared by; (1) mechanical mixing of a pre-synthesised polymer and pre-made NPs powder [143], (2) the *in-situ* polymerisation of monomers [143,144] and (3) the *in-situ* reduction of the metal salt in a polymer matrix [145] . Incorporation of noble metals in polymer via electrospinning prepared by a two-step process in which NPs are synthesised and dispersed into the electrospinning solution has been reported [146]. The two-step process however has some short comings. Protecting agent is always required to prevent NPs from aggregating during solution preparation [147] and the NPs need to be extracted before use [148]. One-step synthesis of nanoparticle-filled polymer nanofibres has been reported where electrospinning is combined with chemical treatment [149], irradiation [123,150] and thermal treatment [151]. Single step approach has acquired significant interest because it minimises time and energy consumption. Some studies have demonstrated that dyes also can be

incorporated in the nanostructures simply by adding the dyes to the polymer solution before the start of the electrospinning process [152,153]. Physical entrapment though simple for immobilisation of dyes/indicators into polymers, the approach suffers from producing inhomogeneity in the material that results in the leaching of the probe. This limits their use for long time monitoring.

As an alternative to physical entrapment, covalent attachment of the molecules into polymeric materials by co-polymerisation or after polymerisation if the polymer contains reactive monomers has been employed. Covalent attachment is the preferred method because it results in molecules that are firmly bound to the polymer backbone and therefore cannot be leached out. However immobilisation of molecules by covalent bonding is tedious. The presence of reactive groups on both the detector agent and the polymer is required, for activation to freely undergo a chemical reaction with the partner. A large variety of probes containing covalently linked dyes have been developed. Such an example is the Remazol procedure, a preferred method for making commercial pH paper strips on celluloses [154] and related hydroxy polymers.

Though the electrospinning process could produce nanofibre with special structures and morphologies, it is difficult to prepare the fibres with desirable surface properties that meet the demands of the intended applications. Post electrospinning modification process however could change or modify the surface properties to satisfy the demands of special applications.

2.6 FUNTIONALISATION OF POLYMER ELECTROSPUN FIBRES

Post electrospinning surface modification of fibres can be done by either inducing some polymerization reactions on the fibre surface or by the adsorption or immobilization of special active agents (such as drugs, some proteins) onto the fibre surface. The most widely

adopted approach to introduce large amounts of reactive groups on chemically inert polymer surfaces is by graft polymerization.

2.6.1 Graft polymerisation

One way of introducing large amount of reactive groups on chemically inert polymer surface is through graft polymerisation. Surface grafting can be achieved via inducing methods such as; photo-induced grafting (UV-induced grafting), thermal-induced grafting, ozone-induced grafting, plasma-induced grafting and redox-grafting techniques either via "grafting-to" or "grafting-from" routes. One approach of polymerization called atom transfer radical polymerization provides a controllable method to modify the surface of some nanostructures. The surface-initiated atom transfer radical polymerization (ATRP) can be conducted consecutive from the surface of a variety of substrates in that the effective initiators were provided. The initiators are commonly some halide groups, such as the benzyl chloride, the benzyl bromide. Two ways could conduct the combining of electrospinning and ATRP reactions. One is to functionalize the polymer molecules (or inorganic particles) through ATRP and then electrospin into nanofibre, the other is to immobilize initiators on the fibre surface and conduct in succession ATRP. Chemical treatment has also been reported as another simple way of introducing desired chemical functionalities onto the surfaces of electrospun nanofibres.

2.6.2 Chemical treatment

Chemical treatment offers the flexibility of surface modification of thick nanofibrous meshes. The approach is normally employed to modify surface wettability property or to create new functionalities (such as carbonyl, hydroxyl, and carboxylic groups) at the surface of the polymer. The oxygen-containing functional groups lead to increased polarity and the ability to form hydrogen bond, which in turn results in the enhancement of wettability and adhesion.

Chemical reactions can be carried out at sites that are susceptible to electrophilic or nucleophilic attacks. Structures such as benzene rings, hydroxyl groups, double bonds, halogens and ester groups qualify for such attacks. Polyester like polyethylene terephthalate (PET) and poly(caprolactone) (PCL) can be treated by amine compounds to introduce amino groups through the aminolysis of the ester groups [155]

In this study we evaluate the feasibility of a fibre as a support for colorimetric probes and even as an alternative solid support for use in lateral flow, dipsticks and micro-fluidic devices. To be a competitive material, electrospun fibres based assay must process small samples in small volumes, complete the test in short duration and be comparable to existing paper based assays in selectivity and sensitivity.

Chapter 3 ASCORBIC ACID & DOPAMINE

3.1 OVERVIEW

The chapter gives an overview of why ascorbic acid and dopamine were chosen as model analytes. The conventional techniques for the detection of the two biomolecules, their advantages and disadvantages are also discussed in this chapter.

3.2 ASCORBIC ACID

Ascorbic acid (AA) also known as vitamin C is a powerful antioxidant naturally present in many foods, especially fruits and vegetables. Rich sources include blackcurrant, citrus fruit, leafy vegetables, and tomatoes, green and red peppers. Most animals synthesise vitamin C, but man, primates, apes, chimps and guinea pigs have lost the ability as they lack the last enzyme (l-glucono-lactone oxidase) on the vitamin C synthesis pathway [156]. Therefore humans depend on exogenous sources of the vitamin C which include fruits and vegetables as well as food supplements and pharmaceutical preparation because the body needs ascorbic acid for its normal physiological functions [157].

For example, AA is involved in the metabolism of several amino acids to produce hydroxyproline, hydroxylysine, norepinephrine, serotonin, homogenistic acid, and carnitine [158,159]. Hydroxyproline, hydroxylysine are components of collagen, a protein that gives structure to bones, cartilages, muscles and blood vessels. The inability for wounds to heal and for fractures to repair is attributed to impaired collagen formation associated with lack of vitamin C. It also aids in the absorption of iron, helps maintain capillaries, bones and teeth. It plays a significant role in regulating the activities of hormonal biosynthesis, enzymatic reactions and transport of neurotransmitters [160,161]. Ascorbic acid is involved in many hydroxylation and decarboxylation reactions for the biosynthesis of many neurochemicals. In

one example tyrosine is metabolized in the presence of ascorbic acid in to catecholamines by hydroxylation and decarboxylation, forming dopamine, norepinephrine, epinephrine, and adrenocrome.

AA plays a major role as an antioxidant that forms part of the body defence system against reactive oxygen species and free radicals, and therefore prevents tissue damage. It donates electrons to free radicals that stabilises them and subsequently prevents free damage to cells. The concentration of AA/ascorbate in biological fluids can be used to assess the extent of oxidative stress in human metabolism. Oxidative stress occurs when the formation of free radicals exceeds the ability to neutralise them and excessive oxidation stress has been linked to cancer, heart disease, and conditions like arthritis [162,163].

AA also used in the food industry as an antioxidant to prevent undesirable changes in colour, taste and odour and subsequently increases the storage life of products. It has also been used for the prevention and treatment of different infectious diseases such as common cold, HIV and influenza. Therefore, the determination of AA content is particularly important in the pharmaceutical and food industry at various levels.

3.3 DOPAMINE

Dopamine (3, 4-Dihydroxyphenylethylamine, (DA) belongs to a group of neurotransmitters called catecholamines. It is involved in the regulation of various actions in the central nervous system including locomotion, cognition, emotion and nueroendrocrine secretion. Dopamine is formed by the decarboxylation of dihydroxyphenylalanine (DOPA) in the brain. Projections originating from brain areas that synthesize this neurotransmitter give rise to four axonal pathways: (1) nigro-striatal (2) mesolimbic, mesocortical (3) tuberoinfundibular. Brain dysfunction has been associated directly or indirectly with the alterations in the neurotransmission of dopamine, for example the nigrostriatal pathway is involved in the

control of movement and its degeneration contributes to the pathogenesis of Parkinson's disease [164]. Parkinson disease is characterised by the inability to execute smooth movement [165,166]. Imbalances in the mesolimbic dopamine pathways are thought to contribute to physcotic disorders such as schizophrenia. The pathway has also been implicated to influence motivated behaviour [167]. The mesocortical on the other hand influences some aspects of learning and memory [168].

Since dopamine and ascorbic acid coexist in real biological samples, the development of sensitive and selective methods for their detection for diagnostic purposes is very important.

3.4 CONVENTIONAL TECHNIQUES FOR DETECTION OF ASORBIC ACID & DOPAMINE

Classic techniques for the detection of AA include titration with an oxidant solution such as dichlorophenol indophenol (DCPIP) [169], potassium iodate or bromate [170]. Volumetric techniques can suffer from lack of specificity that limits their use to samples not containing other reducing agents.

Instrumental techniques developed so far for the detection of both AA and DA include voltammetry [171-173], chromatography especially high performance liquid chromatography with electrochemical detection (HPLC-ECD) [174], flourimetry [175,176], spectrophotometry [177,178]. However, most of the detection methods suffer due to matrix effects, especially as ascorbic acid also co-exists with dopamine and uric acid in real biological samples.

Direct spectrophotometric detection of AA in the UV-region is prone to matrix effects since many organic compounds in complex samples may exhibit ultraviolet absorbance. Lack of

sensitivity for chemiluminescent methods limits their application to real samples and they also require a spectrophotometer for taking measurements.

HPLC-ECD detection is reported to be a selective and sensitive technique for AA assessment in foodstuffs and biological fluids [174]. However, optimisation of sample extraction is still required especially in complex matrices like fruits. The technique has also emerged as the method of choice for the detection of catecholamine. However, analyses of catecholamines consist of three steps. Clean up, separation and detection. Only few methods described have no clean-up of the urine sample, However the protocols made use of different pre-coloumn derivatisation procedures which means total analysis time is not shorter compared to methods using clean-up procedures [179].

Voltammetric techniques though sensitive and fast, they have a limitation of overlapping of peak potentials of uric acid, dopamine and ascorbic acid at conventional electrodes with the pronounced effect, resulting in poor selectivity and reproducibility [180].

There still remain a challenge to develop technically simple methods for the detection of both ascorbic acid and dopamine. The conventional detection techniques also suffer limitations suffer limitations associated with cost, especially for instrument based strategies. The techniques are also time consuming as they rely on extensive sample preparation.

The inter-particle distance dependent colours for the detection of ascorbic acid [181,182] and dopamine [183-186] have been extensively applied in solution phase for colorimetric biodetection but have not received much attention in solid-phase applications which presumably are more suited for practical applications. We envisage colorimetric assays such as a dipstick or test strip are portable and easy to use especially in areas where laboratory facilities are not readily available. The commercially available test strips for ascorbic acid are

not capable of covering a wide range of pH and are therefore either limited to fruit juices or biological samples.

In this study, the ability of target AA to change the inter-particle distance of AuNPs (and therefore the colours) on a nanofibre substrate was examined. Metal NPs have mainly been studied because they exhibit unique optical properties. Alloy NPs on the other hand have received attention because of their catalytic effects [187,188]. When NPs are composed of various metals, both the composition and the actual distribution will determine the resulting physiochemical properties, in particular the optical properties. Alloy may prove to be advantageous to use in colorimetric probes as they offer additional freedom for tuning their optical properties by altering atomic composition and arrangement, hence an approach employing copper-gold (Cu-Au) is reported in this thesis [189].

Chapter 4 EXPERIMENTAL

4.1 OVERVIEW

The chapter presents the experimental aspect of the studies carried out in this work. All the experimental procedures and reagents used for the three colorimetric probes for AA and DA employing NPs, dyes/ligands as detector agents hosted in a nanofibre platform are provided. The colorimetric probes developed are: (1) A colorimetric test strip for ascorbic acid based on copper-gold (Cu-Au) NPs in electrospun nylon6 (2) A colorimetric test strip based on prussian blue for the detection of AA and DA (3) A poly(vinyl benyl chloride) colorimetric test strip based on electrospun nanofibre functionalised with Fe(III) - 2-(2'- pyridyl)-imidazole for the detection of AA and DA.

4.2 CHEMICALS AND REAGENTS

Copper (II) sulphate ($CuSO_4.5H_20$) (98%), gold (III) chloride trihydrate ($HAuCl_4.4H_2O$), 11-mercaptoundecanoic acid (MUA), 4-Mercaptophenyl-boronic acid (MBA), nylon-6, sodium borohydride ($NaBH_4$), azoisobutyronitrile (AIBN) (recrystallized from THF just before use), nylon-6, Ferric chloride ($FeCl_3$), potassium ferricyanide $K_3[Fe(CN)_6]$, ferrous sulphate ($FeSO_4$), pyridine-2-aldehyde 99%, glyoxal solution (40% weight in water) and 4-vinylbenzyl chloride (90%), ascorbic acid (AA), L-lysine, DL-tyrosine, aspartic acid, aspirin, theophylline, sodium sulphite, glutathione were obtained from Sigma Aldrich (St. Louis, USA). Potassium chloride, sodium chloride, calcium chloride, glucose, sucrose, fructose, citric acid, acetic acid (99.5%), and formic acid (99%), tetrahydrofuran (THF), dimethylformamide (DMF), dichloromethane (DCM), (99 %) ethanol, diethyl ether, ethyl acetate, N,N- Tetrahydrofuran (THF), potassium hydroxide (KOH) and sodium hydroxide

(NaOH), 25% ammonia solution, methanol were obtained from Merck (Gauteng, South Africa. merck4ARP@merck.co.za). Sodium dihydrogen phosphate ($NaH_2PO_4.2H_2O$) and potassium hydrogen phthalate ($C_8H_5KO_4$) were from Saarchem Analytic (Krugersdorp, South Africa).

4.3 CHARACTERISATION AND MEASUREMENTS

4.3.1 UV-visible spectroscopy

UV-visible adsorption spectra of solutions were recorded on a Perkin Elmer Precisely UV-visible spectrometer Lambda25 using a 1 cm quartz cell.

4.3.2 Fourier transform infrared spectroscopy (FTIR)

Infrared spectra of the fibres were acquired on a Perkin Elmer System 100 ATR-IR spectrophotometer (4000-650).

4.3.3 Transmission electron microscopy (TEM) and scanning electron microscopy (SEM)

TEM measurements were made on JEOL 1210 operating at 100 kV, SEM images were recorded on a JEOL JSM-7001F with an accelerating voltage of 25 kV, Field emission scanning electron microscope.

4.3.4 X-ray photoelectron spectroscopy (XPS)

Elemental analysis of the fibre was achieved by XPS. The XPS analysis was carried out with a PHI 5000 Versaprobe-Scanning ESCA Microprobe. The surveys were carried out with a 100 µm, 25 W, 15 kV beam using monochromatic Al K_α radiation ($h\nu$ = 1486.6 eV). For higher resolution spectra the hemispherical analyzer pass energy was maintained at 11.8 eV for 30 cycles. Measurements were performed using either a 1 eV/step and 15 min acquisition

time (binding energies ranging from 0-1400 eV, 5 cycles) for survey scans or a 0.1 eV/step and 20-170 min acquisition time for the high resolution scans.

4.3.5 Nuclear magnetic resonance (NMR)

The structure of the ligand was determined by 1H NMR spectroscopy on a bruker AMX 400 NMR MHZ spectrometer and reported relative to tetramethlsilane (TMS) δ 0.00.

4.3.6 Electron paramagnetic resonance (EPR)

EPR spectra were recorded on a Bruker ESP 300E X-band spectrometer, and the spin Hamiltonian parameters were obtained by simulation of the spectra [190]. EPR analysis parameters for Irom(III) complexes are shown in table 1.

Table 4.1:EPR analysis parameters

Fields	
Center Field	3500 G
Sweep Width	8800 G
Resolution	5000 points
Microwave	
Frequency	9.740 GHz
Power	20.000 mW
Reciever	
Receiver Gain	1.00e+003
Mod. Phase	0.00 deg
Harmonic	1
Mod. Frequency	100.00 kHz
Mod. Amplitude	16.05 G
Conversion	5.000 ms
Signal Channel	
Time Constant	20.480
Sweep Time	25.000 s

4.4 ELECTROSPINNING SET-UP

The Polymer solution was fed from a 10 ml syringe equipped with a 24 gauge stainless steel needle and the flow rate was controlled using a digitally controlled pump, (New Era, NE 100). A high voltage supplier from the Department of Electronics and Electrical Engineering at Stellenbosch University (Stellenbosch, South Africa) was linked to the needle through a copper pin.

4.5 pH MEASUREMENTS

Potassium hydrogen phthalate-hydrochloric acid (pH 2.2-4.0), potassium hydrogen phthalate-sodium hydroxide (pH 4.5-5.9) and sodium dihydrogen phosphate-sodium hydroxide (pH 6.0-7.0) were used for preparation of buffer solutions. The pH adjustment monitored by means of a Jenway 3510 pH-meter with a combined glass electrode.

4.6 ASCORBIC ACID TEST STRIP BASED ON COPPER-GOLD ALLOY NANOPARTICLES

4.6.1 *In-situ* synthesis of copper-gold alloy nanoparticles nanocomposite

4.6.1.1 11-mercaptoundecanoic acid stabilised copper-gold alloy nanoparticles nanocomposite

1g of Nylon6, $HAuCl_4.4H_2O$ and $CuSO_4.5H_20$ in the ratio 11: 8, were dissolved in 5 mL formic acid and acetic acid in the ratio 1:1(v/v). The weight percentage of the salts was 10 wt% of nylon6 mass. Formic acid was used as a reducing agent. MUA (11-mercaptoundecanoic acid) was added to stabilize the NPs so as to prevent them from aggregating. The mixture was left to stir constantly at room temperature for 24 h to obtain Cu-Au alloy NPs.

4.6.1.2 Polymer stabilised copper-gold alloy nanoparticles nanocomposite

The approach for MUA stabilised nanocomposite was followed for polymer stabilised (steric stabilisation) NPs, however no additional capping agent was added but the polymer was used as a stabiliser.

4.6.1.3 4-Mercaptophenyl-boronic acid stabilised copper-gold alloy nanoparticles nanocomposite

The production of the test strip was also achieved under the same protocol using an additional capping agent (4-mercaptophenyl-boronic acid (M*B*A)).

4.6.2 Solution studies on a nanocomposite of nylon6 and 11-mercaptoundecanoic acid stabilised copper-gold alloy nanoparticles

4.6.2.1 Effect of ascorbic acid, dopamine & uric acid to a nanocomposite of nylon6 and 11-mercaptoundecanoic acid stabilised copper-gold alloy nanoparticles

AA standard (176. 13 mg L^{-1}), 189.64 mg L^{-1} DA and 168.11 mg L^{-1} uric acid were prepared in water and acetic acid/formic acid (V/V =1:1). The ratio of water: acetic acid/formic acid was 1:5. Aliquots of the polymeric nanocomposite (100 µL) were then added to 4 mL prepared standards of AA, DA and uric acid in four different vials. The contents were left to stand for 10 min before UV-visible absorbances were acquired.

4.6.2.2 Further reduction nanocomposite of nylon6 and 11-mercaptoundecanoic acid stabilised copper-gold alloy nanoparticles by sodium borohydride

The nanocomposite (100 µL diluted by 4 mL in formic acid: acetic acid (V/V=1:1) initially reduced by formic acid was reduced further by 3 mg $NaBH_4$.

4.6.2.3 Linearity studies on the nanocomposite of nylon6 and 11-mercaptoundecanoic acid stabilised copper-gold alloy nanoparticles

The linearity studies were carried out using the polymeric nanocomposite prior to electrospinning. A series of AA standards solutions were prepared in a concentration range of

100 mg L^{-1} - 400 mg L^{-1}. The standards were prepared in water and acetic acid/formic acid (V/V =1:1). The ratio of water: acetic acid/formic acid was 1:5. Aliquots of NPs polymeric composite (20 µL) were then added to 3 mL AA of different concentrations. Colour change was observed at 5 min and maximum absorbance was at 10 min. Therefore all nanocomposite absorbance were carried out at 730 nm after 10 min.

4.6.3 Electrospinning

4.6.3.1 11-mercaptoundecanoic acid stabilised copper-gold alloy nanoparticles electrospinning conditions

The nanocomposite was electrospun at a positive voltage of 17 kV, and a flow rate of 0.5 mL/h. The nanofibres were collected on the grounded collector that was covered with aluminium foil and the distance from tip of the nozzle to the collector was 10 cm.

4.6.3.2 Polymer stabilised copper-gold alloy nanoparticles electrospinning conditions

The nanocomposite was electrospun at a voltage of 17 kV at a flow rate of 0.5 mL/h. The nanofibres were collected on the grounded collector that was covered with aluminium foil and the distance from tip of the nozzle to the collector was 10 cm.

4.6.3.3 11-mercaptoundecanoic acid and 4-mercaptophenyl-boronic acid stabilised copper-gold stabilised alloy nanoparticles electrospinning conditions

The solution was electrospun at a voltage of 17 kV, flow rate of 0.5 mL/h and at the distance of 10 cm between collector and nozzle.

4.6.4 Investigations on ascorbic acid test strip based on copper-gold alloy nanoparticles

4.6.4.1 Colorimetric detection of ascorbic acid using 11-mercaptoundecanoic acid stabilised copper-gold alloy nanoparticles based test strip

A stock solution of 176 mg L^{-1} AA was prepared in the pH range 2-7. The test strip was subsequently exposed to ascorbic acid in the standard solutions. The buffers used to adjust the pH were potassium hydrogen phthalate-hydrochloric acid (pH 2.2-4.0), potassium hydrogen phthalate-sodium hydroxide (pH 4.5-5.9) and sodium dihydrogen phosphate-sodium hydroxide (pH 6.0-7.0). Possible biological, foodstuff and pharmaceutical interferences were evaluated at pH 3 (pH for pharmaceuticals and fruit juices), pH 7 which is a physiological pH. Possible interfering compounds evaluated include glucose, sucrose, fructose, citric acid, oxalic acid, aspartic acid, maleic acid, sodium chloride, calcium chloride, lysine, glutathione, aspirin, alanine, tyrosine, sodium sulphite. The response for dopamine and uric acid was evaluated at the physiological pH only.

4.6.4.2 Colorimetric detection of ascorbic acid by 11-mercaptoundecanoic acid and 4-mercaptophenyl-boronic acid stabilised copper-gold alloy nanoparticles based test strip

The protocol for MUA Cu-Au alloy NPs was followed for the colorimetric detection of AA and the evaluation of possible interferences.

4.6.4.3 Colorimetric detection of ascorbic acid by polymer stabilised copper-gold alloy nanoparticles test strip

The protocol for MUA stabilised Cu-Au alloy NPs was followed for the colorimetric detection of AA and the evaluation of possible interferences

4.7 EVALUATION OF THE FEASIBILITY OF A FIBRE AS A SOLID SUPPORT FOR NANOPARTICLES

4.7.1 Polymerisation of poly(vinylbenzyl chloride)-styrene (PVBC-styrene)

Bulk polymerisation of the monomers 4-vinylbenzylchloride (15 mmol) and styrene (35 mmol) were achieved by using excess (0.04g, 0.19) azobisisobutyronitrile (AIBN) as the initiator in a stoppered flask. The mixture was heated overnight at 70 ˚C. The obtained polymer was precipitated with methanol, filtered and air dried. The procedure for polymerisation is summarised in scheme 2.

4.7.2 *In-situ* synthesis of copper-gold alloy nanoparticles nanocomposite

4.7.2.1 Synthesis of copper-gold alloy nanoparticles *in-situ* in nylon6

The protocol was carried out as described in section 5.6.1.1.

4.7.2.2 Synthesis of copper-gold alloy nanoparticles *in-situ* in cellulose acetate

Cellulose acetate (0.6 g), $HAuCl_4.4H_2O$ and $CuSO_4.5H_20$ in the ratio 11: 8, 6 mg MUA was dissolved in was dissolved in ratio 4:1 (wt/v) dichloromethane and methanol. The weight percentage of the salts was 10 wt% of nylon6 mass. $NaBH_4$ was used as a reducing agent.

4.7.2.3 Synthesis of copper-gold alloy nanoparticles *in-situ* in poly(vinylbenzy chloride)-styrene

PVBC-styrene $HAuCl_4.4H_2O$ and $CuSO_4.5H_20$ in the ratio 11: 8, 6 mg MUA was dissolved in ratio 1:1 (wt/wt) tetrahydrofuran and dimethylformamide. The weight percentage of the salts was 10 wt% of nylon6 mass $NaBH_4$ was used as a reducing agent.

4.7.3 Electrospinning

4.7.3.1 Electrospinning conditions for the composite of nylon6 and copper-gold alloy nanoparticles

Electrospinning conditions are as described in section 4.6.3.1.

4.7.3.2 Electrospinning conditions for the composite of cellulose acetate and copper-gold alloy nanoparticles

Cellulose Acetate (CA) was electrospun at a positive voltage of 20 kV a flow rate of 9 mL/h, and a working distance of 14 cm.

4.7.3.3 Electrospinning conditions for the composite of poly(vinylbenzyl chloride)-styrene copper-gold alloy

PVBC-styrene was electrospun at a positive voltage of 20 kV, flow rate of 2.6 mL/h, and a working distance of 11 cm.

4.7.4 Leaching investigations in nylon6, poly(vinylbenzyl chloride)-styrene, and cellulose acetate based test strips

Ascorbic acid standards of different concentrations (from 1.76 $x10^{5}$ mg L^{-1} to1.76 $x10^{-2}$ mg L^{-1}) were prepared in deionised water. The test strips were cut into 1 cm^{2}, exposed to into 3 ml of each standard for 5 min to allow for colour change of the fibre. The solutions were then checked for leaching by taking the UV-visible absorption readings of the same standard solutions which the fibres were exposed to.

4.7.5 Thermal stability of nylon6 based test strip

MUA Cu-Au alloy nanoparticles test strip was left in the oven at 60 °C and others at 80 °C for 3 days. After this period they were cut into 1 cm^{2} and exposed to 3 ml of each standard for 5 min to allow for colour change of the fibre. Leaching was investigated from the standard solutions using UV-visible absorption spectrometer.

4.8 ASCORBIC ACID AND DOPAMINE TEST STRIP BASED ON A PRUSSIAN BLUE

4.8.1 Nylon6, ferric chloride and ferricyanide based test strip

4.8.1.1 Synthesis of nylon6, ferric chloride and ferricyanide composite

$FeCl_3$ (ferric chloride) and $K_3[Fe^{III}(CN)_6]$ (ferricyanide) mass in the ratios 3:2 were weighed into a vial containing 1 g nylon-6. The contents were dissolved in a mixture of formic and acetic acid in the ratio 1:1 (v/v). The mixture was left to stir constantly at room temperature for 24 h.

4.8.1.2 Solution studies on nylon6, ferric chloride and ferricyanide composite

4.8.1.2.1 Effect of ascorbic acid, dopamine & uric acid to a composite of nylon6, ferric chloride and ferricyanide

To determine the effect of AA, DA and uric acid on the composite of nylon6 and the iron salts 176. 13 mg L^{-1}AA, 189.64 mg L^{-1} DA and 168.11 mg L^{-1} uric acid standards were prepared in water and acetic acid/formic acid (V/V =1:1). The ratio of water: acetic acid/formic acid was 1:5. Aliquots of polymeric composite (20 µL of $K_3[Fe^{III}(CN)_6]$, $FeCl_3$ and nylon6 composite) was then added to 4 mL prepared standards of AA, DA and uric acid in four different vials. The contents were left to stand for 1 h before UV-visible absorbencies were acquired.

4.8.1.2.2 Effect of ascorbic acid, dopamine and uric acid on ferricyanide and nylon6 composite

AA standard (176. 13 mg L^{-1}), 189.64 mg L^{-1} DA and 168.11 mg L^{-1} uric acid were prepared in water and acetic acid/formic acid (V/V =1:1). The ratio of water: acetic acid/formic acid was 1:5. Aliquots of polymeric composites (10 µL of $K_3[Fe^{III}(CN)_6]$ and

nylon-6 composite) was then added to 4 mL prepared standards of AA, DA and uric acid in four different vials. The contents were left to stand for 1 h before UV-visible absorbencies were acquired.

4.8.1.2.3 Effect of ascorbic acid, dopamine and uric acid on ferric chloride and nylon6 composite

The same protocol was followed using $FeCl_3$ instead of $K_3[Fe^{III}(CN)_6]$ to determine the effect of AA, DA, and uric acid on ferric chloride composite

4.8.1.3 Nylon6, ferric chloride and ferricyanide composite electrospinning conditions

The composite of $FeCl_3$, $K_3[Fe^{III}(CN)_6]$ and nylon6 was electrospun at a voltage of 21 kV, flow rate of 0.5 mL/h and a working distance of 12 cm.

4.8.1.4 Colorimetric detection of ascorbic acid and dopamine by Nylon6, ferric chloride and ferricyanide based test strip

The colorimetric response of the test strip was evaluated in 1.76 $x10^5$ mg L^{-1} AA and 1.89 $x10^5$ mg L^{-1} DA standards pH ranges 2-7. The response of other species like the saccharides, amino acids, and organic acids that may co-exist with either ascorbic acid or dopamine in biological samples were also evaluated. The interferences evaluated include glucose, fructose, sucrose, benzoic acid, citric acid, oxalic acid, analine, aspartic acid, lysine, glutathione, sodium sulphite, calcium chloride, sodium chloride.

4.8.2 Soluble prussian blue (Turnsbull's pigment) based test strip

4.8.2.1 Synthesis of soluble prussian blue polymeric composite (Turnsbull's pigment)

To produce prussian blue (soluble' Turnsbull's blue pigment), the same protocol was followed using ferrous sulphate ($FeSO_4$): $K_3[Fe^{III}(CN)_6]$ mass in the ratios 3:2.

4.8.2.2 Solution studies on soluble prussian blue polymer composite

4.8.2.2.1 Linearity studies; effect of ascorbic acid and dopamine on soluble prussian blue polymer composite

Solution studies were carried out using prussian blue polymeric nanocomposite prior to electrospinning. A series of AA standards solutions were prepared in a concentration range of 50 mg L^{-1} - 200 mg L^{-1}. The standards were prepared in water and acetic acid/formic acid (V/V =1:1). The ratio of water: acetic acid/formic acid was 1:5. Aliquots of prussian blue polymeric composite (20 µL) was then added to 4 mL AA of different concentrations. The same protocol was followed for DA using 10 µL prussian blue polymeric composite instead of 20 µL. Absorbance of Prussian blue was monitored every 15 min for 60 min using a 200 mg L^{-1} AA and DA standards at a maximum wavelength of 690 nm. It was observed that absorbance for DA increased for the first 45 min and remained stable after 60 min and decreased within the first 15 min for AA and remained stable for 1 h. Therefore all nanocomposite absorbance were carried out at 690 nm after 1 h.

4.8.2.3 Soluble prussian blue composite electrospinning conditions

The prussian blue composite was electrospun at a voltage of 21 kV, flow rate of 0.5 mL/h and at a working distance of 12 cm.

4.8.2.4 Colorimetric detection of ascorbic acid and dopamine by soluble prussian blue strip

The same protocol for the detection of AA and DA by Nylon6, ferric chloride and ferricyanide based test strip was followed; refer to section 4.7.1.4 for details.

4.9 ASCORBIC ACID AND DOPAMINE TEST STRIP BASED ON POLY(VINYLBENYLCHLORIDE) ELECTROSPUN FIBRE FUNCTIONALISED WITH FE(III) - 2-(2′-PYRIDYL)-IMIDAZOLE

4.9.1 Synthesis

4.9.1.1 Synthesis of the 2-(2′-pyridyl)-imidazole

The ligand 2-(2′-pyridyl)-imidazole (PIMH) was prepared following the procedure Gerber *et.al*. [191]. Briefly 10.70 g of pyridine-2-aldehyde was weighed in 10 mL ethanol. The solution was then mixed with 20 mL of a 40% aqueous glyoxal solution in a round bottom flask stirring over ice. This was followed by addition of 30 ml ice cold 20% aqueous ammonia. The yellow solution thus obtained was left to stir under ice for 30 min, and then allowed to stand overnight at room temperature. Ethanol was boiled off followed by liquid-liquid extraction with 50 mL aliquots of diethyl ether. The ether was evaporated using a rotary evaporator and the yellow solid crystals thus obtained were recrystallised from ethyl acetate. Scheme 4.1 summarises the synthetic procedure for PIMH.

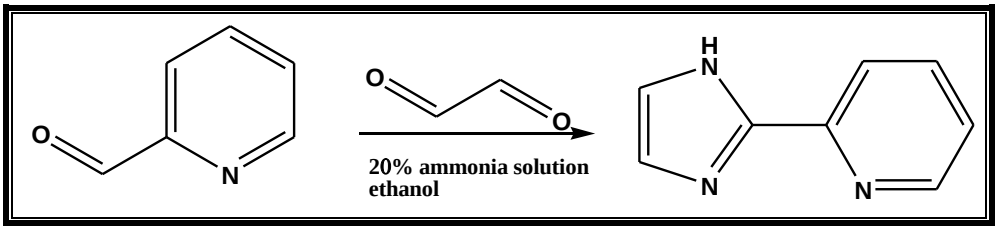

Scheme 4.1: Synthesis of 2-(2′-pyridyl)-imidazole

4.9.1.2 Synthesis of poly(vinylbenyl chloride)

Bulk polymerisation of the monomer 4-vinylbenzylchloride was achieved by using excess (0.04g, 0.19) azobisisobutyronitrile (AIBN) as the initiator in a stoppered flask. The mixture

was heated overnight at 70 ˚C. The obtained polymer was precipitated with methanol, filtered and air dried. The synthetic procedure for poly(vinylbenyl chloride) (PVBC) is summarised in scheme 4.2.

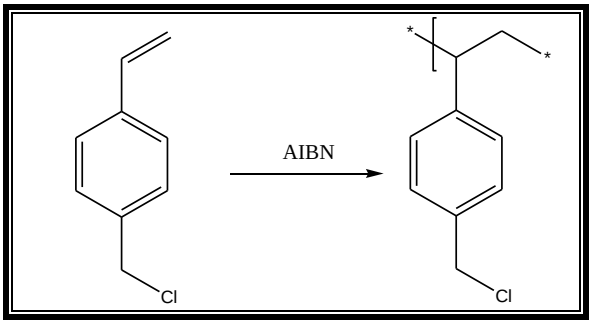

Scheme 4.2: polymerisation of 4-vynl benzyl chloride

4.9.2 Preparation of Fe(III) - 2-(2′- pyridyl)-imidazole complex

Fe(III) (0.0003 moles) and PIMH (0.0001 moles) in the ratio 1:3 were dissolved in 30ml EtOH: H_2O $(V/V = 10:20)$.

4.9.3 Linearity studies; Effect of ascorbic acid and dopamine on iron(III) - 2-(2′-pyridyl)-imidazole complex

The stock and working solution of AA were prepared every day. A series of AA standards solutions were prepared in a concentration range of 1.76 $x10^5$ mg L^{-1}-17.6 mg L^{-1}. 500 µL Fe(III)-PMIH reagent was then added to 3 mL AA of different concentrations. Colour change was observed immediately and absorbances were carried out at 730 nm after 10 min. The same protocol was followed for DA using 100 µL Fe(III)-PMIH reagent instead of 500 µL Fe(III)-PMIH. A blue colour was observed immediately for DA.

4.9.4 Optimisation of pH for iron(III) - 2-(2′-pyridyl)-imidazole complex

Fe(III)-PMIH moles in the ratio 1:3 were prepared at pH range from 2 to 7. UV-vis spectrospcopic measurements of each solution were taken.

4.9.5 poly(vinylbenyl chloride) electrospun fibres synthetic procedures

PVBC was dissolved in DMF: THF 1:1 to make a 40% solution and was left to stir overnight.

4.9.6 Electrospinning conditions for poly(vinylbenyl chloride)

The polymer was electrospun at a positive voltage of 21 kV, and a flow rate of 3 mL/h. The nanofibres were collected on the grounded collector that was covered with aluminium foil at a working distance of 11 cm.

4.9.7 Post-electrospinning functionalisation of the poly(vinylbenyl chloride) electrospun fibre

A strip of fibre weighing 0.79 g was placed in a 30 mL methanol solution of 7.0 g (0.048 mol) PIMH and 4 g KOH. The contents were refluxed for 48 h and the fibre was filtered in methanol and air dried. It was then soaked in 0.15 g $FeCl_3$ dissolved in 20 mL ethanol and water 1:1 v/v for 30 min, then air dried for 3 h. Excess Fe(III) was then rinsed in ethanol. The functionalisation procedure for PVBC is summarised in scheme 4.3.

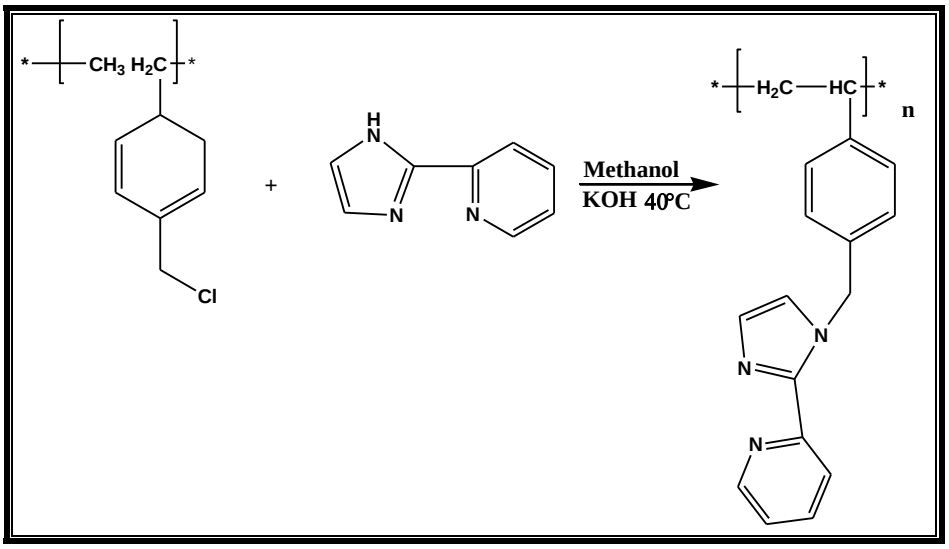

Scheme 4.3: Post functionalisation of poly(vinylbenyl chloride) with 2-(2′- pyridyl)-imidazole

4.9.8 Colorimetric detection of ascorbic acid and dopamine by poly(vinylbenyl chloride) electrospun fibre functionalised with Fe(III) - 2-(2′-pyridyl)-imidazole

A stock solution of 176 mg L^{-1} ascorbic acid was prepared in the pH range 2-7. The test strip was subsequently exposed to ascorbic acid in the standard solutions. Possible biological, foodstuff and pharmaceutical interferences were evaluated at pH 3 (pH for pharmaceuticals and fruit juices), and at a physiological pH 7. Possible interfering compounds evaluated include glucose, sucrose, fructose, benzoic acid, citric acid, maleic acid, oxalic acid, aspartic acid, lysine, glutamic acid, glutathione, sodium chloride, calcium chloride, sodium sulphite. The response for dopamine and uric acid was evaluated at the physiological pH only.

Chapter 5 RESULTS & DISCUSSION

5.1 TEST STRIP FOR ASCORBIC ACID BASED ON COPPER-GOLD ALLOY NANOPARTICLES

5.1.1 11-mercaptoundecanoic acid stabilised copper-gold nanoparticles based test strip

5.1.1.1 Solution studies on the polymeric matrix after formic acid reduction

Formic acid, like other aldehyde containing groups has been used as a reducing agent for the synthesis of NPs [192,193]. Formic acid simultaneously reduced copper and gold in the polymeric matrix. The simultaneous reduction of Cu and Au in the same solution resulted in the formation of Cu-Au alloy NPs as illustrated in Fig. 5.1 [189,194]

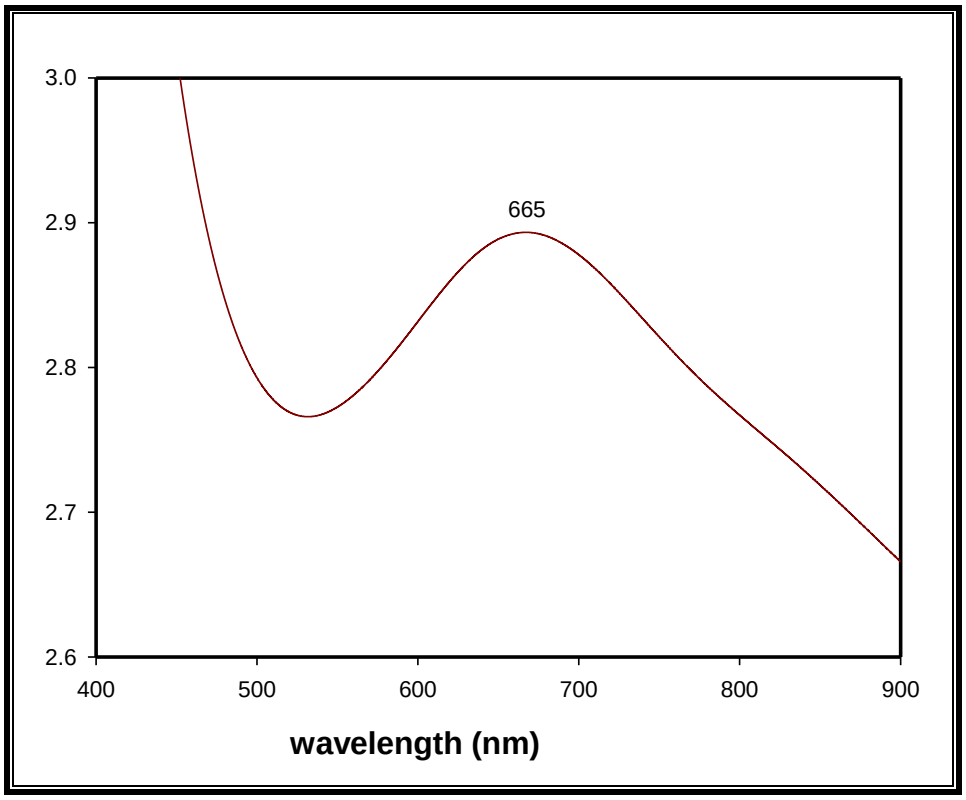

Figure 5.1: UV-visible absorption spectra of gold-copper alloy nanoparticle

The alloy formation was concluded from the fact that the optical absorption spectrum shows only one peak at 665 nm. Two bands would have been expected as demonstrated in Fig. 5.2 in case of a mixture of AuNPs and CuNPs [195,196]. A single band spectra cannot be obtained either due to a simple physical mixture of monometallic Au and Cu colloidal dispersions or due to formation of core shell Au-Cu NPs, where there are two characteristic absorption peaks [189,194].

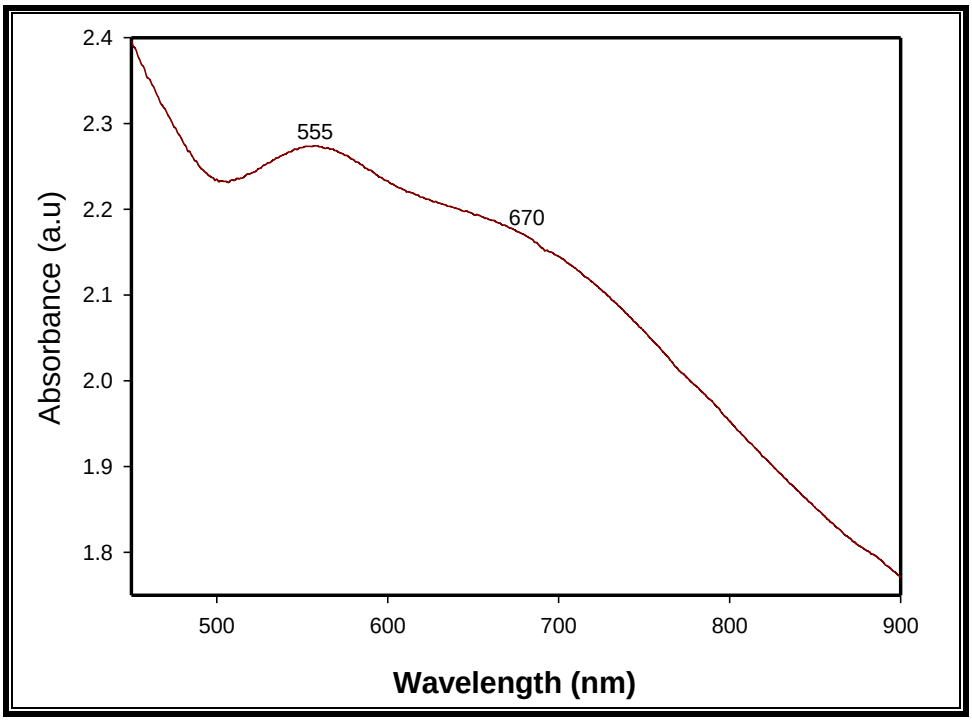

Figure 5.2: UV-visible absorption spectra showing two plasmon absorption bands originating from copper gold mixture

The absorption spectra for Au monometallic NPs, Cu-Au alloy NPs and Cu monometallic NPs are shown in Fig. 5.3. Gold exhibits an SPR at 533 nm, which is consistent with SPR of AuNPs size in the nanometre range and CuNPs exhibit an SPR at 721 nm consistent with CuNPs size in the nanometre range [161-163]. Cu-Au alloy NPs exhibit a single SPR peak at position different from either monometallic Au or Cu. The alloy SPR is at the intermediate position between pure Au and CuNPs SPR peaks and is not addative to the spectra of the pure compounds [161-163]. The TEM image of the nanocomposite of Cu-Au alloy NPs in Fig. 5.4 revealed NPs in the size range of 2-6 nm,

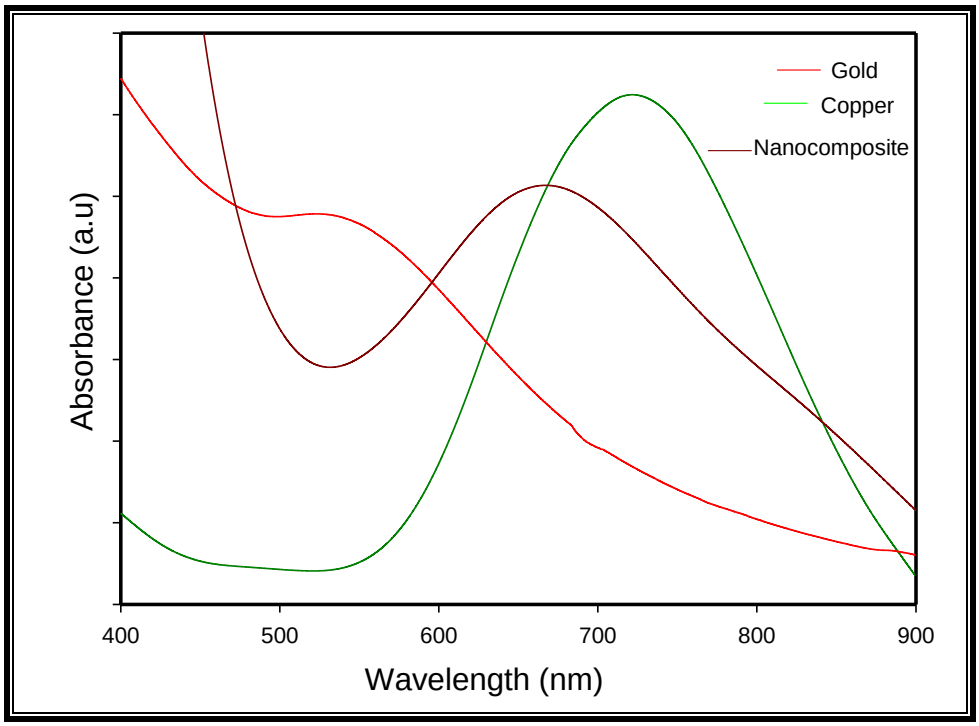

Figure 5.3: UV-visible absorption spectra for monometallic gold nanoparticles copper-gold and copper monometallic nanoparticle

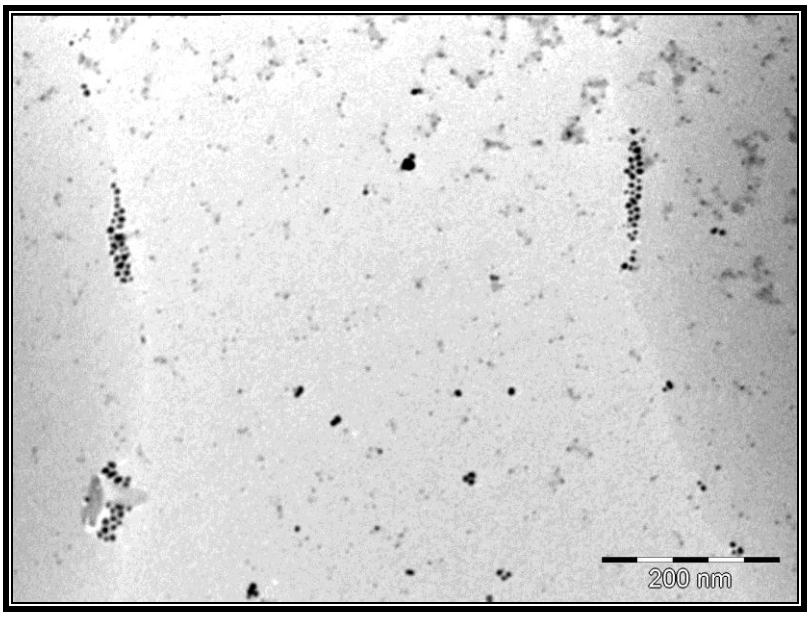

Figure 5.4: Transmission electron micrograph of the copper-gold alloy nanoparticles nanocomposite

On addition of AA to a nanocomposite of nylon-6 and the Cu-Au alloy NPs, the colour changed from green to deep blue as illustrated in Fig. 5.5.

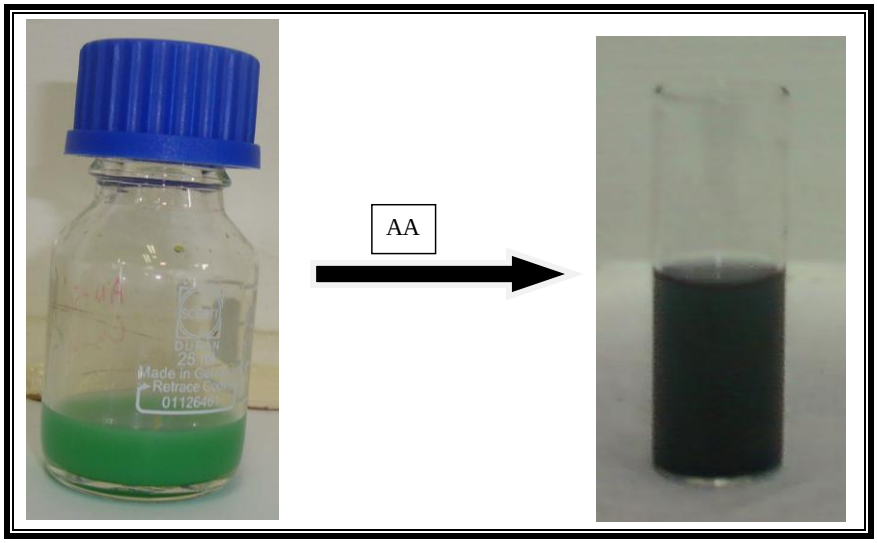

Figure 5.5: Colour change exhibited by nylon-6 and copper-gold alloy nanocomposite after addition of ascorbic acid

The UV- visible spectra of the deep blue mixture (with AA) was red shifted to 746 nm (Fig. 5.6 and 5.7). This bathochromic shift was attributed to an increase in the particle size of Cu-Au NPs [161]. Small NPs are oscillated by light in a dipole mode, light cannot polarise the nanoparticle homogeneously as it increases in size, this leads to a bathocromic shift as observed in Fig. 5.6 and 5.7 [197]. It was also observed that the absorption peak of the nano-composite without AA was relatively narrow and symmetrical, indicating a narrow size distribution of NPs. After addition of ascorbic acid, the absorption peak of the blue mixture solution broadened indicating broad size distribution. Uric acid did not cause any shift to the UV-visible spectra absorption of the mixture while the SPR after dopamine addition was featureless (Fig 5.7).

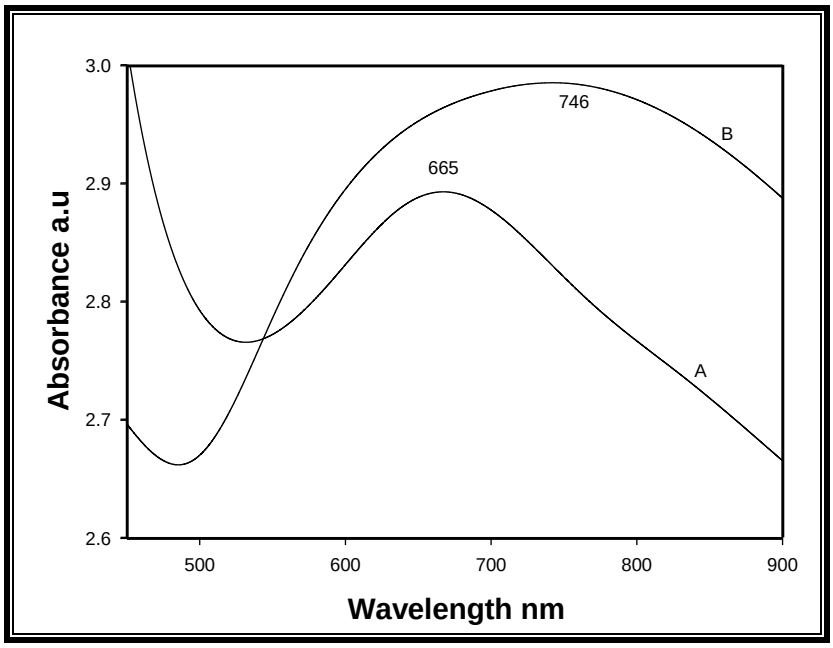

Figure 5.6: UV-visible absorption spectra of copper-gold alloy nanocomposite and the nanocomposite with ascorbic acid

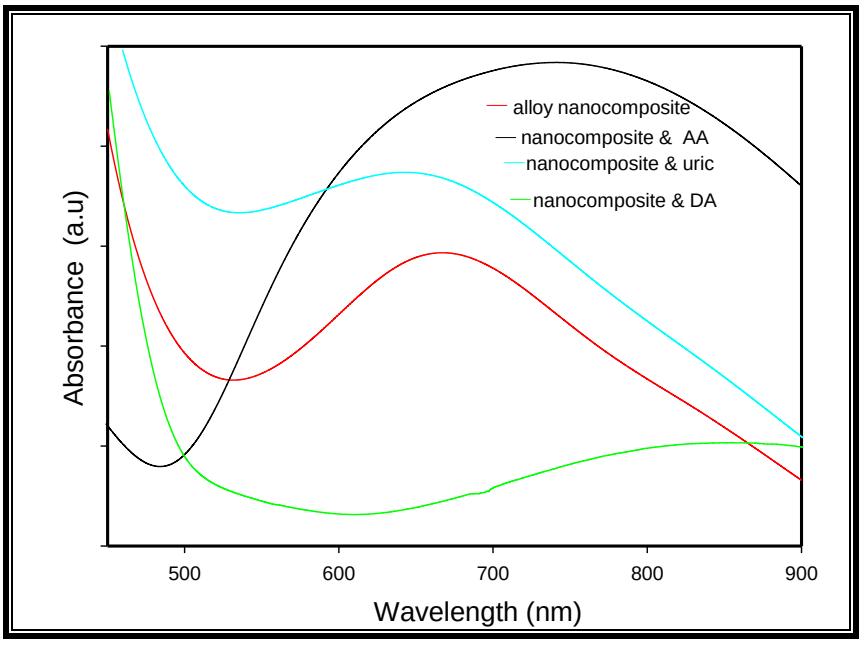

Figure 5.7: UV-visible absorption spectra of copper-gold alloy nanocomposite, the nanocomposite with ascorbic acid, the nanocomposite with uric acid and the nanocomposite with dopamine

The bathochromic shift by AA demonstrated a good agreement with the TEM images of the alloy particles shown in Fig. 5.8. It was observed that the particles were larger and showed core-shell structures (Fig. 5.8 insert). The core was attributed to the crystalline metal particles and the shell was related to the surfactant [72]. AA thus induced the growth of the NPs as well as its stabilization giving rise to the core shell.

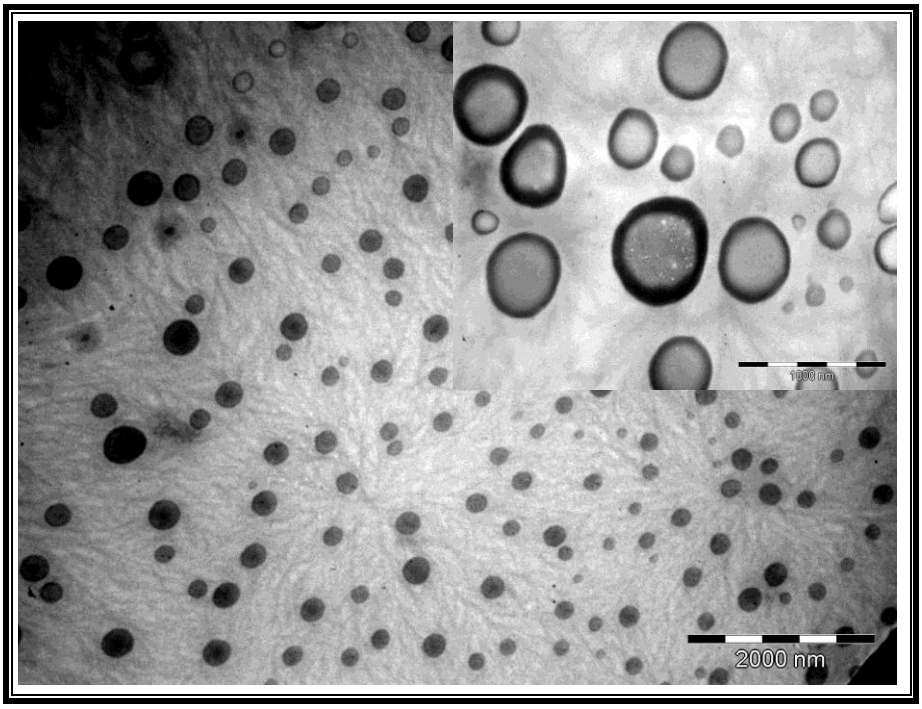

Figure 5.8: Transmission electron micrographs of copper-gold alloy nanoparticles in a polymer matrix after addition of ascorbic acid

The polymeric matrix nanocomposite formed by formic acid was further reduced with $NaBH_4$. Reduction by $NaBH_4$ involves the hydrolysis of the borohydride accompanied by the evolution of the hydrogen gas as shown in equation 5.

$BH_4^- + 2H_2O \rightarrow BO_2^- + 4H_2$ .....eqn 5

The general mechanism for particle growth has been studied and reported in detail [17-21]. The most accepted mechanism suggests a two-step process, i.e. nucleation and then successive growth of the particles. In the initial stage metal NPs are nucleated by the reduction reaction and collision between ions, atoms, and clusters to form an irreversible seed. Successive growth from the metal seed NPs may be carried out in specific conditions, i.e surfactants and polymers may be used in various ratios to control the size and shape of the NPs. With addition of $NaBH_4$, the solution turned deep blue (black) and the SPR was blue shifted to 595 nm as illustrated by the UV absorption spectra in Fig. 5.9. This was the same colour observed when polymeric nanocomposite was exposed to AA. The absorption spectra of the Cu-Au seed formed by formic acid and NPs after further reduction by $NaBH_4$ are compared in Fig. 5.9. Formic acid reduced part of the metal ions in the polymeric matrix, the atoms thus formed agglomerated to form a mixture of bimetallic alloy seed and bimetallic alloy NPs. The remaining metal ions present either were adsorbed on the seed or just remained in the bulk solution. $NaBH_4$, as a strong reducing agent promotes the formation of new particles instead of particle growth and therefore suppresses nucleation hence the blue shift.

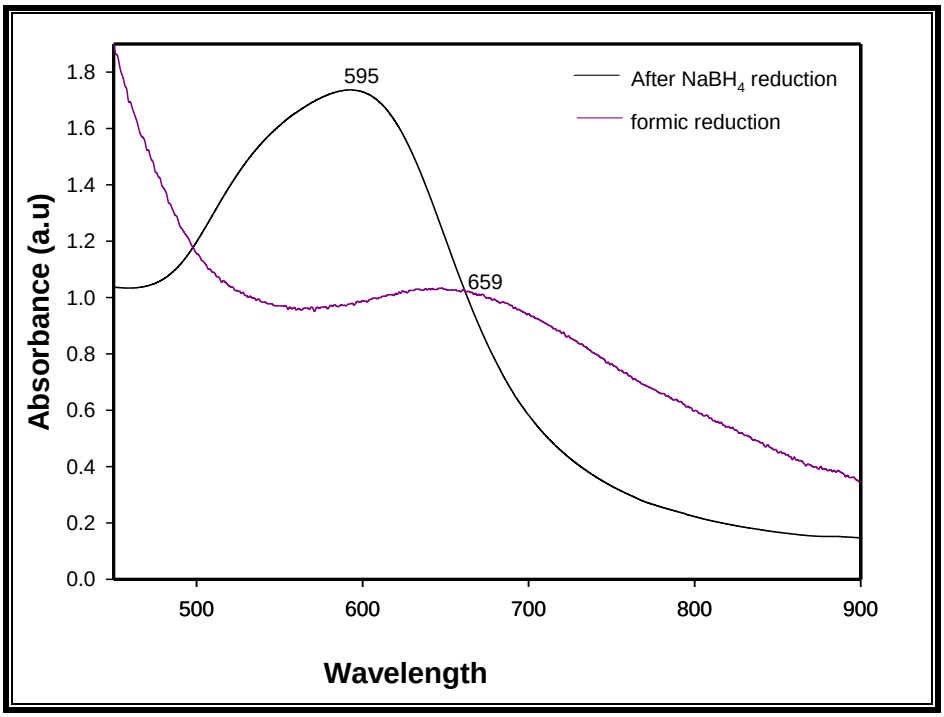

Figure 5.9: UV-visible absorption spectra of polymer matrix after reduction with formic and after reduction with sodium borohydride

Figure 5.10 (A-G SPR absorbances) shows that absorbance corresponding to the plasmon of NPs intensified as the concentration of AA increased linearly range from 100 mg L^{-1} to 400 mg L^{-1} (Fig. 5.11). The bathochromic shift and broadening of the SPR evident in Fig. 5.10 was attributed to the reduction of Cu-Au ions on the seed/ nucleation centre by AA and subsequent growth of the NPs.

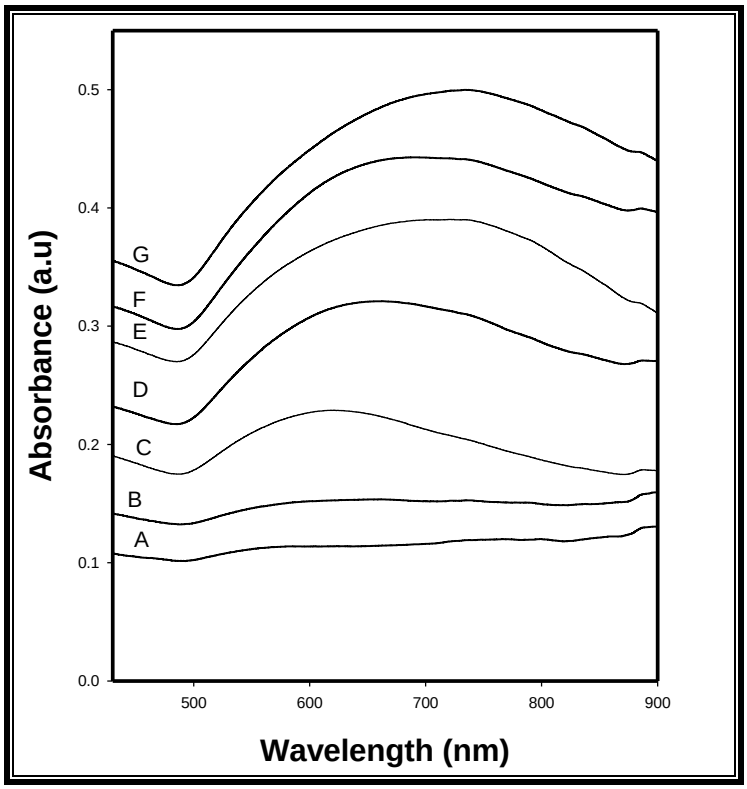

Figure: 5.10: The different plasmon absorbance graphs for copper-gold nanoparticles at 730 nm for different concentrations of ascorbic acid

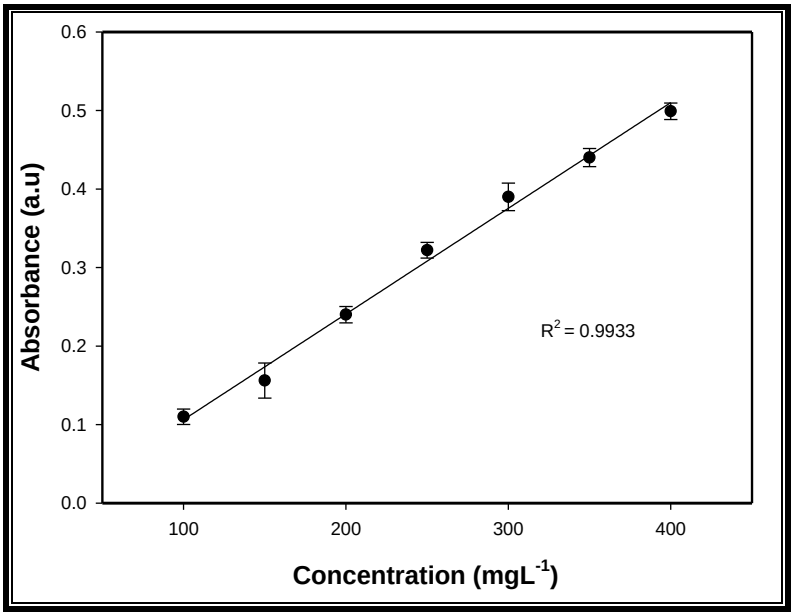

Figure: 5.11: The linear relation of plasmon absorbance of copper-gold nanoparticles at 730 nm for different concentrations of ascorbic acid

Investigations for possibility of analyte induced aggregation of NPs were extended to the solid support (nanofibre).

5.1.1.2 Investigations on 11-mercaptoundecanoic acid stabilised copper-gold test strip

The alloy formation on a solid support (nanofibre) was further confirmed by x-ray photoelectron spectroscopic (XPS) analysis. The binding energy (E_B) for Au $4f_{7/2}$ and $4f_{5/2}$ was located at 84 eV and 88 eV respectively as illustrated by Fig. 5.12, consistent with the gold atom while E_B for Cu $2p_{3/2}$ and $2p_{1/2}$ was found at 933 eV and 953 eV respectively as shown Fig. 5.12.

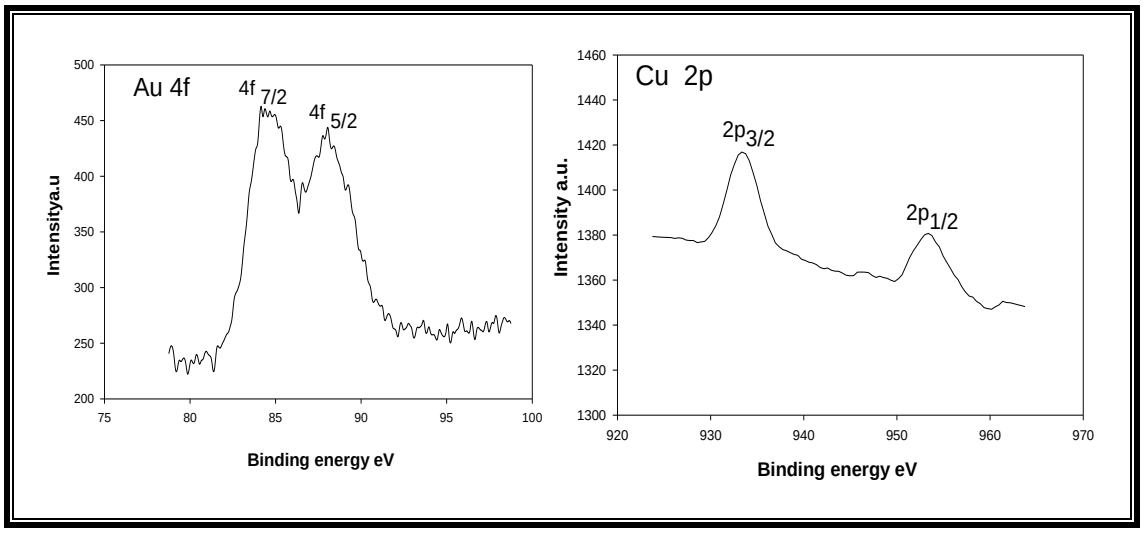

Figure 5.12: XPS spectra of Au 4F and Cu 2p

Figure 5.13 shows SEM micrographs of the electrospun nano-composite of Cu-Au alloy NPs in nylon-6. However, NPs were not visible from the micrographs of the nanofibres because there were encapsulated within the fibrous mesh.

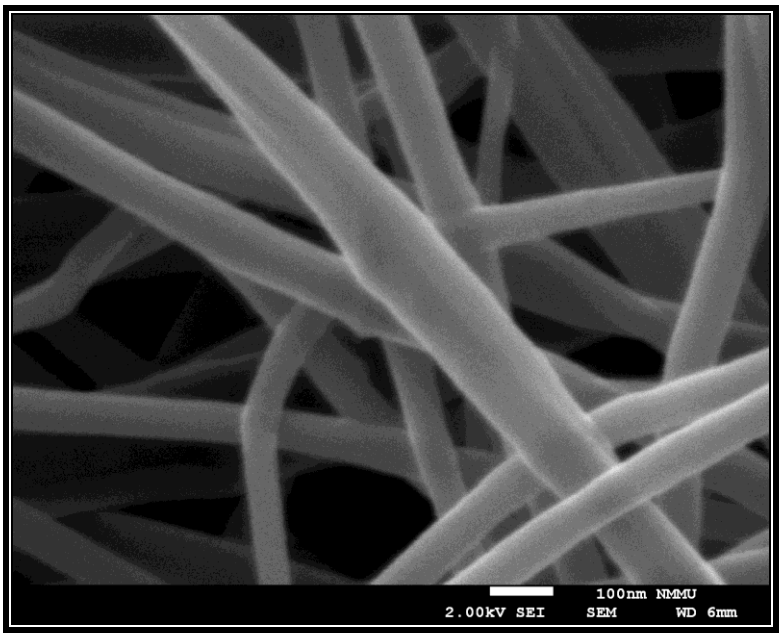

Figure 5.13: SEM micrographs of 11-mercaptoundecanoic acid stabilised copper-gold nanoparticles electrospun nanofibres from a nanocomposite of and nylon-6.

The test strip corresponding to the smooth fibre was white (Fig. 5.14). Upon interaction with AA it turned blue /black in less than 3 min in a 176 mgL^{-1} AA standard solution in the pH range of 2- 7 as shown in Fig. 5.15.

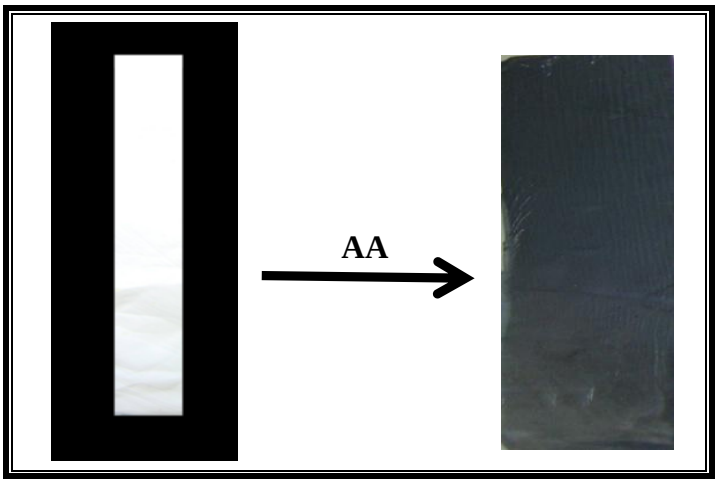

Figure 5.14: Colour change by 11-mercaptoundecanoic acid stabilised copper-gold alloy nanoparticles based test strip after interaction with ascorbic acid

Figure 5.15: Colour change exhibited by 11-mercaptoundecanoic acid stabilised copper-gold alloy nanoparticles based test strip in 176 mg L^{-1} ascorbic acid standard from pH 2-7

AA induced growth of NPs that resulted in colour change as illustrated by SEM images in Fig. 5.16. The degree of growth and subsequent colour change showed dependence on the concentration of AA. Figure 5.17 exhibits growth observed in a 1.76 mgL^{-1} ascorbic acid solution. It could be concluded from the micrograph that the lower the concentration of the analyte the smaller the degree of growth.

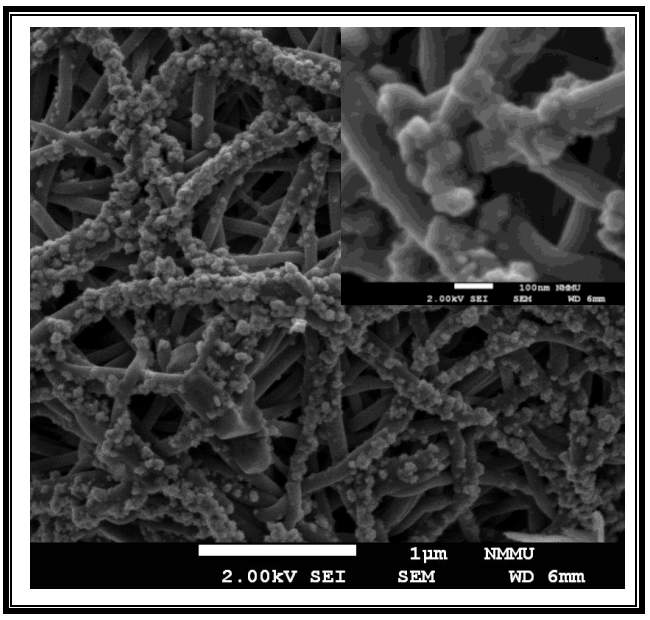

Figure 5.16: Scanning electron micrographs of 11-mercaptoundecanoic acid stabilised copper-gold alloy nanoparticles based test strip in 1.76 x10^5 mg L^{-1} ascorbic acid

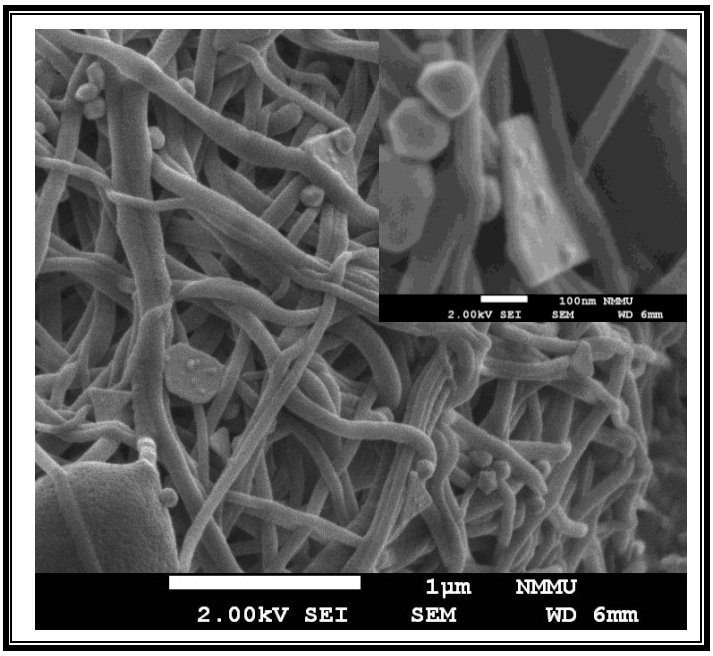

Figure 5.17: Scanning electron micrographs of 11-mercaptoundecanoic acid stabilised copper-gold alloy nanoparticles based test strip in 1.76 mg L^{-1} ascorbic acid

The possible interfering compounds evaluated could not show the same colour change observed for AA at the same concentration and pH. Among the interfering candidates evaluated, aspirin and oxalic acid showed some pink response after 30 min at pH 3 (Fig. 5.18). At pH 7, the colorimetric test strip remained white as shown in Fig. 5.19 and Fig 5.20. in all the compounds evaluated, however oxalic acid gave a purple response after 30 min. Even though glucose has been used for the reduction of metal ions to synthesise NPs, it could not reduce metal ions in a polymeric matrix at room temperature.

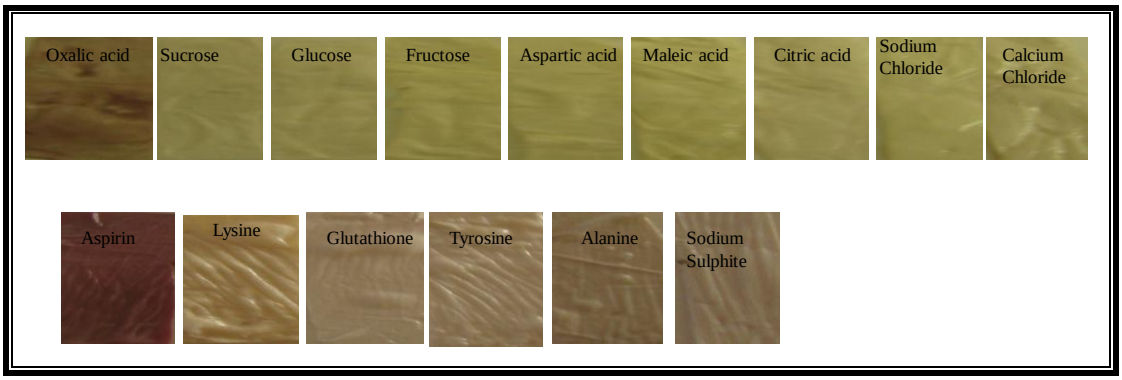

Figure 5.18: 11-mercaptoundecanoic acid stabilised copper-gold alloy nanoparticles based test strip after exposure to oxalic acid, sucrose, glucose, fructose aspartic acid, maleic acid, citric acid, sodium chloride, calcium chloride aspirin, lysine, glutathione, tyrosine , alanine, and sodium sulphite at pH 3

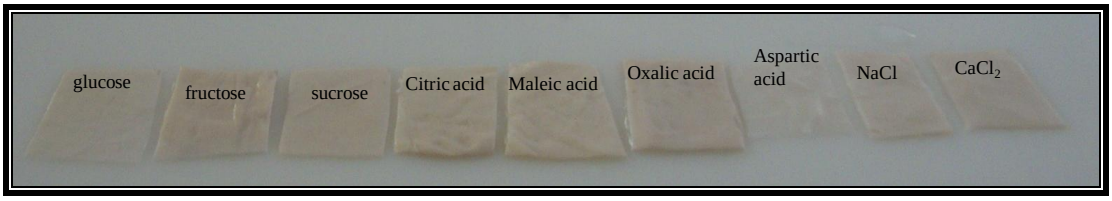

Figure 5.19: 11-mercaptoundecanoic acid stabilised copper-gold alloy nanoparticles based test strip after exposure to oxalic acid, sucrose, glucose, fructose aspartic acid, maleic acid, citric acid, sodium chloride and calcium chloride at pH 7

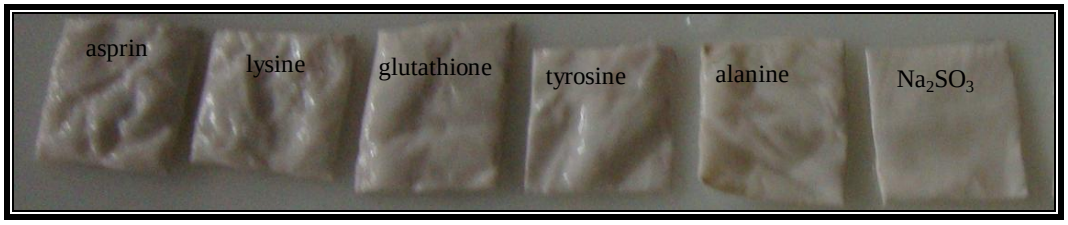

Figure 5.20: 11-mercaptoundecanoic acid stabilised copper-gold alloy nanoparticles based test strip after exposure to aspirin, lysine, glutathione, tryosine, alanine and sodium sulphite at pH 7

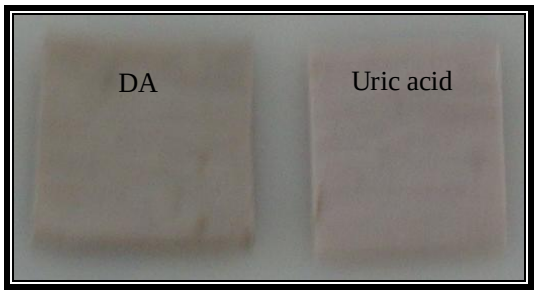

Figure 5.21: 11-mercaptoundecanoic acid stabilised copper-gold alloy nanoparticles based test strip after exposure dopamine and uric acid at pH 7

DA and uric acid did not cause colour change as shown on test strips in Fig. 5.21 nor did they cause aggregation of NPs on the nanofibre as evident in Fig.5.22.

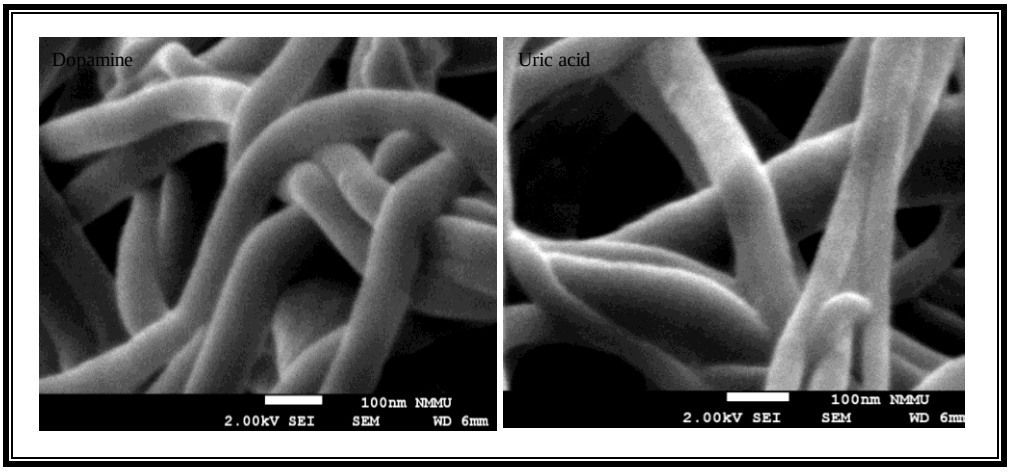

Figure 5.22: Scanning electron micrograph of 11-mercaptoundecanoic acid stabilised copper-gold alloy nanoparticles based test strip in: 1.89 x10^5 mg L^{-1} dopamine and 1.68 x10^5 mg L^{-1} uric acid

The growth of NPs (Fig. 5.23) and subsequent colour change was observed in a mixture of 176 mg L^{-1} ascorbic acid, 1.89 x10^5 mg L^{-1} dopamine and 1.68 x10^5 mg L^{-1} uric acid. It was then concluded that the optical response resulting from ascorbic acid was not affected by the co-existence of dopamine and uric acid. Pure copper and gold stabilised NPs could not cause

any colour change when in contact with ascorbic acid, dopamine and uric acid. It was therefore concluded that Cu-Au alloy NPs were responsible for the selective recognition of AA.

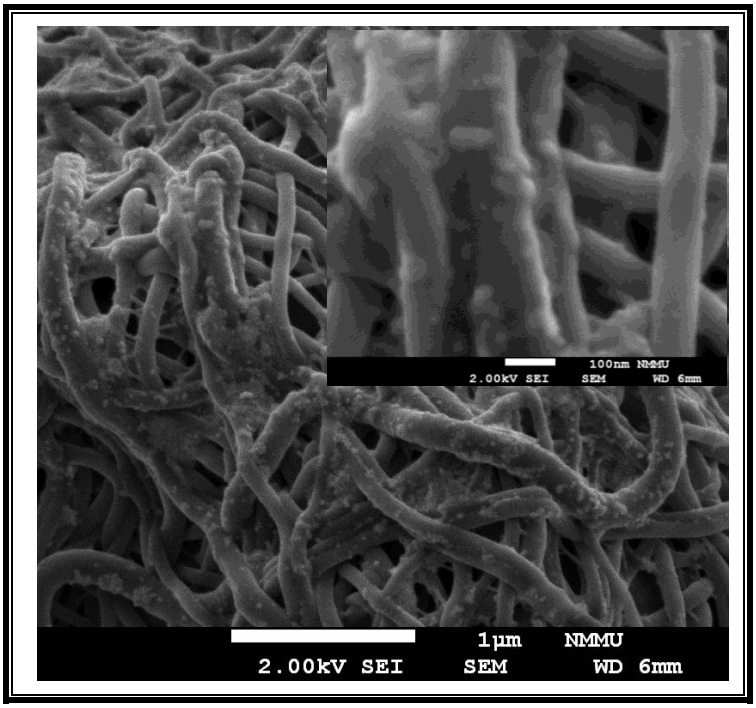

Figure 5.23: Scanning electron micrographs of 11-mercaptoundecanoic acid stabilised copper-gold alloy nanoparticles based test strip in a mixture of 176 mg L^{-1} ascorbic acid, 1.89 x10^{5} mg L^{-1} dopamine and 1.68 x10^{5} mg L^{-1} uric acid

The lowest concentration detected by the test strip was 1.76 x10^{-2} mg.L^{-1} as shown in Fig, 5.24. The response by the probe in 1.76 x10^{5} mg L^{-1} to 17.6 mg L^{-1} concentrations of AA was observed in less than 5 min comparable to that reported with the paper assay developed by Martinez et al.[17] based on HRP, glucose oxidase, and potassium iodide. Concentrations in the range 1.76 mg L^{-1} to 1.76 x10^{-2} mg L^{-1} showed a response after 1 h.

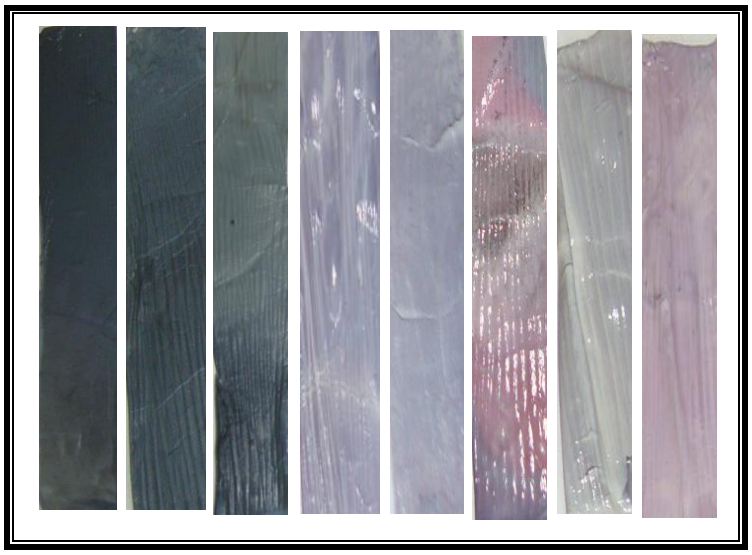

Figure 5.24: 11-mercaptoundecanoic acid stabilised copper-gold alloy nanoparticles based test strip in different concentrations of ascorbic acid from 1.76 x10^{-2} mg L^{-1} to 1.76 x10^{5} mg L^{-1}

5.1.1.3 Sensing mechanism for ascorbic acid by 11-mercaptoundecanoic acid stabilised copper-gold alloy nanoparticles based test strip

Generally metal NPs agglomerate due to high active surface area. Capping agents, that act as a steric barrier, may be introduced to the surface of a nanoparticle to prevent agglomeration. Various surfactants, polymers, dendrimers, biological templates and biomacromolecules have been used for this purpose [159].

AA is a well-known antioxidant that scavenges free radicals. AA therefore being a mild reducing agent reduced Cu-Au ions adsorbed on the Cu-Au seed, Cu-Au NPs or in the bulk and induced growth of the NPs. The porous morphology of the nanofibres permits diffusion and interaction of AA with the ions encapsulated within the polymer. The ascorbic acid diffuses to the surface of the seed or NPs where electron transfer takes place resulting in the formation of the atoms [195] and subsequently growth of the clusters to NPs. Alternatively agglomeration of MUA stabilised Cu-Au seed through hydrogen induced by AA lead to the colour change observed or both processes occurred at the same time. The mechanism resulted

in a colour change of the fibre from white to blue due to coupling of plasmons. AA showed distinct colours because; compared to DA and uric acid it has more hydrogen bond donors which are more flexible to bind to the MUA stabilised NPs.

5.1.1.4 Application of 11-mercaptoundecanoic acid stabilised copper-gold alloy nanoparticles based test strip to real samples

To confirm the practicality of the test strip for routine monitoring of AA in food, pharmaceuticals and biological samples, the test strip was applied to 15 fruit juices of three different brands with varying concentrations of AA from 132 mg L^{-1} – 450 mg L^{-1}, vitamin C tablets, 30 mg L^{-1} fortified serum samples, urine samples with AA concentrations of 200 mg L^{-1}- 1000 mg L^{-1}. The test strips confirmed the presence of AA in all samples tested. Colorimetric images of the applied strips in fruit juices, urine, serum and AA tablets, are in Figs 5.25, 5.26, 5.27 and 5.28 respectively.

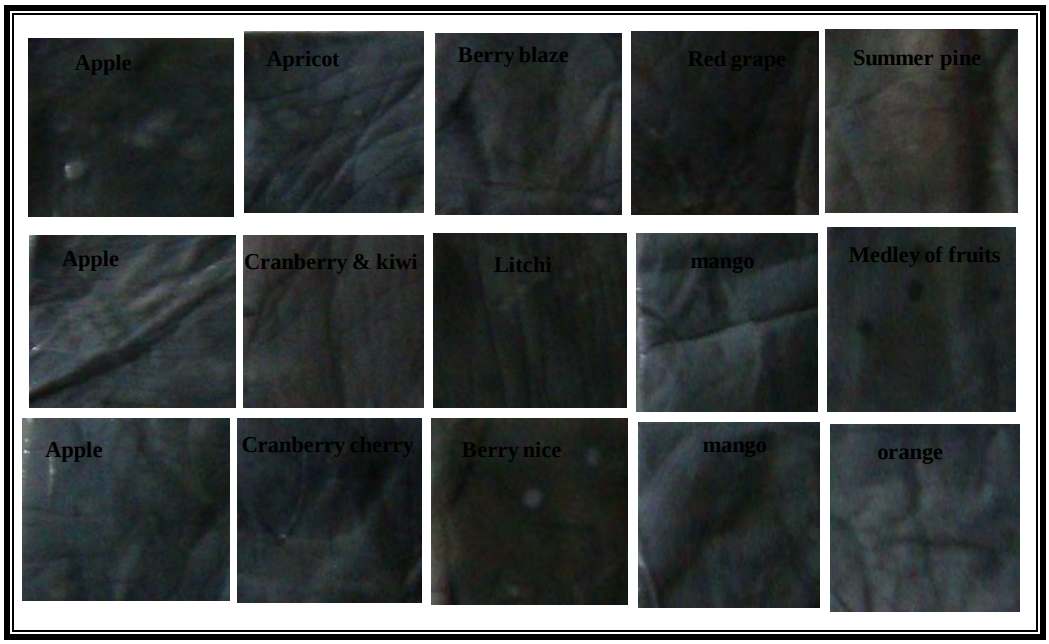

Figure 5.25: Colour change exhibited by 11-mercaptoundecanoic acid stabilised copper-gold alloy nanoparticles based test strip test strip in fifteen fruit juices of three different brands

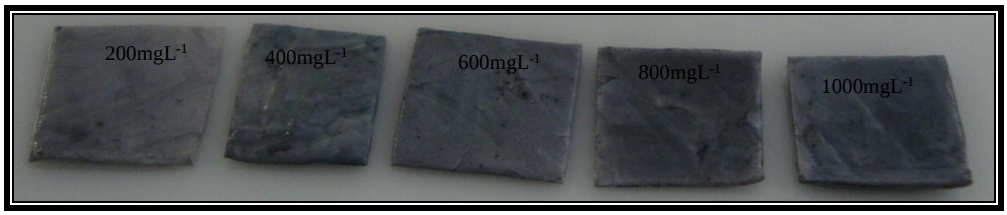

Figure 5.26: Colour change exhibited by 11-mercaptoundecanoic acid stabilised copper-gold alloy nanoparticles based test strip in ascorbic acid fortified urine samples

Figure 5.27: 11-mercaptoundecanoic acid stabilised copper-gold alloy nanoparticles based test strip in serum before and after fortification with 30mg L^{-1} of ascorbic acid

Figure 5.28: Colour change exhibited by 11-mercaptoundecanoic acid stabilised copper-gold alloy nanoparticles based test strip in ascorbic acid tablets from 1000 mg L^{-1}, 500mg L^{-1}, 250mg L^{-1}, 100 mg L^{-1} and 50mg L^{-1}

5.1.2 11-mercaptoundecanoic acid and 4-mercaptophenyl-boronic acid stabilised copper-gold alloy nanoparticles based test strip

The test strip based on MUA and MBA stabilised Cu-Au alloy NPs remained white in all the possible interferences evaluated at pH 3, however DA interfered at pH 7. The interference by DA was attributed to the stable boronate complexes formed between boronic acids from MBA and the diols in DA.

The test strip however responded well to fruit juices (pH 3-4) showing the same response as the MUA capped Cu-Au-alloy NPs test strip as depicted Fig 5.29.

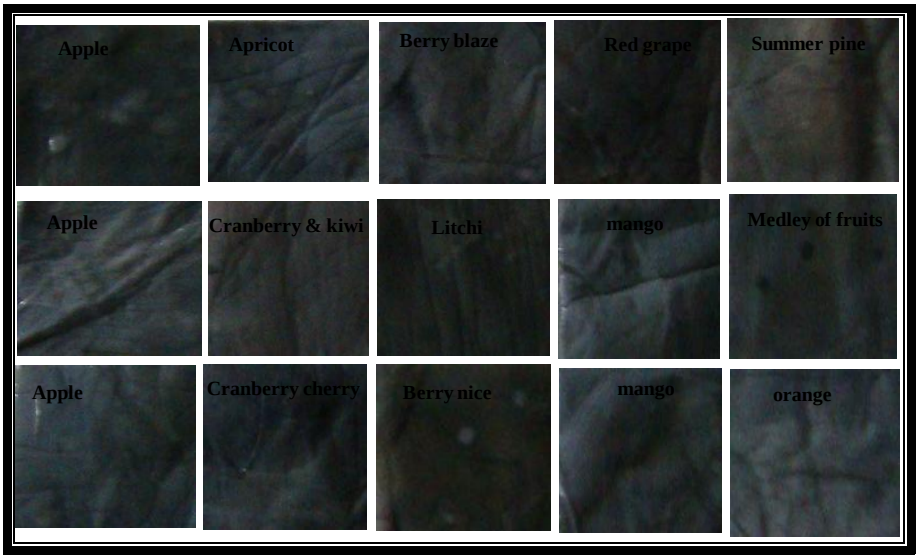

Figure 5.29: **11-mercaptoundecanoic acid and 4-mercaptophenyl-boronic acid stabilised copper-gold alloy nanoparticles based test strip in fifteen fruit juices of three different brands**

5.1.3 Polymer stabilised Cu-Au alloy nanoparticles based test strip

The white test strip, incorporated with NPs stabilised by steric hindrance, showed the same response in AA, dopamine and uric acid as the test strip with MUA stabilised NPs as observed in Fig. 5.30A and 5.30B. However, in addition to aspirin and oxalic acid, sodium sulphite also showed some pink response after 30 min at pH 3. Sodium sulphite however rarely co-exists with AA in real samples, therefore its interference is not significant. However, sodium sulphite interefence could mean that thiolated substances are potential interferences in polymer stabilised nanoparticles test strips because of the affinity of sulfur to nanoparticles. Where the polymer coverage on the NPs is incomplete the sulfur bonds to the NPs, which alters composition of the medium at the surface of the NPs and produces an SPR shift.

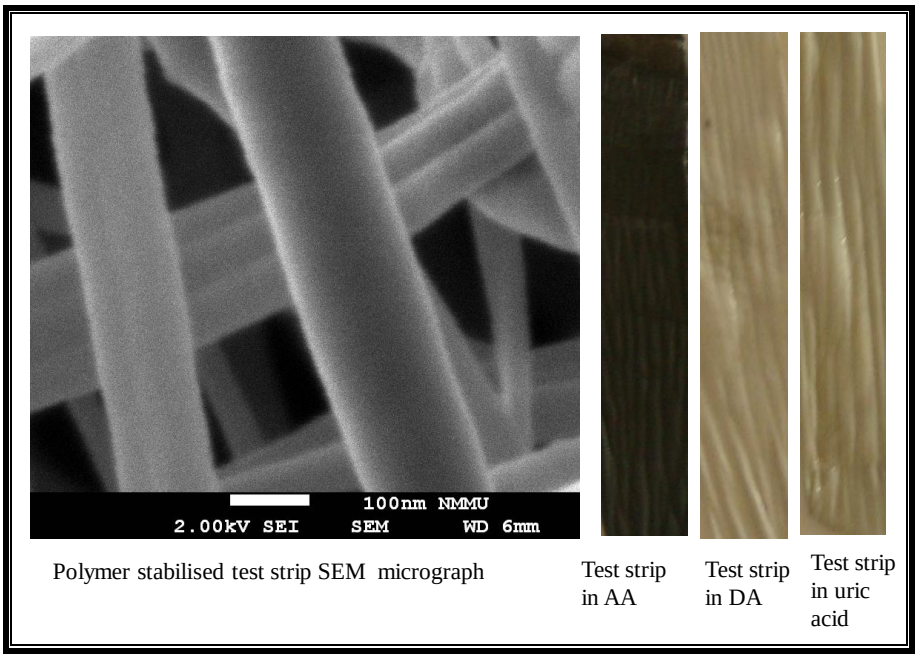

Figure 5.30: SEM micrographs of polymer stabilised test strip and colour change exhibited by the fibre in ascorbic acid, uric acid, and dopamine solutions

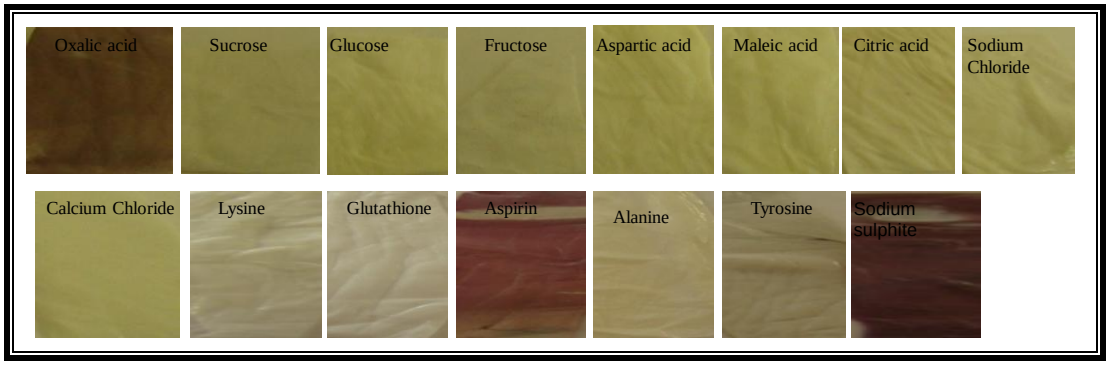

Figure 5.31: Polymer stabilised copper-gold alloy nanoparticles based test strip after exposure to oxalic acid, sucrose, glucose, fructose aspartic acid, maleic acid, citric acid, sodium chloride, calcium chloride, lysine, glutathione, aspirin, alanine, tyrosine and sodium sulphite at pH 3

AA still induced growth of the NPs that resulted in colour changes as illustrated by SEM image in Fig. 5.32 of the test strip in 1.76 $x10^{5}$ mg L^{-1} AA. It was also observed in that dopamine, uric acid and water had no effect on the polymer stabilised NPs test strip consistent with SEM data in Fig. 5.33.

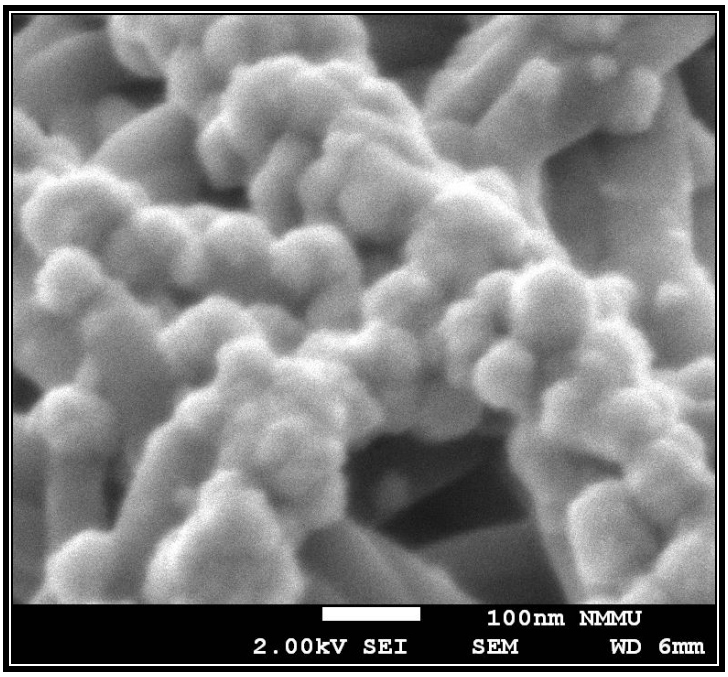

Figure 5.32: SEM micrographs of polymer stabilised copper-gold alloy nanoparticles based test strip 1.76 x10^{5} mg L^{-1} ascorbic acid

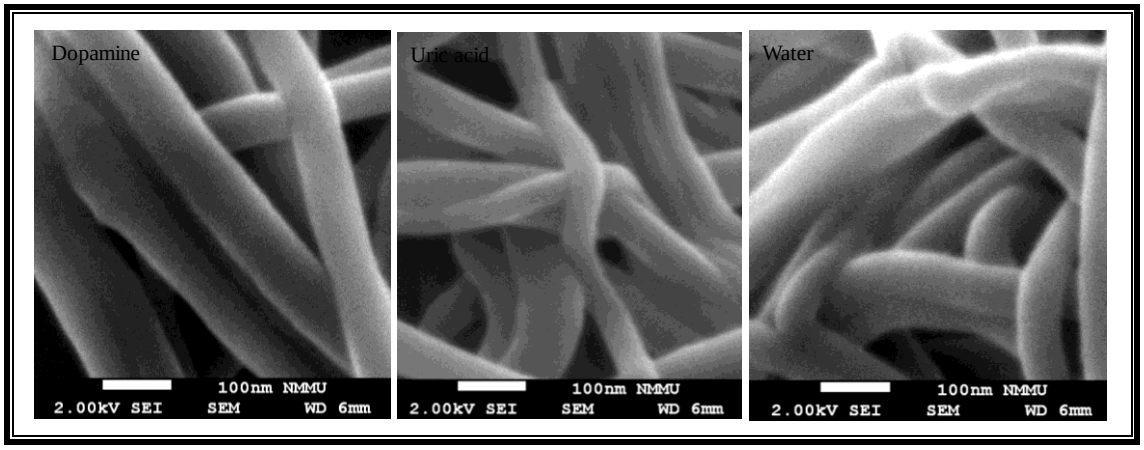

Figure 5.33: SEM micrographs of polymer stabilised copper-gold alloy nanoparticles based test strip in 1.89 x10^{5} mg L^{-1}, dopamine, 1.68 x10^{5} mg L^{-1} uric acid and water

The lowest concentration detected by the test strip was 1.76 x10^{-2} mg L^{-1}. The response by the probe in 1.76 x10^{5} mg L^{-1} to 17.6 mg L^{-1} concentrations of AA was observed in less than 5 min. The test strip responded after 1 h in the concentration range of 1.76 mg L^{-1} to 1.76 x10^{-2} mg L^{-1}.

5.1.3.1 Sensing mechanism of a polymer stabilised copper-gold alloy nanoparticles based test strip

In this approach, no surfactant was added to stabilize the NPs and to prevent them from aggregation. However, reduction occurred in nylon-6, therefore the particles were not expected to agglomerate due to steric hindrance.

As an antioxidant AA is well known to scavenge free radicals, as a mild reducing agent it can be used to reduce ions on the seed as a slower growth process is required. Therefore ascorbic acid reduces Cu-Au ions adsorbed on the Cu-Au seed or in the bulk and induces anisotropic growth of the nanoparticle. The porous morphology of the nanofibres permits diffusion and interaction of ascorbic acid with the seed encapsulated within the polymer. The ascorbic acid diffuses to the surface of the seed or NPs where electron transfer takes place resulting in the formation of the atoms [195] and subsequently growth of the clusters to nanoparticles.

5.2 EVALUATION OF THE FEASIBILITY OF A FIBRE AS A SOLID SUPPORT FOR NANOPARTICLES

5.2.1 Solution chemistry investigation on nylon6, poly(vinylbenzyl chloride-styrene) and cellulose acetate nanocomposites

A study to evaluate electrospun nanofibres as a possible host for NPs in view to their application as support material for point of use and point of care was carried out. Three polymers were employed for the study: (1) nylon6 (2) PVBC-styrene and (3) cellulose acetate. Investigations were carried out in the polymeric nanocomposites prior to test strips.

For nylon6 solution studies, section 5.1.1.1 may be referred to. Solution studies were done for PVBC-styrene and cellulose acetate alloy NPs. A narrow SPR for the PVBC-styrene and

cellulose acetate alloy NPs were observed at 450 nm and 560 nm respectively as illustrated in Figs.5.34. The results were in agreement with the TEM image of the polymeric nanocomposite in Fig 5.35 that revealed NPs of a narrow size distribution between 3-5 nm for and 3-7 nm for PVBC-styrene cellulose acetate respectively. $NaBH_4$, a fast and strong reducing agent used in both cases promoted nucleation rate thus making a high number of nuclei which resulted in reduced nanoparticles with narrow size distribution. Colour change was observed for both polymers accompanied by a blue shift in SPR after addition of AA to 570 nm and 590 nm in PVBC-styrene (Fig 5.34A) and cellulose acetate (Fig. 5.35B) respectively. TEM image revealed aggregated NPs after AA addition in both polymeric matrices. As illustrated in Figs 5.34A and 5.34B. AA induced agglomeration of MUA NPs through hydrogen bonding.

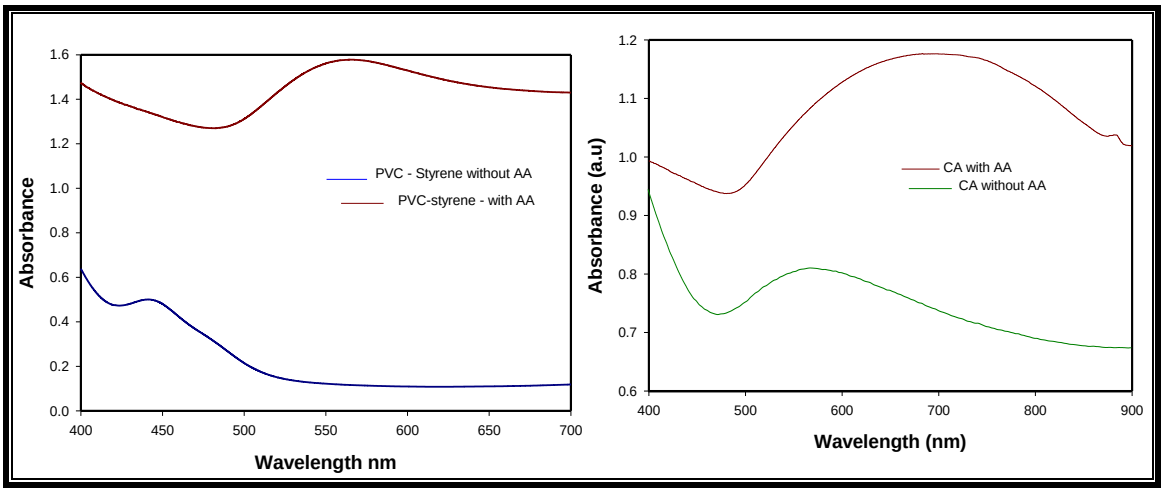

Figure 5.34: Change in UV/VIS absorption spectra of polv(vinylbenzyl chloride)-styrene before and after ascorbic acid and cellulose acetate before and after ascorbic acid

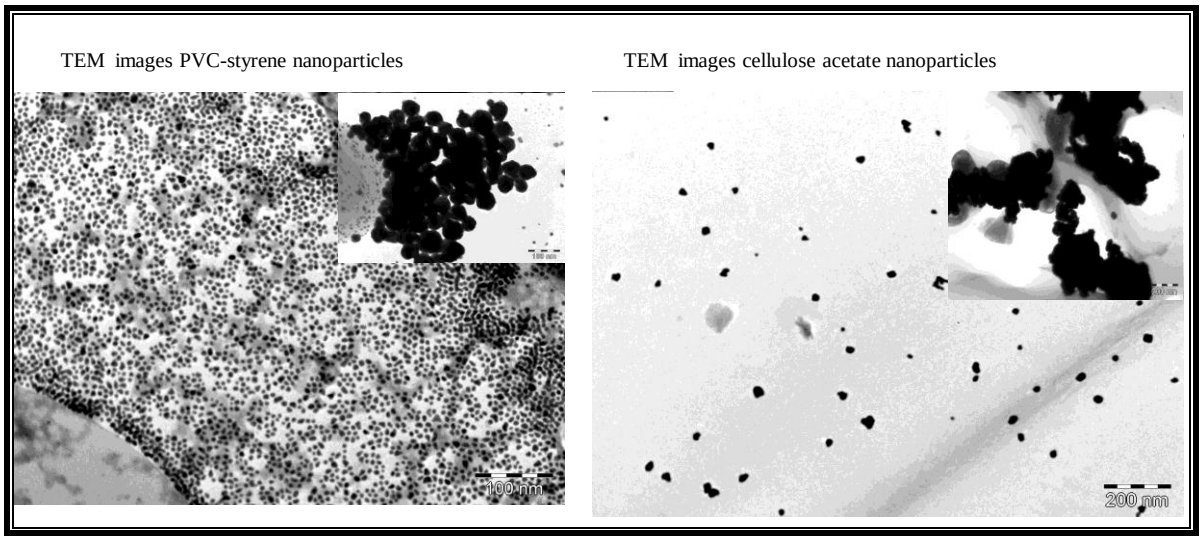

Figure 5.35: TEM images of Au-Cu alloy nanoparticles in: polv(vinylbenzyl chloride)-styrene before and after interaction with ascorbic acid and cellulose acetate before and after ascorbic acid

5.2.2 Investigations on nylon6, poly(vinylbenzyl chloride)-styrene and cellulose acetate based test strips

The test strip responded in AA inducing nanoparticle growth and subsequent colour change to blue in all polymers. Nylon6 changed from white, PVBC-styrene from pink while cellulose acetate changed from brown. The morphology of the test strips before and after interaction with the analyte as observed under SEM are shown Figs 5.36 and 5.37 PVBC-styrene and cellulose acetate respectively. For the morphology of nylon6 test strips section5.1.1.2.2 should be referred to. NPs were visible on the surface of PVBC-styrene and cellulose acetate test strips, while nylon6 appeared smooth before interaction with AA. This was because in PVBC-styrene and cellulose acetate test strips had more NPs as a result of the high nucleation rate promoted by $NABH_4$ reduction, while in nylon6 there were more Cu-Au ions due to incomplete reduction.

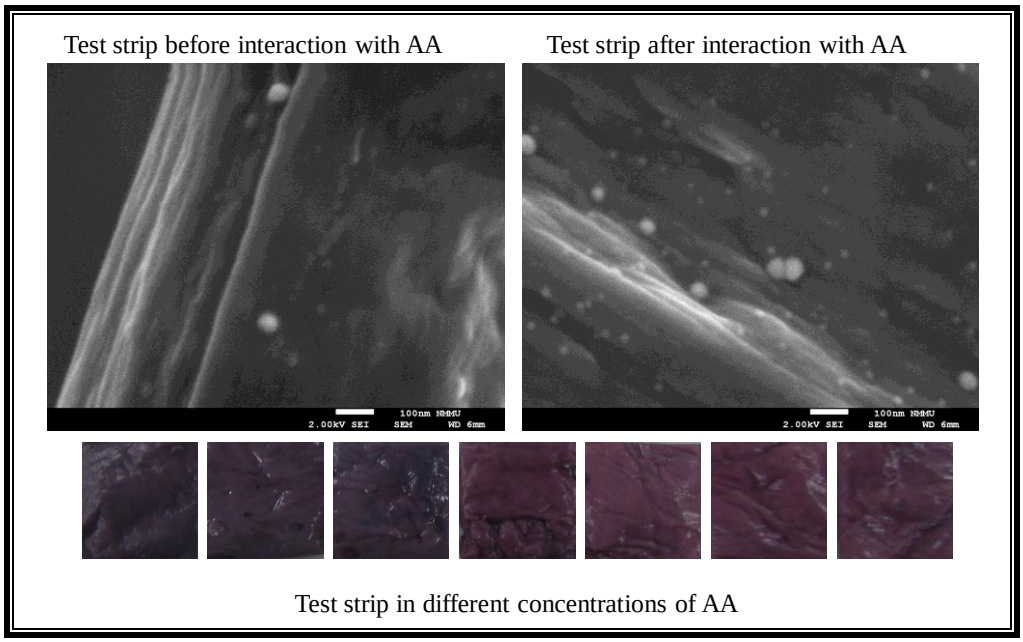

Figure 5.36: Scanning electron micrograph of poly(vinylbenzyl chloride)-styrene based test strip before after interaction with ascorbic acid and colour change exhibited by poly(vinylbenzyl chloride)-styrene based test strip in different concentrations of ascorbic acid

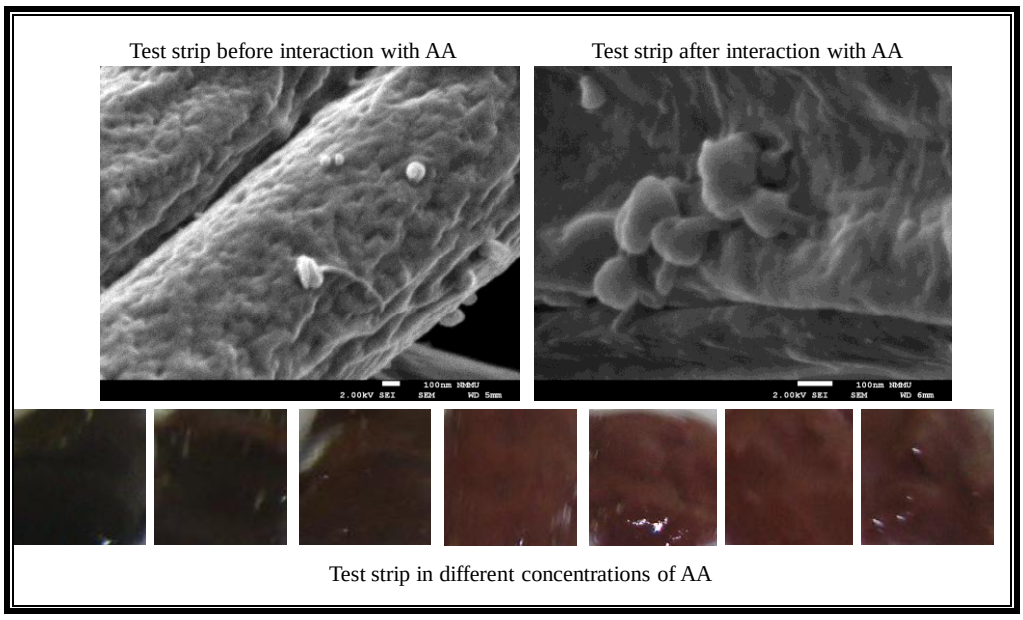

Figure 5.37: Scanning electron micrograph of cellulose acetate based test strip before after interaction with ascorbic acid and colour change exhibited by cellulose acetate based test strip in different concentrations of ascorbic acid

5.2.3 Leaching investigations on nylon6, poly(vinylbenzyl chloride)-styrene and cellulose acetate based test strips

After verifying the performance of the test strip for AA, leaching investigations were carried out. The presence of NPs in the analyte solution after interaction with the test strip was investigated. Because leaching was not obvious with naked eye detection, investigations were carried out using a UV-visible spectrometer. The absorbance at 700 nm confirmed the presence of NPs in the solutions after interaction with AA for nylon 6, cellulose acetate and PVBC-styrene test strips respectively as shown by graphs in Fig 5.38. Leaching was inevitable in these particular probes because, TEM micrographs had revealed that NPs grow on the surface of the test strip and are therefore likely to fall off into the analyte solution. Leaching could be avoided by assaying small volumes (µl) onto test strip impregnated with NPs [193] rather than immersing them in an analyte solution.

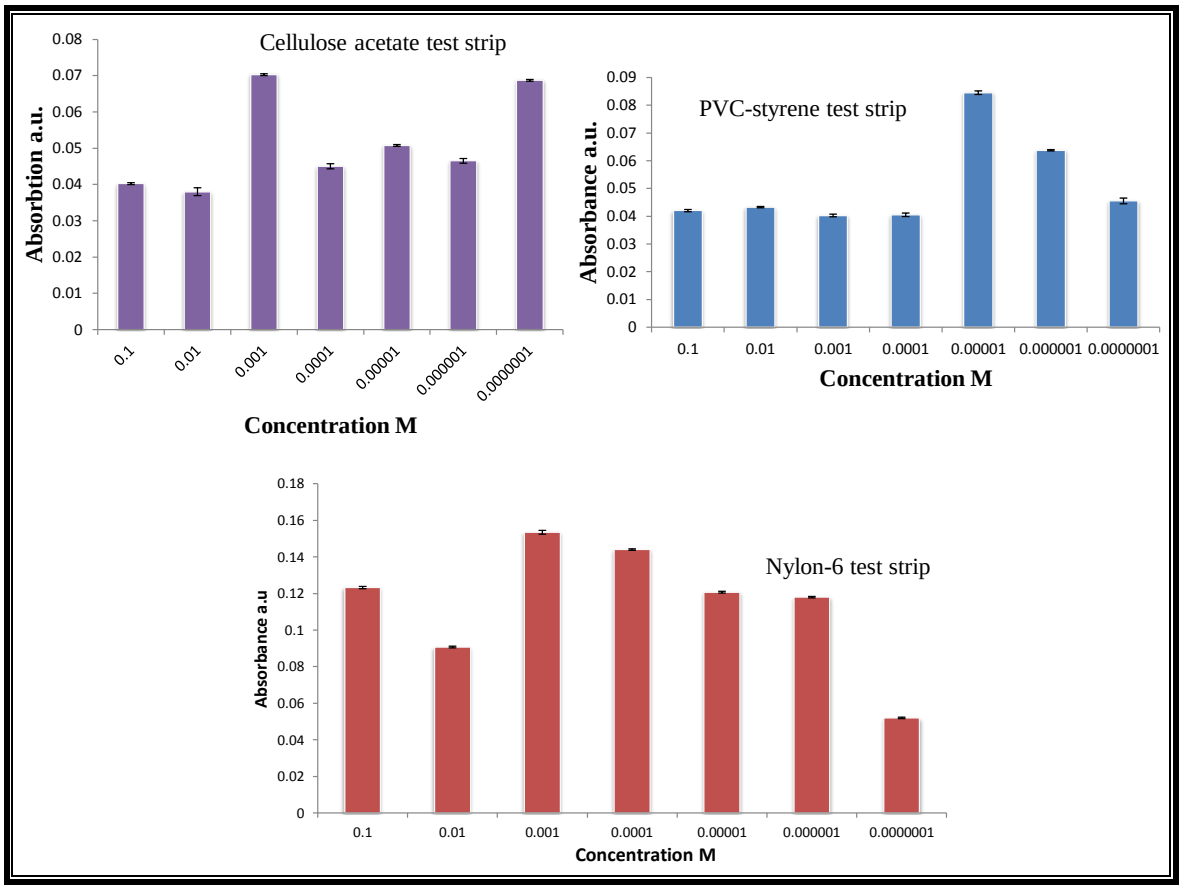

Figure 5.38: Graphs showing leaching trends in: cellulose acetate, poly(vinylbenzyl chloride) - styrene and nylon6 test strips

It was observed that leaching varied according to the polymer and the method of NPs production. Nylon6, exhibited the highest leaching compared to cellulose acetate and PVBC-styrene. It had been expected that nylon6 with amide functionalities would retain the nanoparticles due to their affinity for the amide group. However, it was observed that growth was more prominent on the surface of nylon-6 than test strips of other polymers at the same concentration of the analyte. The extent of incomplete reduction of Cu-Au ions in nylon6 during synthesis of the nanoparticles led to the high degree of growth of the nanoparticles. Polymers also impart steric hinderance (polymer barrier) that prevents nanoparticles from agglomeation. Steric stabilisation is less sensitive towards ionic strength, but the thickness of

the polymer is more effective [197]. It is therefore evident from the structures of nylon-6, cellullose acetae and PVBC-styrene in Fig. 5.39 that nylon6 exhibit less steric strain compared to others.

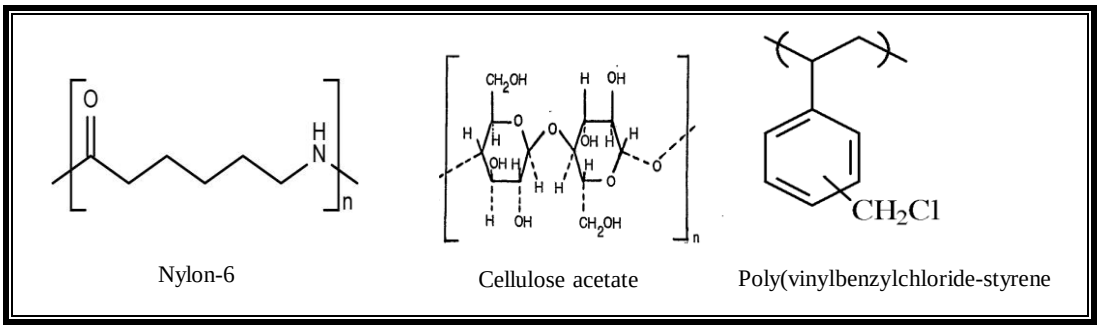

Figure 5.39: Structure of nylon-6, cellulose acetate and poly(vinylbenzyl chloride) - styrene

5.2.4 Thermally stability of nylon6 based test strip

The other parameter investigated to check the possibility of using electrospun nanofibres as support for colorimetric probes was thermal stability, however this was only investigated in nylon-6. It was observed that after heat treatment for two days at 60 ˚C, leaching did not increase, however at 80 ˚C leaching was increased. Heat treatment of the fibre at 80˚C for more than three days resulted in a colour change from white to purple test strip as an indication of agglomeration of NPs. When temperature is raised the diffusion and subsequently agglomeration of NPs is promoted [198].

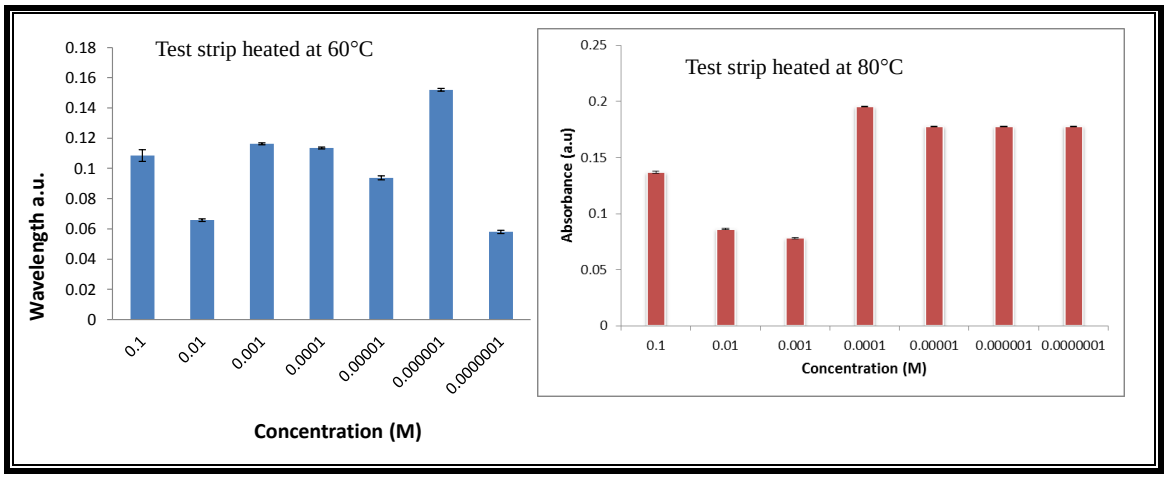

Figure 5.40: Graphs showing leaching trends after heating nylon-6 based test strip at 60°C and 80°C at 555 nm

The test strip did not lose its colorimetric detection performance after heat treatment at 60˚C for two days nor did they show colour decay suggesting their thermal stability at this temperature. Thermal stability up to 60˚C also suggests that a fibre protects the incorporated NPs from agglomeration and degradation induced by external stimuli like heat. The performance of the test strip was evaluated in fruit juices, pharmaceuticals and urine after long term storage and it still functioned well ten months after production. Even after ten months of storage in a locker the fibres did not show colour decay. For the application of nylon6 test strips to real samples refer to section 5.1.1.4.

Because AA and DA co-exists in real biological samples, the development of simple detection methods for their detection without trading sensitivity and selectivity for diagnostics, pharmaceutical and food industry is also a necessity. Therefore two colorimetric test strip based on (1) Prussian blue incorporated in an electrospun nylon6 fibre (2) poly(vinylbenyl chloride) electrospun fibre functionalised with Fe(III) - 2-(2′-Pyridyl)-imidazole that are capable of detecting either AA or DA without the interference of the other

were developed. Prussian blue based test strip for the detection of either AA or DA is discussed in the section that follows.

5.3 PRUSSIAN BLUE BASED TEST STRIP FOR ASCORBIC AND DOPAMINE

5.3.1 nylon6, ferric chloride and ferricyanide based test strip for ascorbic acid and dopamine

5.3.1.1 Solution studies on nylon6, ferric chloride and ferricyanide polymeric matrix

The composite of the polymer and the iron salts (Ferric chloride and potassium ferricyanide) exhibited some yellowish colour as shown in Fig.5.41. A colour change to blue was observed as shown in Fig. 1E, when dopamine and ascorbic acid were added to the composite indicating the formation of prussian blue. Uric acid initially formed prussian green, which gradually turned blue. The visible colour changes were attributed to the ability of DA, AA and uric acid to reduce Fe^{III} to Fe^{II} which in turn reacted with Fe^{III} to form prussian blue ($Fe^{III}_4[Fe^{II}(CN)_6]_3$).

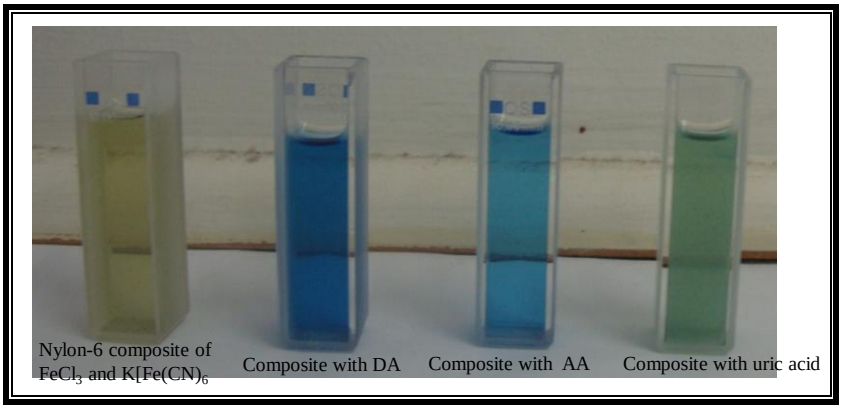

Figure 5.41: Colour changes exhibited by: nylon6 composite of ferric chloride and ferricyanide, the composite with dopamine, the composite with ascorbic acid and the composite with uric acid

The UV-visible spectra of the composite of nylon 6, $FeCl_3$ and $K_3[Fe^{III}(CN)_6]$ in Fig. 5.42A showed a very weak absorption around 700 nm. However a very sharp peak was observed around 710 nm (Fig 5.42B-D), typical of prussian blue after the addition of DA, AA and uric acid to the composite of nylon 6, $FeCl_3$ and $K_3[Fe^{III}(CN)_6]$. The absorption around 710 nm was due to the inter-metal charge transfer band from Fe^{2+} to Fe^{3+} in prussian blue particles [199].

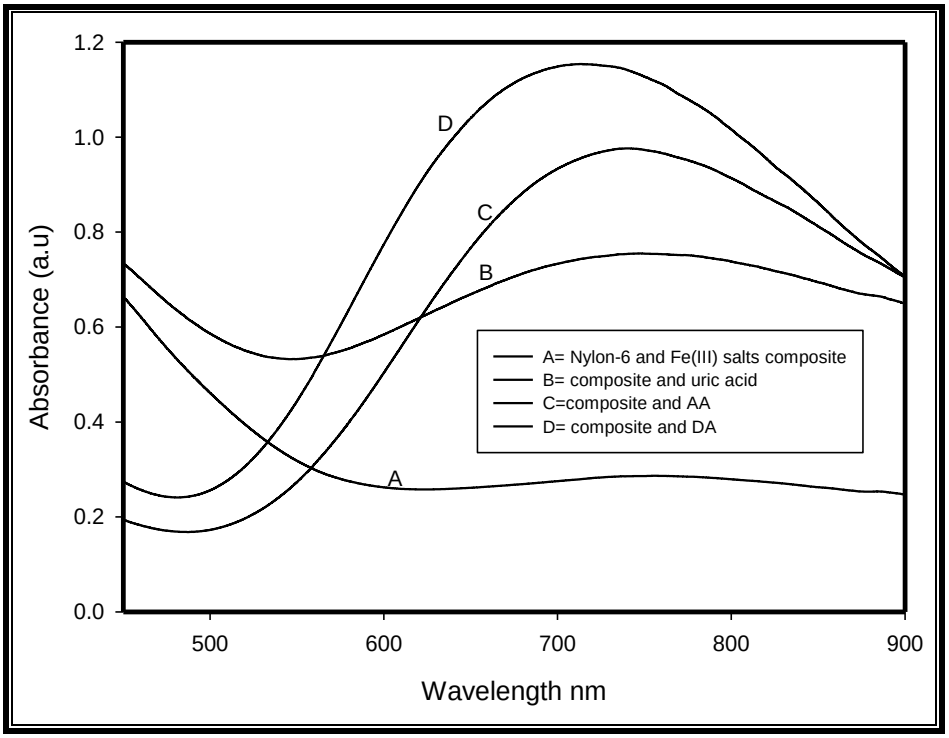

Figure 5.42: UV-visible spectra of ferric chloride and ferricyanide and polymer composite, the composite with ascorbic acid, the composite with dopamine and the composite with uric acid

AA donates an electron to the $K_3[Fe^{III}(CN)_6]$ metal centre and forms $K_4[Fe^{II}(CN)_6]$ which in turn reacts with $FeCl_3$ to produce an insoluble Prussian blue. To confirm that it was $K_3[Fe^{III}(CN)_6]$ reduced instead of $FeCl_3$, the UV-visible absorption spectra of the composite

of nylon 6 and $K_3[Fe^{III}(CN)_6]$ was acquired as in Fig. 2. The composite exhibited a very weak absorption band around 650 nm, upon addition of DA, uric acid and AA a sharp absorption band around 650 nm was observed. The peak was due to ligand to charge transfer from the auxochrome found in ascorbic acid and dopamine to reduce $K_3[Fe^{III}(CN)_6]$ to $K_4[Fe^{II}(CN)_6]$. The reduced $K_4[Fe^{II}(CN)_6]$ reacted with $FeCl_3$ to form insoluble Prussian blue as summarised in eqn 6.

$$4FeCl_3 + 3K_3[Fe^{II}(CN)_6] \rightarrow Fe^{III}_4[Fe^{II}(CN)_6]_3 + 9KCl \quad \text{.....eqn 6}$$

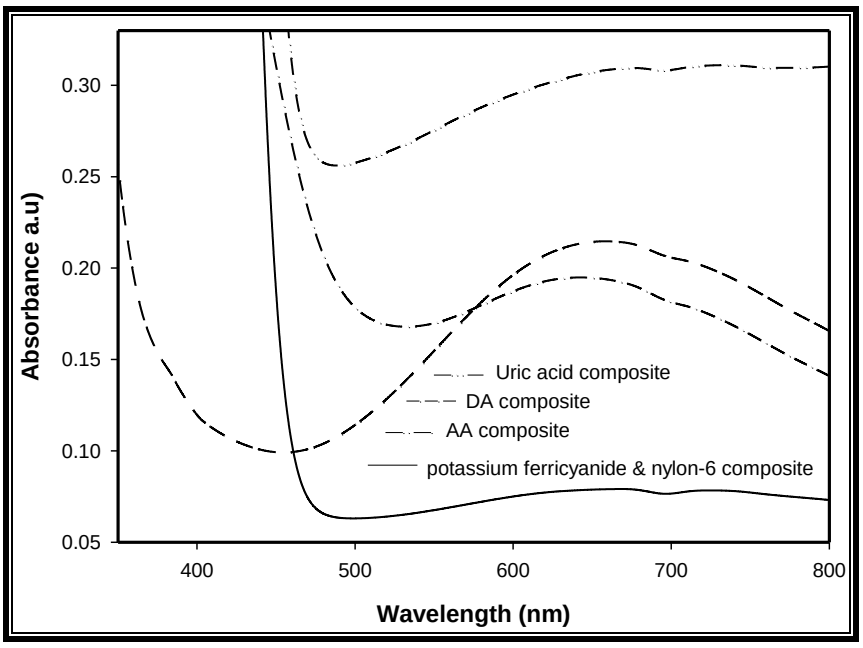

Figure 5.43: UV-visible spectra of nylon6 and ferricyanide composite, the composite with ascorbic acid, the composite with dopamine and the composite with uric acid

The UV-visible absorption spectrum of the composite of nylon6 and $FeCl_3$ is shown in Fig. 5.44. The addition of dopamine, uric acid and ascorbic acid did not cause any observable changes to the absorption spectra, a confirmation that $K_3[Fe^{III}(CN)_6]$ reduced instead of $FeCl_3$.

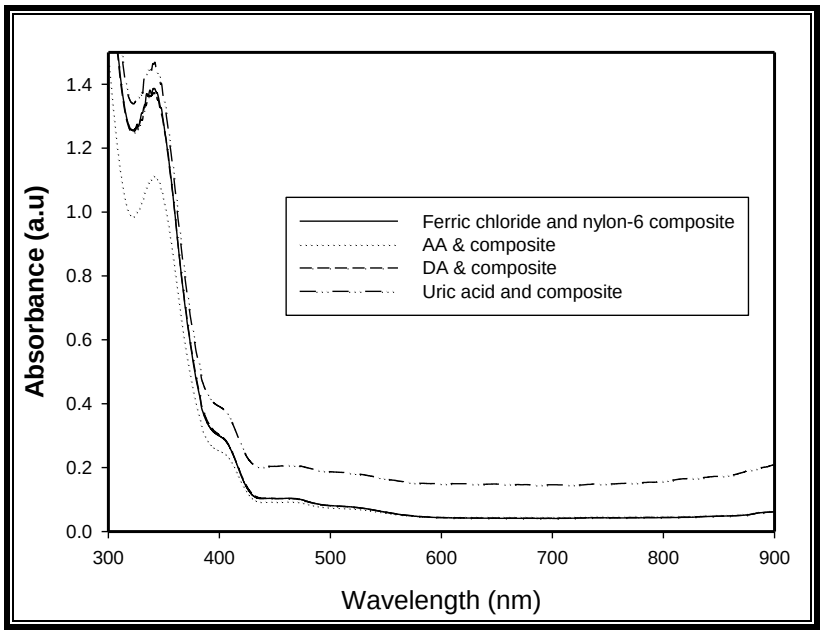

Figure 5.44: UV-visible spectra of nylon6 and ferric chloride composite, the composite with ascorbic acid, dopamine and uric acid

5.3.1.2 Colorimetric detection of ascorbic acid by nylon6, ferric chloride and ferricyanide based test strip

A light green test strip was obtained from the polymer composite of $FeCl_3$ and $K_3[Fe^{III}(CN)_6]$. The test strip exhibited different colours in ascorbic acid, dopamine and uric acid as shown in Fig. 5.45. Interferences were experienced from glutathione and citric acid as they showed the same response as ascorbic acid (Fig. 5.46). Glutathione like ascorbic acid is a powerful antioxidant that scavenges for free radicals that may cause cell damage. Glutathione is found in almost all fruits and vegetables and its interference is a crucial challenge. Citric acid also co-exists with ascorbic acid and its interference is a concern.

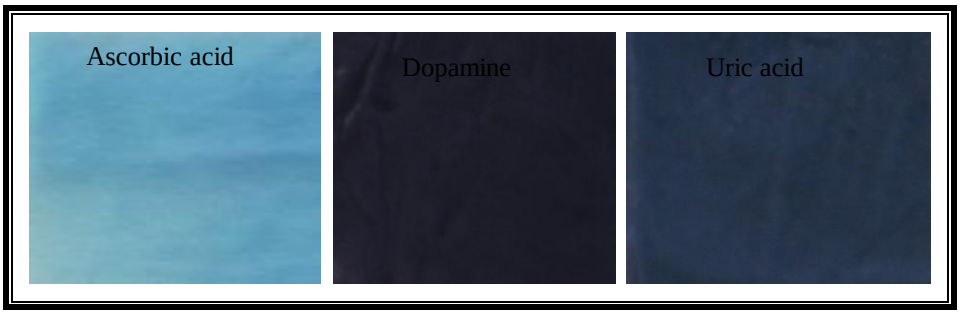

Figure 5.45: Colour change exhibited by nylon6, ferric chloride and ferricyanide based test strip in ascorbic acid (pH 3), dopamine (pH 7) and uric acid (pH 7)

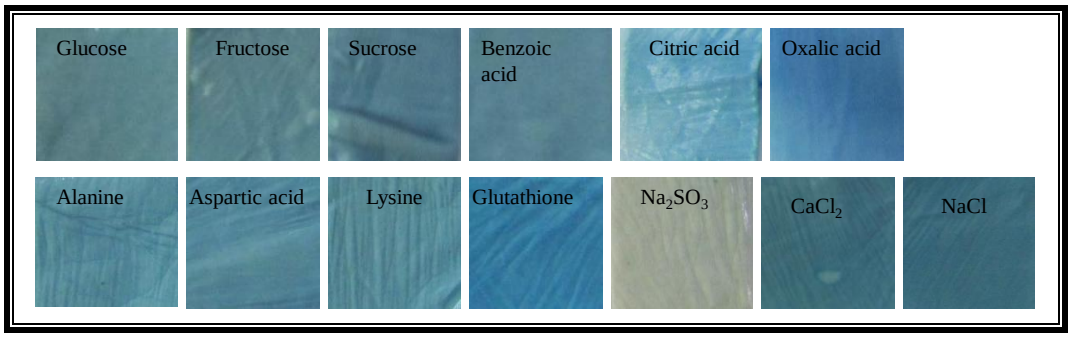

Figure 5.46: Colour change exhibited by nylon6, ferric chloride and ferricyanide based test strip in glucose, fructose, sucrose, benzoic acid, citric acid, oxalic acid, alanine, aspartic acid, lysine, glutathione, sodium sulphite, calcium chloride and sodium chloride at pH 3

Catecholamines showed a purplish test strip similar to dopamine as illustrated in Fig. 5.47. The concentration of catecholamines (norepinephrine, epinephrine and 3, 4-Dihydroxy-L-phenylalanine) and dopamine in body fluids is clinically relevant for neurological disorders diagnosis. The catecholamine test is usually carried out to diagnose an adrenal gland tumor called pheochromocytoma and to diagnose euroblastoma.

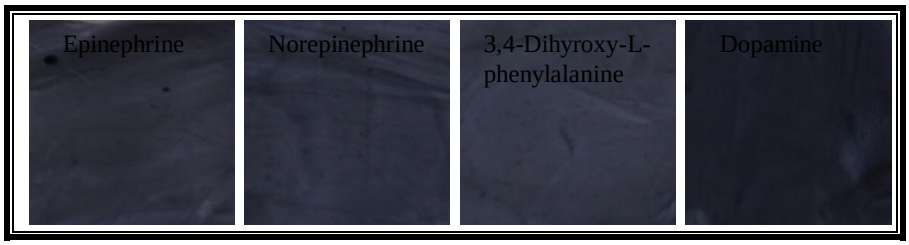

Figure 5.47: Colour change exhibited by nylon6, ferric chloride and ferricyanide test strip in catecholamines at pH 7

5.3.2 Soluble prussian blue based test strip for ascorbic acid and dopamine

5.3.2.1 Solution studies on soluble prussian blue polymeric matrix

In an attempt to improve selectivity, a prussian blue based test strip was fabricated directly from ferrous sulfate ($FeSO_4$) and potassium ferricyanide ($K_3[Fe^{III}(CN)_6]$). An intense blue colour was observed on mixing ferrous sulfate and ferricyanide salts in nylon-6. Eqn 7 summarises the formation of 'soluble' Turnsbull's blue pigment.

$$FeSO_4 + K_3[Fe^{III}(CN)_6] \rightarrow KFe^{III}[Fe^{II}CN)_6] + 2K^+ \quad \text{.....eqn 7}$$

The UV-visible spectrum of the polymer-prussian blue composite in Fig. 5.48, showed an absorption band around 700 nm, typical of prussian blue. The morphology of prussian blue nanoparticles in a polymeric matrix as observed under TEM is shown in Fig. 5.49.

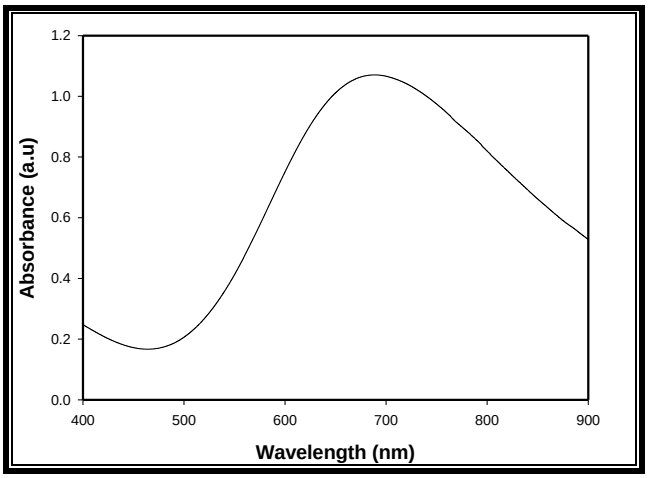

Figure 5.48: UV-visible spectra of soluble prussian blue in nylon6

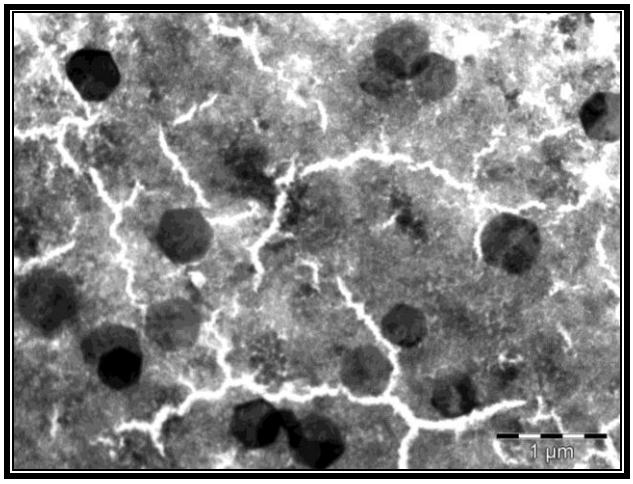

Figure 5.49: Transmission electron micrograph of prussian blue nanoparticles in nylon6

Upon addition of AA to the prussian blue nylon-6 composite, a lighter blue colour was observed. This was in agreement with the UV-visible absorbance spectra in Fig. 5.50 of the composite with AA. The absorbance of the polymeric matrix is linearly dependent upon the concentration of added AA, with a linearity range from 50 mg L^{-1} - 200 mg L^{-1} (Fig. 5.51). The fading of the prussian blue colour by AA was attributed to the reductive power of

ascorbic acid which reduces Fe^{III} to Fe^{II} eliminating the intervalence charge transfer that forms the prussian blue's colour.

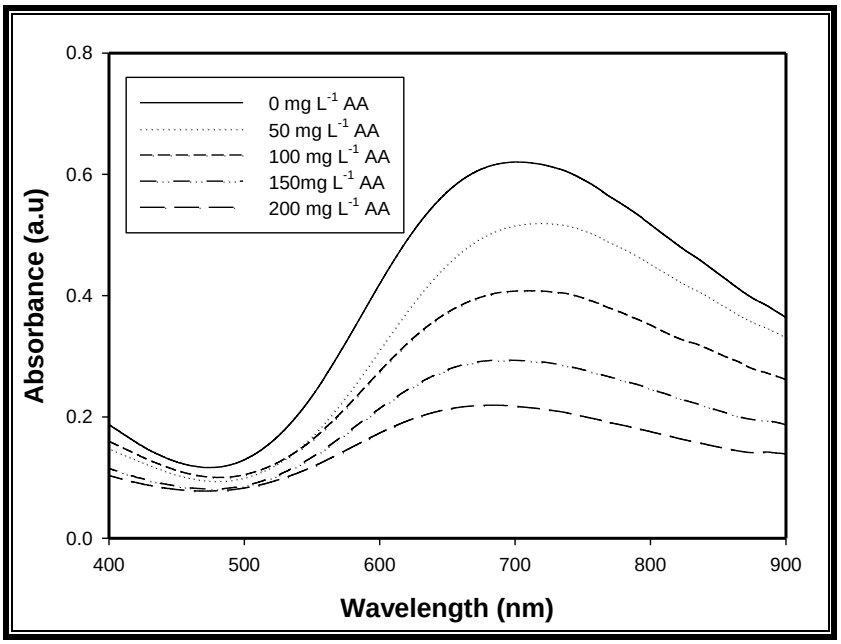

Figure 5.50: The decrease in absorbance of prussian blue with increase in ascorbic acid

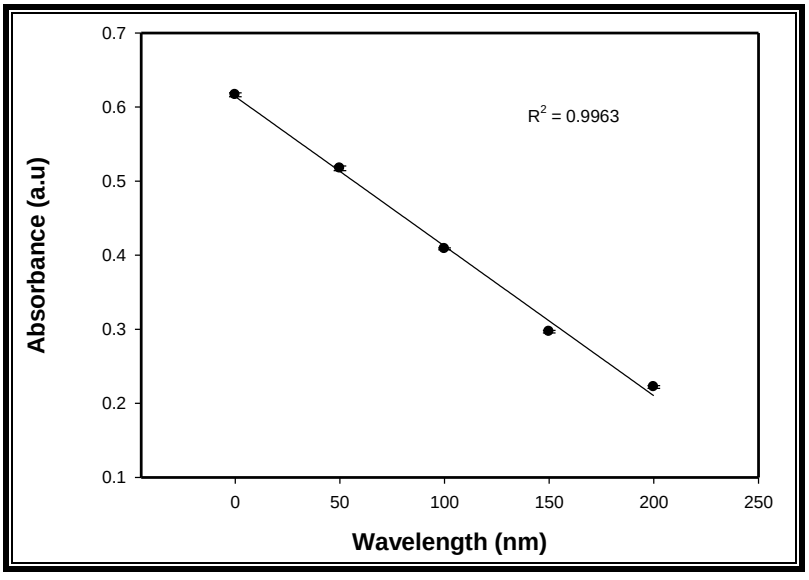

Figure 5.51: The linear relation of soluble prussian blue at 730 nm for different concentrations of ascorbic acid

A deep blue colour was observed when DA was added to prussian blue nylon6 composite. This was in agreement with UV-visible absorbance of the composite with DA in Fig 5.52, which showed the absorbance of the polymeric matrix is linearly dependent upon the concentration of added DA, with a linearity range from 50 mg L^{-1} - 200 mg L^{-1} (Fig. 5.53). It is not yet understood how dopamine enhances electrochromism of prussian blue.

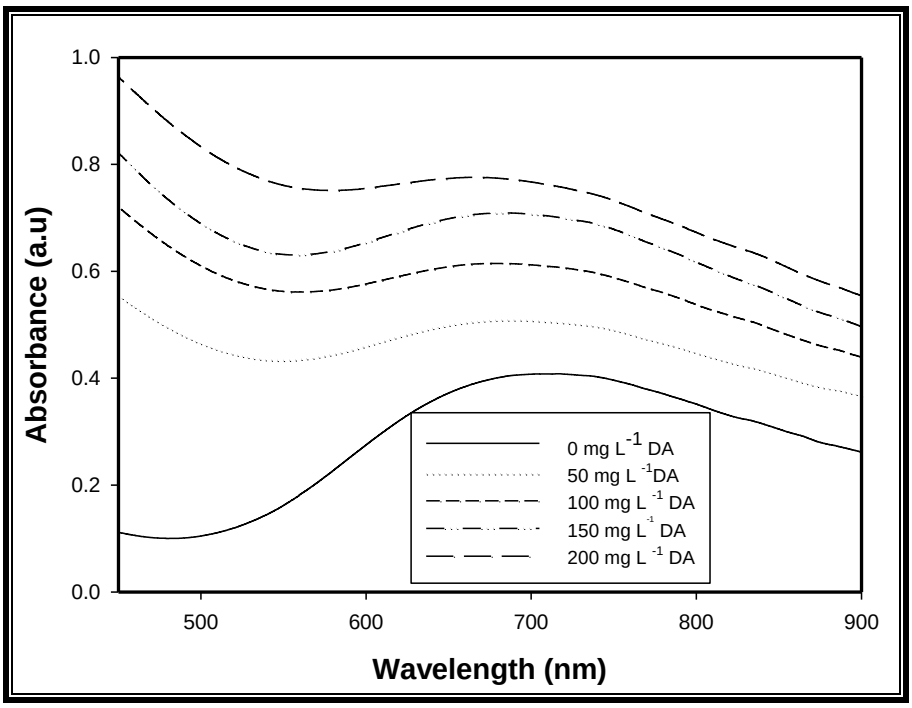

Figure 5.52: The increase in absorbance of prussian blue with increase in dopamine at 700 nm

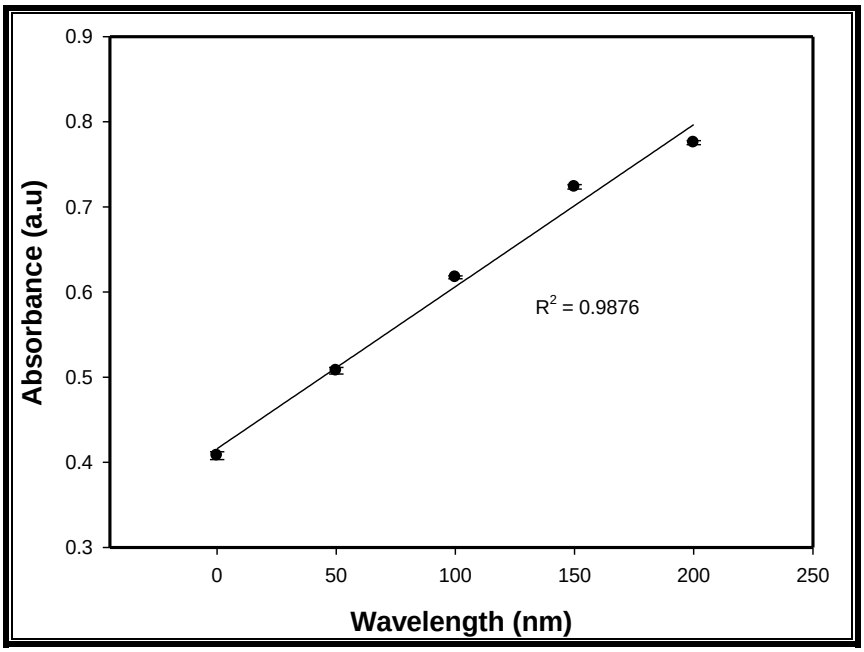

Figure 5.53: The linear relation of soluble prussian blue at 700 nm for different concentrations of dopamine

5.3.2.2 Investigations on a soluble prussian blue test strip

The FT-IR spectra of the test strip showed a peak at 2078 cm^{-1} attributed to the CN stretching in the Fe^{2+}–CN–Fe^{3+} of prussian blue [199,200] The band at 1660 cm^{-1} was assigned to the vibration of the C=O and that at 3298 cm^{-1} to N-H vibration both in nylon-6. The other peaks such as band at 2920 and 2859 cm^{-1} were due to CH stretching of the polymer. The morphology of prussian blue NPs in a polymeric matrix as observed under TEM as shown in Fig. 3.

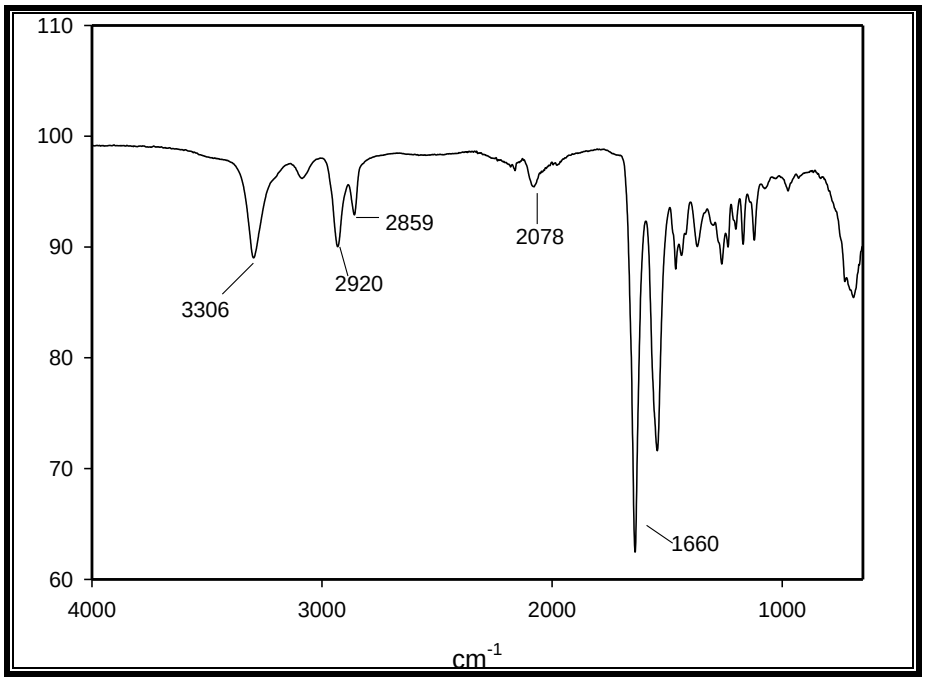

Figure 5. 54: Infrared spectra of a soluble prussian blue based test strip

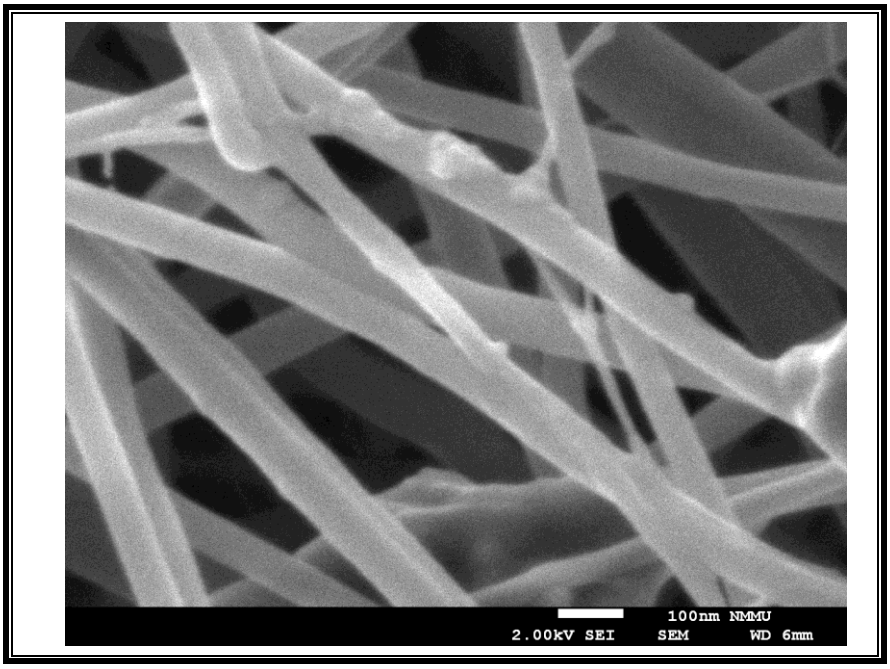

Figure 5.55: Scanning electron micrograph of the soluble prussian blue based test strip

The test strip was blue in colour, like in a polymeric solution, AA discoloured prussian blue on the fibre platform giving a distinct shade of blue from DA and uric acid as illustrated in Fig. 5.56. DA gave a purple response, a colour different from either AA or uric acid.

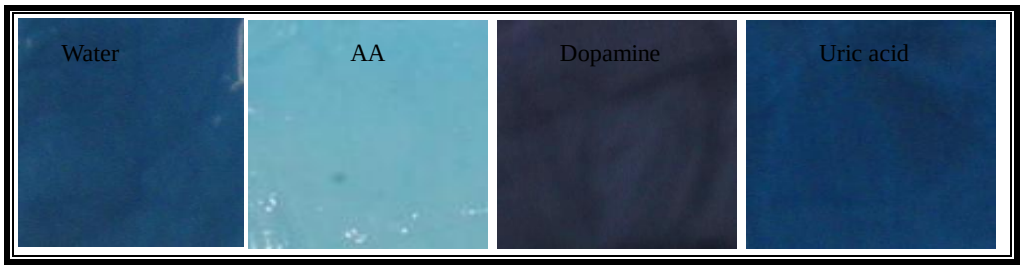

Figure 5.56: Colour changes exhibited by soluble prussian blue based test strip in water, 1.76 x10^5 mg L^{-1} ascorbic acid, 1.89 x10^5 mg L^{-1} dopamine and 1.68 x10^5 mg L^{-1} uric acid

Possible interfering species like the sacharrides, organic acids and amino acids in Fig. 5.57 did not show the same response as AA at pH 3 neither did they respond as DA at pH 7 as depicted in Fig. 5.58. The other catecholamines (norepinephrine, epinephrine and 3, 4-Dihydroxy-L-phenylalanine) evaluated also turned the test strip purple, giving a similar response to $FeCl_3$ and $K_3[Fe^{III}(CN)_6]$ test strip in section 5.3.1.2. The concentration of catecholamines in body fluids is only clinically relevant in neurological disorders diagnosis.

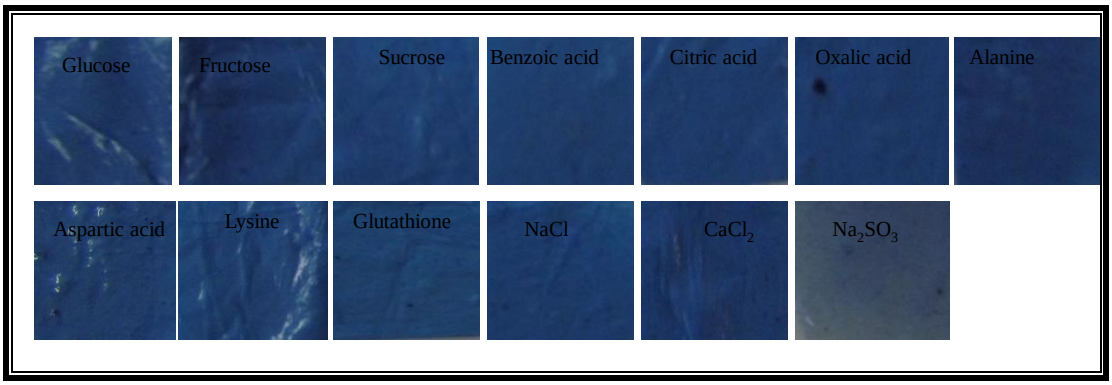

Figure 5.57: Colour changes exhibited by soluble prussian blue based test strip in glucose, fructose, sucrose, benzoic acid, citric acid, oxalic acid, alanine, aspartic acid, lysine, glutathione, sodium sulphite, calcium chloride, sodium chloride at pH 3

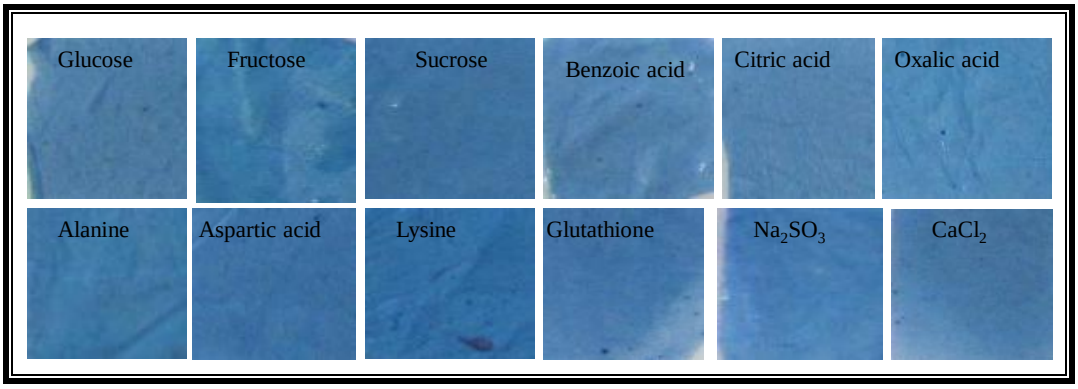

Figure 5.58: Colour changes exhibited by soluble prussian blue based test strip in glucose, fructose, sucrose, benzoic acid, citric acid, oxalic acid, alanine, aspartic acid, lysine, glutathione, sodium sulphite, calcium chloride at pH 7

The influence of pH on the performance of the test strip was evaluated for AA and DA. The faded blue colour was observed for a fibre in AA in a pH range of 2 – 5 as shown in Fig. 5.59. The purple colour exhibited by DA was enhanced at the physiological pH (pH 6.5 – 7) as shown in Fig. 5.60 while a distinct colour (faded navy blue) was observed for AA at the same pH range (Fig. 5.59). The detection limit of the test strip was 17.6 mg L^{-1} and 18.9 mg L^{-1} as shown in Figs. 5.61 and 5.62 for AA and DA respectively.

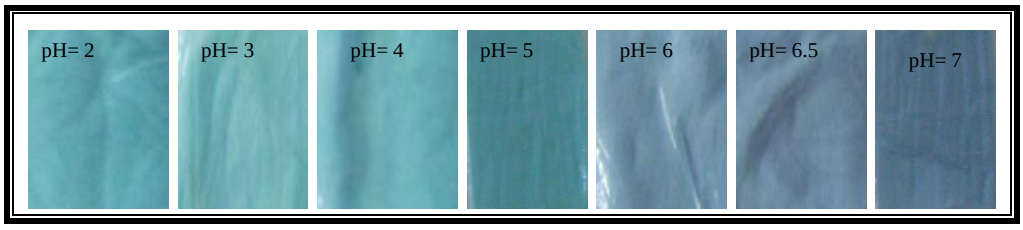

Figure 5.59: Colour change exhibited by soluble prussian blue based test strip in 176 mg L^{-1} ascorbic acid from pH 2-7

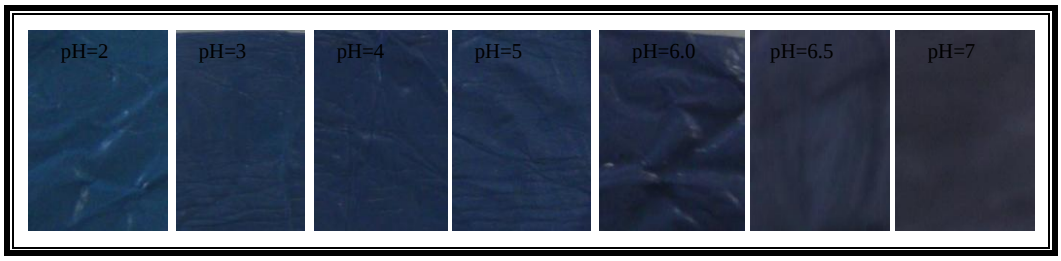

Figure 5.60: Colour change exhibited by soluble prussian blue based test strip in 189 mg L^{-1} dopamine from standard from pH 2-7

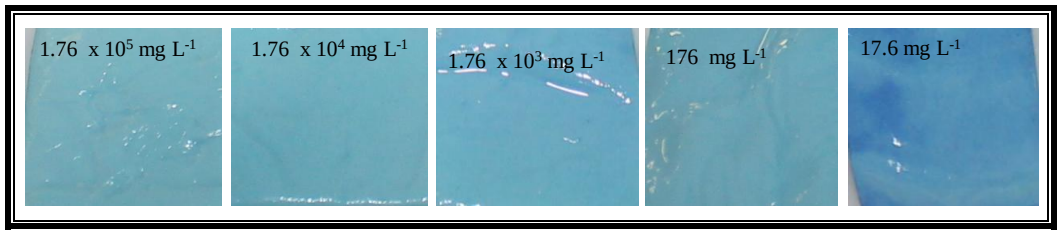

Figure 5.61: Soluble Prussian blue based test strip in different concentrations of ascorbic acid from 1. 76 x10^5 mgL^{-1} to 17.6 mg L^{-1}

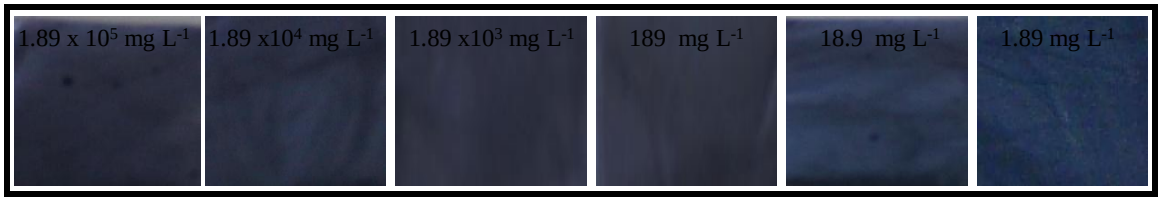

Figure 5.62: Soluble prussian blue based test strip in different concentrations of dopamine 1.89x10^5 mg L^{-1} to 18.9 mg L^{-1}

In order to confirm the suitability of the test strip for analytical applications in real samples, it was evaluated for AA in fifteen fruit juices of three different brands. The strip perfomance was also evaluated for both AA and DA in fortified urine samples. Colorimetric images corresponding to test strip in fruit juices, AA and DA fortified urine are in shown in in Fig. 5.63. In all cases the fibre performed effeciently. The test strips were applied to real samples after 10 months of storage in a shelf.

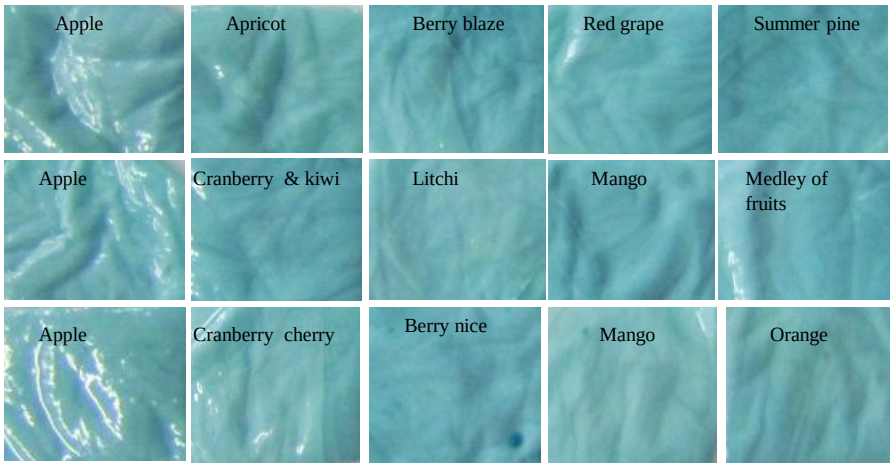

Test strips in fruit juices

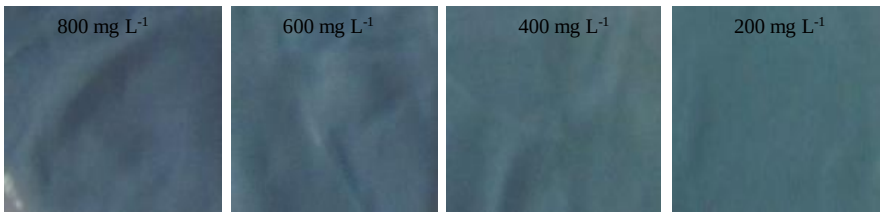

Test strips in ascorbic acid fortified urine

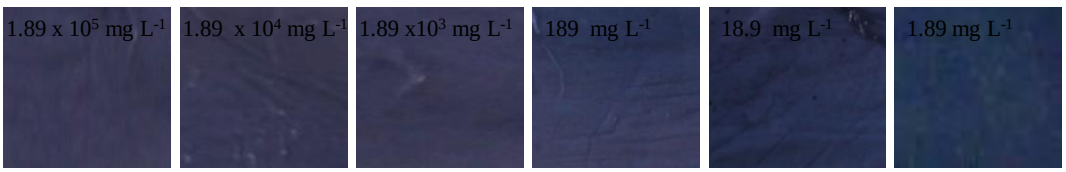

Test strips in dopamine fortified urine

Figure 5.63: Colour changes exhibited by soluble prussian blue based test strip in: fifteen fruit juices of three different brands, ascorbic acid fortified urine sample and in dopamine fortified urine samples

5.4 POLY-(VINYLBENYLCHLORIDE) ELECTROSPUN FIBRE FUNCTIONALISED WITH FE(III) - 2-(2′-PYRIDYL)-IMIDAZOLE TEST STRIP FOR ASCORBIC ACID AND DOPAMINE

5.4.1 Solution studies on Fe(III)- 2-(2′-pyridyl)-imidazole complex

PIMH was successfully synthesised as confirmed by ^{1}H NMR in Fig 5.64. ^{1}H NMR (600 MHz, CDCl3) δ ppm: 11.35 (s, NH, imidazole), 8.51 (d, *J* = 6 Hz, 1H, pyridine), 8.20 (d, *J* = 6 Hz, 1H, imidazole), 7.78 (t, *J* = 17, 1H, imidazole), 7.27- 7.13 (m, 3H, pyridine).

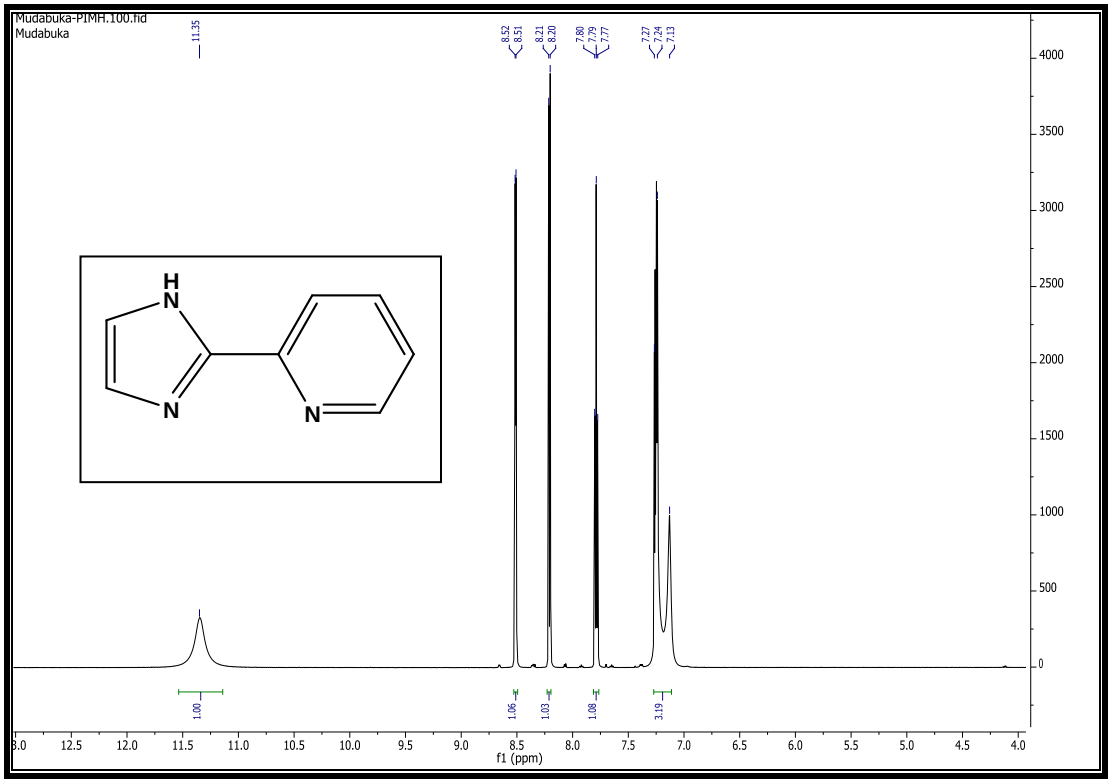

Figure 5.64: ^{1}H NMR of 2-(2′- pyridyl)-imidazole ligand recorded in $CDCl_3$

The detection mechanism was based on the reduction of PIMH-Fe(III) to PIMH-Fe(II), resulting in a red complex. Reaction pH was optimised and it was observed that AA could form a red complex from pH 2 to 5, but from pH 6-7, a red precipitate was formed. However

an optimum pH for the formation of the complex was illustrated in Fig. 5.65A because is soluble at lower pH's Fe(III). The red precipitate at pH above 4 was due to the hydrolysis of Fe(III) which formed hydroxide hence a decrease in absorbance observed. At pH 4 Job's method of continuous variation and molar ratio was applied to ascertain the stoichiometric composition of the ligand and Fe(III) in Fig 5.65B. It was confirmed from Job's plot in Fig. 1B that three ligands were coordinated to Fe(III). So Fe(III)-PIMH complex in the ratio 3:1 at pH 4 was used for AA detection.

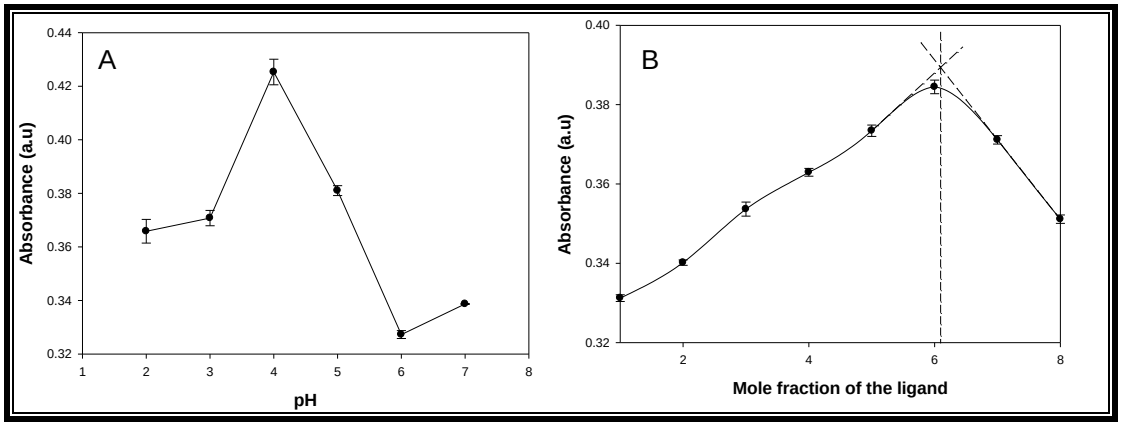

Figure 5.65: The effect of pH on the absorbance intensity of Fe(III) - 2-(2′- pyridyl)-imidazole and the plot of Job's method of continuous variation for determination of the stoichiometry of the Fe(III) - 2-(2′-pyridyl)-imidazole complex at pH 4

From literature, iron with an oxidation state of +3 cannot bind with ligands system having donor atoms such as nitrogen and oxygen [201] , as a result, giving rise to a low crystalline field energy at Fe^{3+} (Fig 5.66). This is what brings about the observed iron high-spin state. Iron is in the high-spin state S = 5/2. The EPR line recorded at g = 4.10-4.30 represents a typical signal from the Fe^{3+} ion in a system of low, rhombic symmetry in an octahedral or tetrahedral surrounding [201-205] while the signal at g = 6.03 is due to trivalent iron in PIMH with oxidation state III.

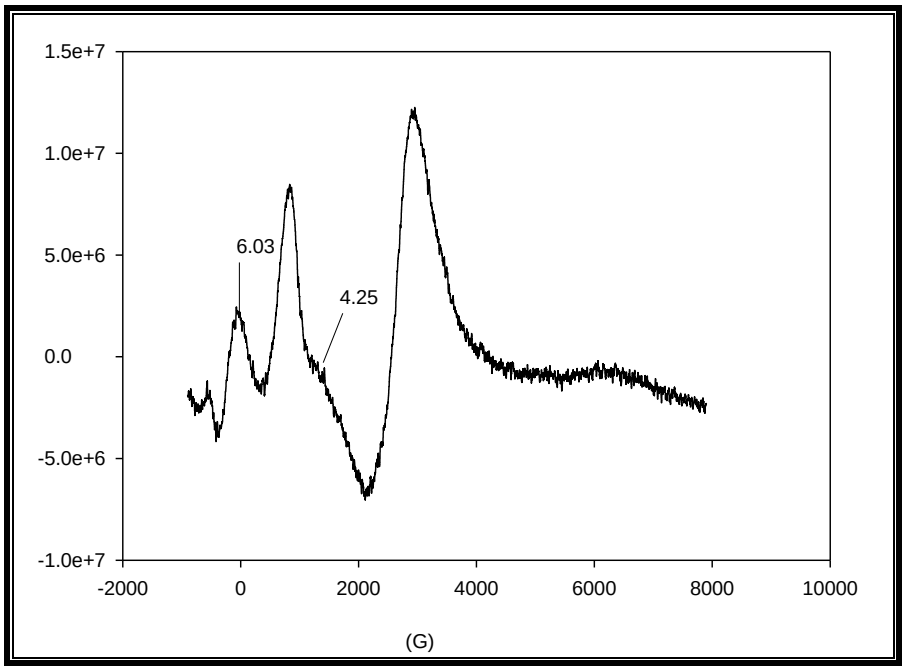

Figure 5.66: EPR characterisation of the complex

Figure 5.67 shows the UV-visible absorbance of Fe(III)-PIMH complex, Fe(III)-PIMH, AA and Fe(III)-PIMH, DA. The strong band observed on the Fe(III)-PIMH complex in the range 275-295 nm was due to an intra-ligand charge transfer transition. The weak broad absorption band in the range 308-335 nm may be assigned to the electronic transition associated with the CH=N- linkages. The band around 390 nm was due to ligand to metal charge transfer (LMCT).

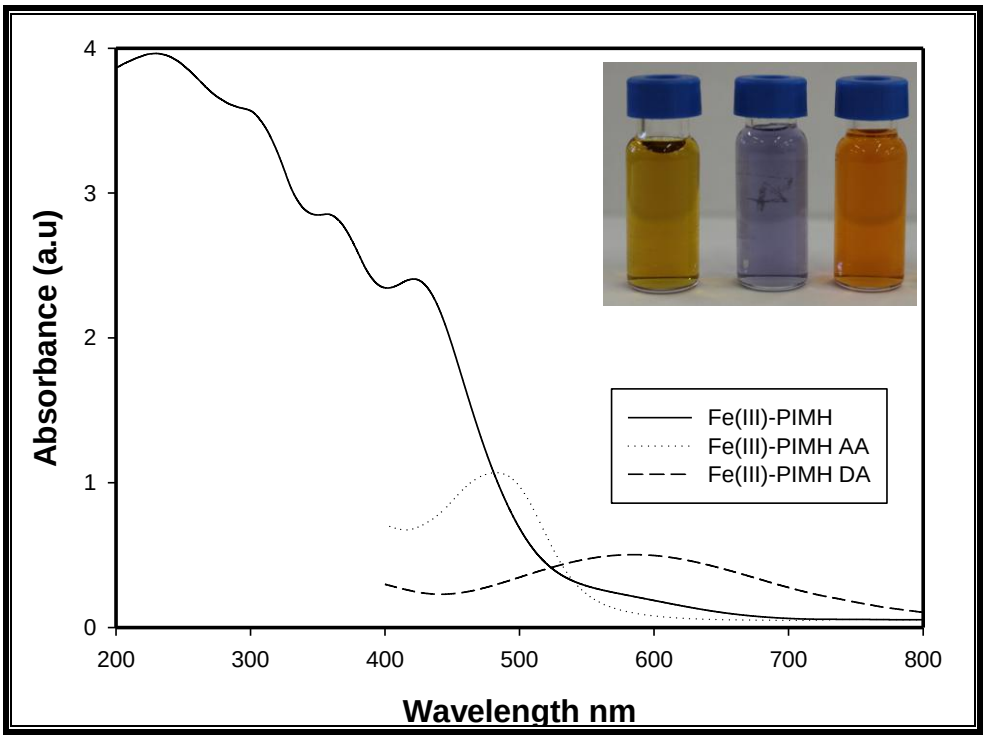

Figure 5.67: UV-visible of Fe(III) - 2-(2′-pyridyl)-imidazole complex, complex with ascorbic acid and the complex with dopamine

It was observed from the spectrum that ascorbic acid formed a red complex that absorbed at 480 nm while dopamine formed a blue complex that showed absorption around 600 nm. When AA was introduced to the high spin Fe(III) - PIMH complex (d5), it donated an electron to the metal centre and formed a low spin (d6) stable Fe(II)-PIMH complex. Detection methods where ascorbic acid reduced a metal ion to lower oxidation state that is then complexed with suitable ligand to produce a coloured complex have been reported.

In Fe^{2+} the outer electrons could occupy all the lower T_2g level (low spin) or they could occupy both T_2g and Eg level (high spin). A high spin PIMH complex with electrons occupying both T_2g and Eg level formed in the presence of dopamine hence the blue colour observed. The ^1H NMR of Fe(III)-PIMH with DA in Fig 5.68 (blue complex) exhibited a paramagnetic character with peak broadening, which is indicative of a high spin Fe(II).

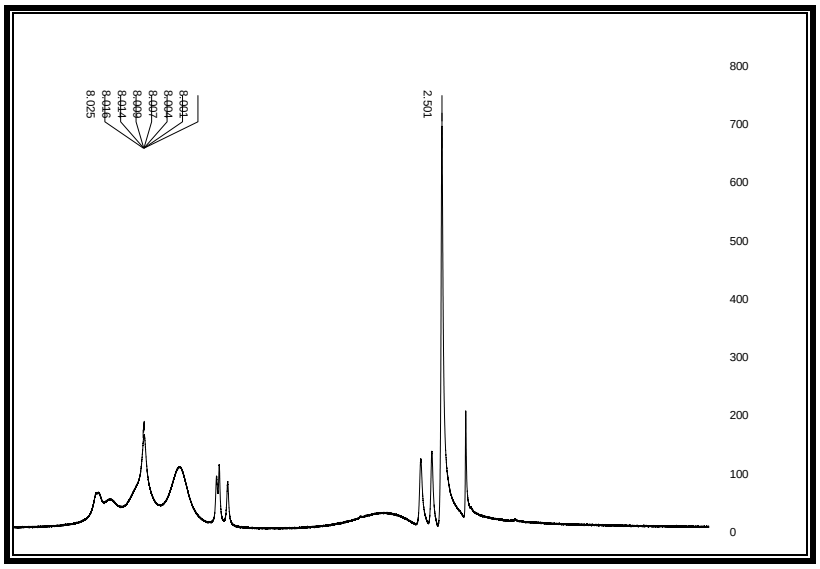

Figure 5.68: ^{1}H NMR of Fe(III) 2-(2′-pyridyl)-imidazole reagent with dopamine recorded in $CDCl_3$

Glutathione showed absorbance at the same region as AA in Fig 5.69, indicating it also reduced Fe (III) to Fe (II). All other potential interferences did not show any colour change.

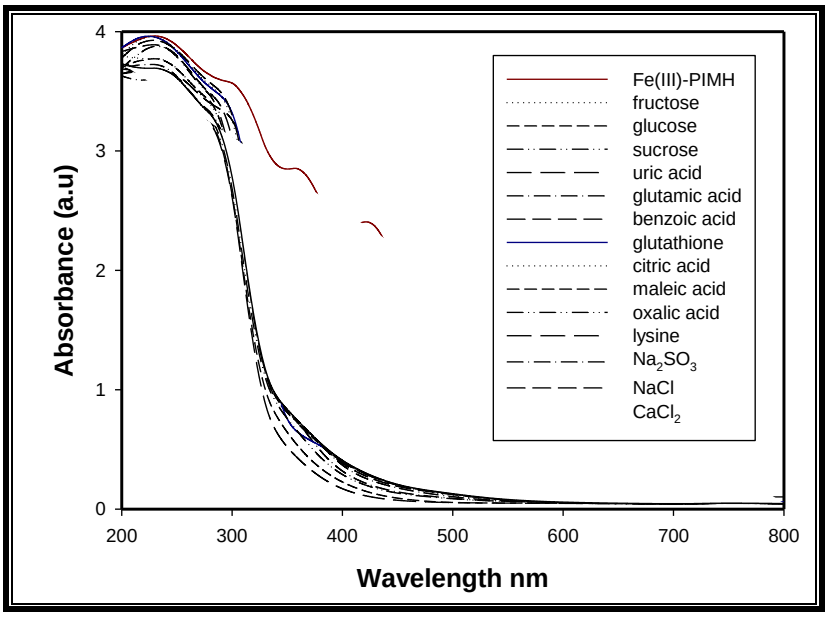

Figure 5.69: UV-visible of Fe(III) - 2-(2′-pyridyl)-imidazole complex and complex with potential interferences

Figure 5.07 shows that absorbance corresponding to the complex intensified as the concentration of AA increased with a linearity of 0.176 mg L^{-1} to 176 mg L^{-1} for AA and DA.

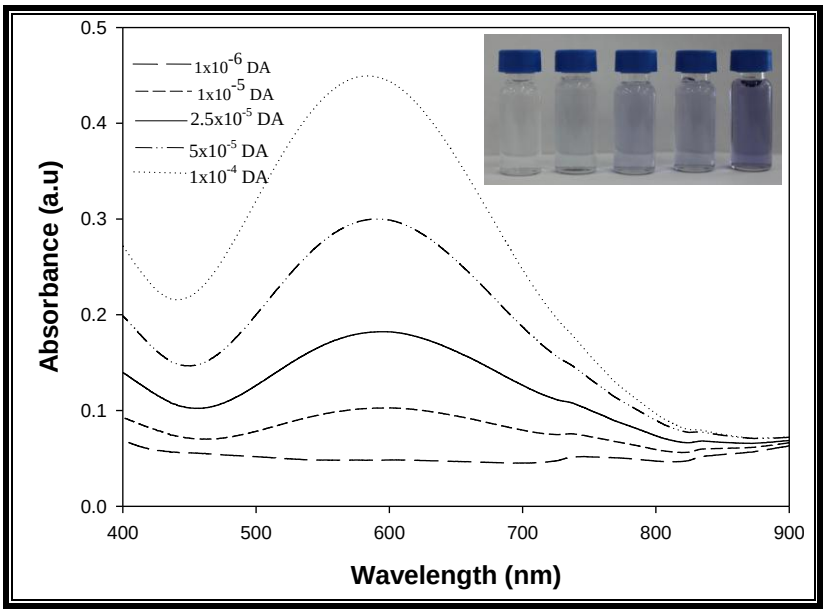

Figure 5.70: Absorption spectral changes of 2-(2′-pyridyl)-imidazole - Fe^{2+} complex with increasing concentrations of dopamine

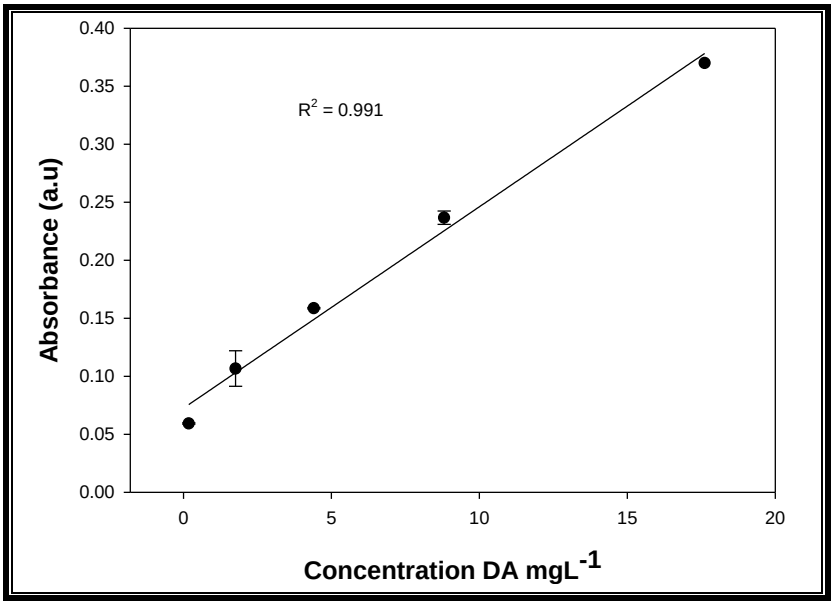

Figure 5.71: The linear relation of 2-(2′- pyridyl)-imidazole - Fe^{2+} complex with increasing concentrations of dopamine

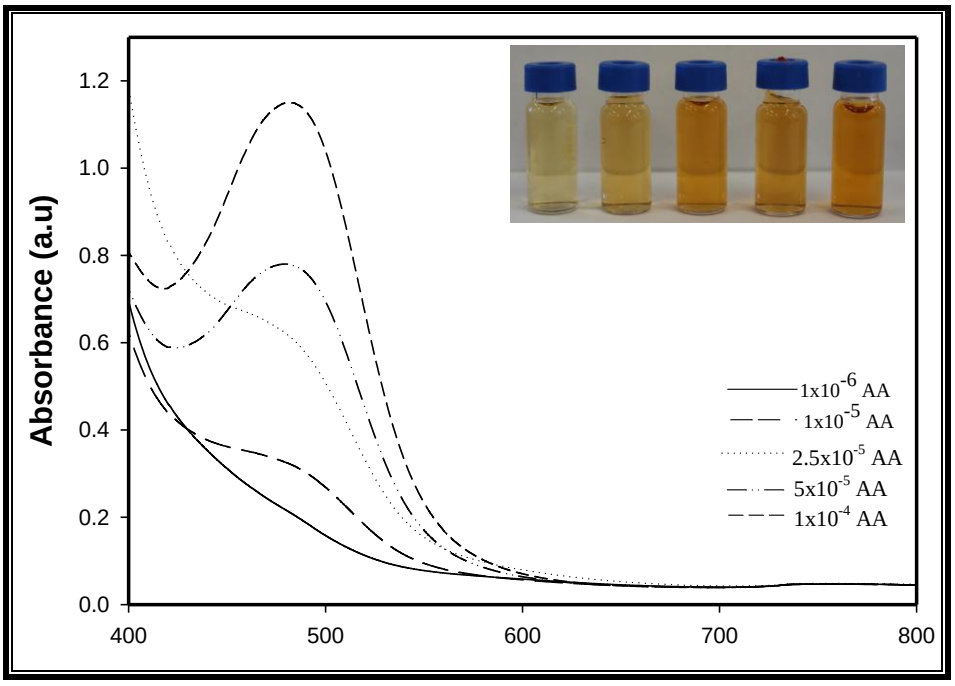

Figure 5.72: Absorption spectral changes of 2-(2′- pyridyl)-imidazole - Fe^{2+} complex with increasing concentrations of ascorbic acid

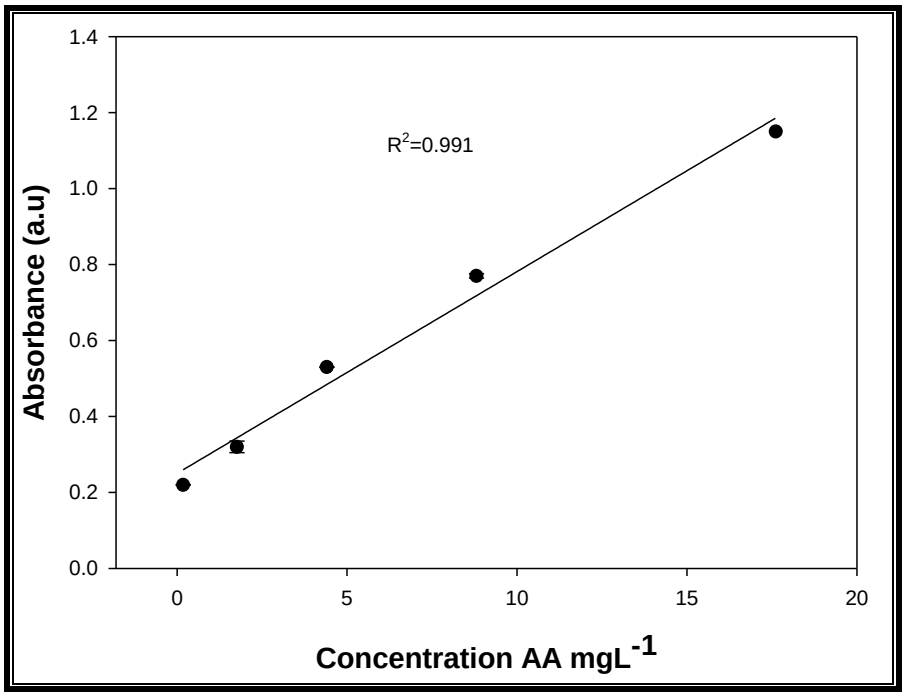

Figure 5.73: The linear relation of 2-(2′- pyridyl)-imidazole - Fe^{2+} complex with increasing of ascorbic acid

5.4.2 Investigations on Fe(III) - 2-(2′-pyridyl)-imidazole functionalised poly(vinylbenzyl chloride) test strip

FTIR was used to confirm the functionalisation of PVBC fibre with PIMH. The disappearance of C-Cl band of the polymer at 672 cm^{-1} and the appearance of the N-H band of the ligand around 3100 in Fig 5.74 confirmed post functionalisation of the test strip. The presence of all the expected functionalities was further confirmed by EDX. Figure 5.75A shows PVBC fibre and the expected functionalities (C and Cl). The appearance of nitrogen in the PVBC fibres functionalized by PIMH in Fig. 5.75A was an indicator that the ligand had been successfully attached to the polymer back bone. Fe(III) appeared in a fibre further soaked in $FeCl_3$ in 5.75B confirming the presence of all functionalities integrated in the test strip.

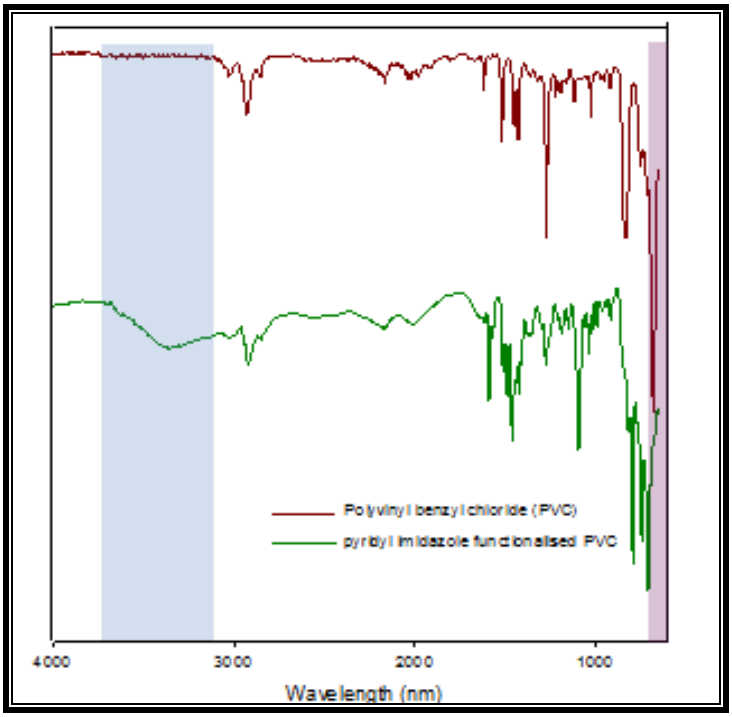

Figure 5.74: Infrared spectra of poly(vinylbenzyl chloride) functionalised with 2-(2′-pyridyl)-imidazole

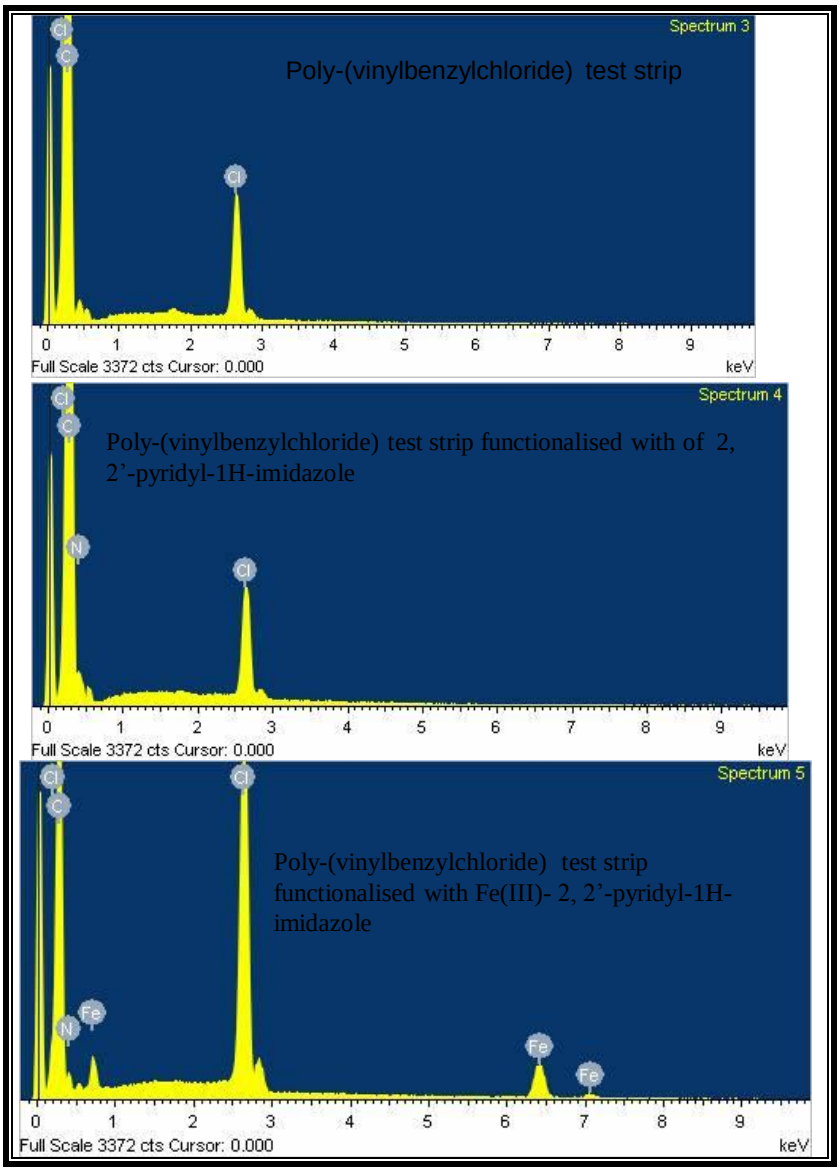

Figure 5.75: EDX of electrospun fibre of: poly(vinylbenzyl chloride) , poly(vinylbenzyl chloride) fibre functionalised with of 2-(2′-pyridyl)-imidazole and poly(vinylbenzyl chloride) fibre functionalised with Fe(III) - 2-(2′-pyridyl)-imidazole

The test strip exhibited a red colour in AA at pH 3, dark blue colour in DA at pH 7 and remained yellow in uric acid at pH 7 as illustrated in Fig. 5.76. The possible interfering compounds evaluated could not show the same colour change observed for AA and DA at the same concentration and pH as shown in Figs 5.77 and 5.78. Only glutathione showed the same response as AA at pH 3.

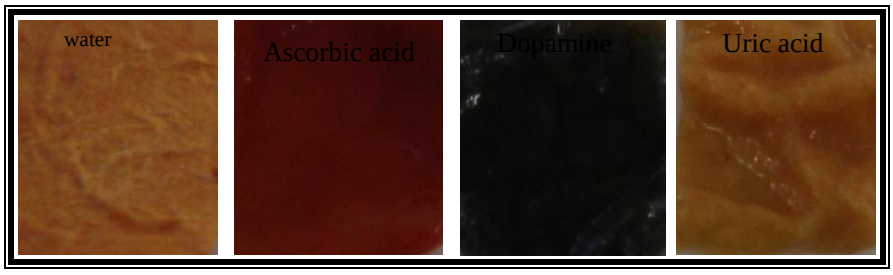

Figure 5.76: Colorimetric response of Fe(III) - 2-(2′-pyridyl)-imidazole functionalised poly(vinylbenzyl chloride) test strip in water, ascorbic acid at pH 3, dopamine at pH 7, and uric acid at pH 7

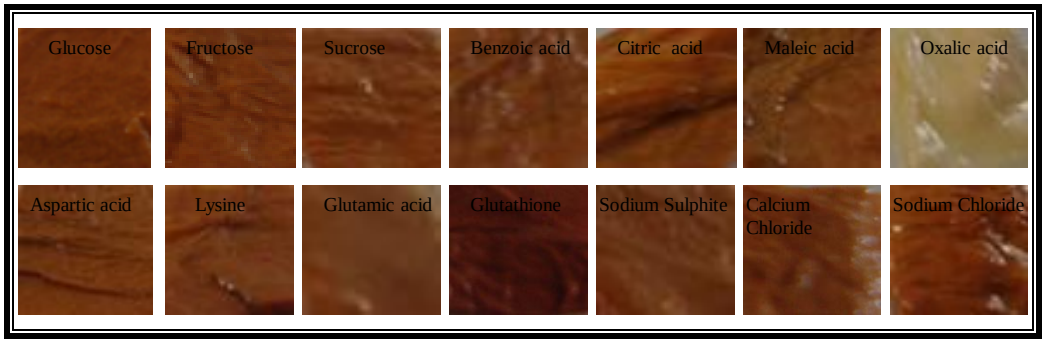

Figure 5.77: Colorimetric response of Fe(III) - 2-(2′-pyridyl)-imidazole functionalised poly(vinylbenzyl chloride) test strip in glucose, fructose, sucrose, benzoic acid, citric acid, maleic acid, oxalic acid, aspartic acid, lysine, glutamic acid, glutathione, sodium sulphite, calcium chloride, sodium chloride at pH 3

Figure 5.78: Colorimetric response of Fe(III) - 2-(2′- pyridyl)-imidazole functionalised poly(vinylbenzyl chloride) test strip in glucose, fructose, sucrose, benzoic acid, citric acid, maleic acid, oxalic acid, aspartic acid, lysine, glutamic acid, glutathione, sodium sulphite, calcium chloride, sodium chloride at pH 7

The detection limit of the test strips was 17.6 mg L^{-1} for AA and 18.4 mg L^{-1} for dopamine respectively. Figure 5.80 and 5.81 show the test strips in different concentrations of AA (1.76 x 10^5 mg L^{-1} - 1.76 mg L^{-1}) and DA (1.89 x 10^5 mg L^{-1} to 1.89 mg L^{-1}) respectively.

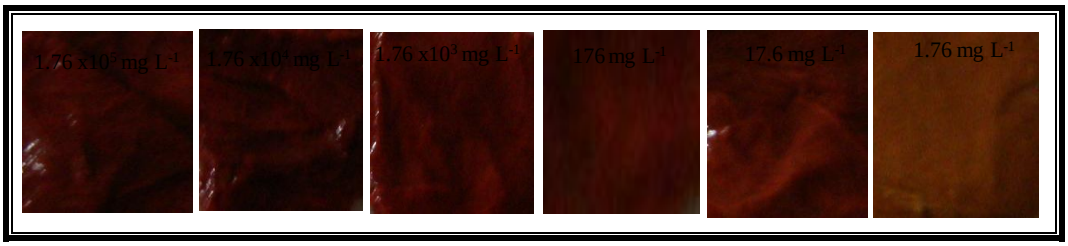

Figure 5.79: Fe(III) - 2-(2′-Pyridyl)-imidazole functionalised poly(vinylbenzyl chloride) test strip in different concentrations of ascorbic acid from 1. 76 x10^5 mgL^{-1} to 1.76 mg L^{-1}

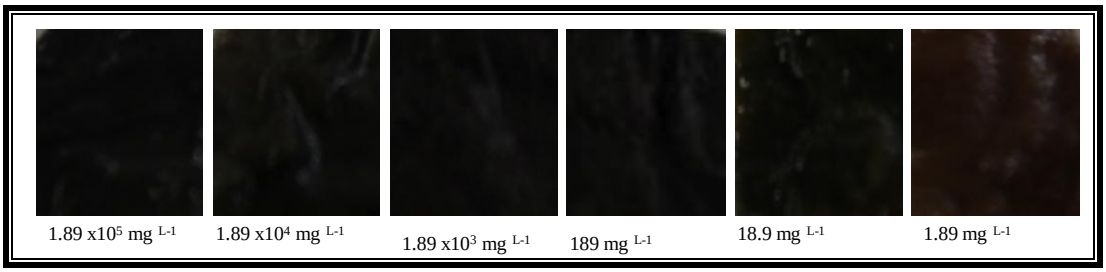

Figure 5.80: Fe(III) - 2-(2′-Pyridyl)-imidazole functionalised poly(vinylbenzyl chloride) test strip in dopamine concentrations from 1.89x10^5 mg L^{-1} to 18.9 mg L^{-1}

We demonstrated the analytical application of the test strip by detecting AA in fruit juices and DA fortified urine sample as in Fig. 5.81. The test strip was applied to real samples after storage in a shelf for 10 months confirming their stability.

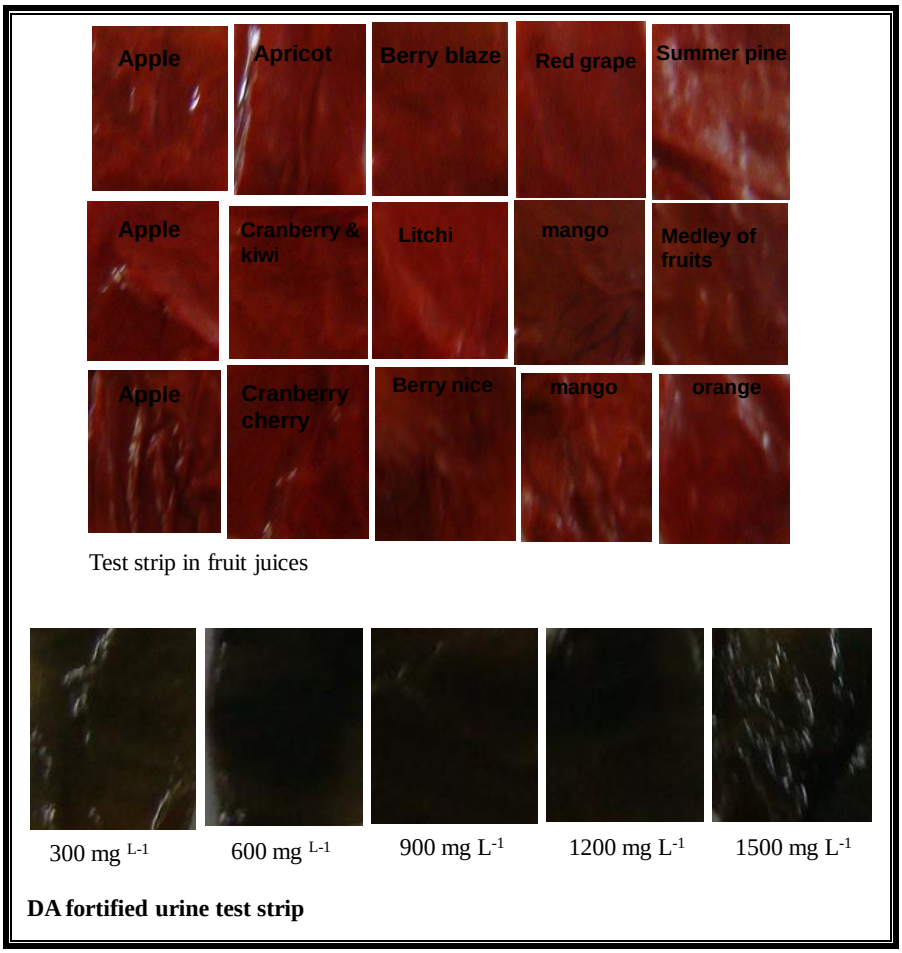

Figure 5.81: Colorimetric response of Fe(III) - 2-(2′-Pyridyl)-imidazole functionalised poly(vinylbenzyl chloride) test strip in: fifteen fruit juices of three different brands and dopamine fortified urine samples

Chapter 6 CONCLUSION

The application of electrospun nanofibre as a host for detector agents such as dyes and nanoparticles was demonstrated for the detection of ascorbic acid and dopamine in studies conducted and reported in this thesis. The colorimetric detection of analytes demonstrated in the study present a low cost easy to use alternative to conventional methods. Chemical reactions in solution form that result in colour change were also observed on the solid substrate. However, better sensitivity was attained for the metal nanoparticles based test strips. Although metal nanoparticles exhibit strong extinction bands in the visible region of the spectrum, and therefore bright and gaudy colours reminiscent of molecular dyes, their origins are different. The spectra of molecular dyes can be understood only in terms of quantum mechanics, while the extinction spectra of metal nanoparticles can be treated in terms of classical electromagnetism. Moreover, metal nanoparticles also scatter light with high efficiency and, unlike molecular dyes, their extinction spectra are really a combination of both absorption and scattering thus rendering nanoparticles more sensitive than dyes in colorimetric detection [206]. The colorimetric test strips could be applied to samples without sample pre-treatment and visual results were obtained within minutes rendering the test strips simple and rapid.

The protocol employing nanofibres as a support for colorimetric probes developed in this thesis present an alternative platform for simple colorimetric ‘point of use’ and ‘point of care’ devices. The polymer electrospun substrates were shown to have excellent properties for use in the cost-effective, easy-to-use colorimetric assay agents. The polymer porous morphology permits diffusion and interaction of analytes with the reagents incorporated within the

substrate. Moreover, electrospun polymers can be functionalised, thus tuning properties towards analytes of interest to achieve high selectivity. Electrospinning offers researchers an opportunity to alter fibre diameter and orientation that gives the analyst an advantage of modifying the platform porosity and pore size to meet application requirement. Again electrospinning being applicable to many polymers offers an opportunity of a wide variety of polymers to choose from for the development of POU and POC devices. Electrospun fibres have also shown to withstand long-term storage effects without discolouration and to be thermally stable up to 60 ˚C making an ideal platform for POU and POC devices.

For future studies, electrospun nanofibres may be exploited for mulitiplex assay format. Electrospinning however generally utilises toxic organic solvents to dissolve polymers. The solvents may affect the structural properties of proteins in the development of lateral flow devices. There is therefore a need to replace toxic organic solvents with less toxic solvents.

REFERENCES

1. Colloidal Gold lateral flow strips development (cited 20.10.13) Available: http://www.creative-diagnostics.com/Colloidal-Gold-Lateral-Flow-Strips-Development.html?gclid=CLOu--aSm7oCFcLHtAodJkIAzw

2. Free AH, Adams EC, Kercher ML, Free HM, Cook MH (1957) Simple specific test for urine glucose. Clinical chemistry 3 (3):163-168

3. Urine testingusng the multistick (cited 20.1013) Available: . http://www.pointofcare.net/procedures/AriaHealth1209/UrineTestingUsingtheMultistick.pdf
4. diagnostics SMs. http://en.wikipedia.org/wiki/Urine_test_strip.

5. Martinez AW, Phillips ST, Whitesides GM, Carrilho E (2010) Diagnostics for the developing world: Microfluidic paper-based analytical devices. Analytical Chemistry 82 (1):3-10

6. Martinez AW, Phillips ST, Whitesides GM (2008) Three-dimensional microfluidic devices fabricated in layered paper and tape. Proceedings of the National Academy of Sciences of the United States of America 105 (50):19606-19611

7. Klasner SA, Price AK, Hoeman KW, Wilson RS, Bell KJ, Culbertson CT (2010) Paper-based microfluidic devices for analysis of clinically relevant analytes present in urine and saliva. Analytical and Bioanalytical Chemistry 397 (5):1821-1829

8. Bruzewicz DA, Reches M, Whitesides GM (2008) Low-cost printing of poly(dimethylsiloxane) barriers to define microchannels in paper. Analytical Chemistry 80 (9):3387-3392

9. Khan MS, Fon D, Li X, Tian J, Forsythe J, Garnier G, Shen W (2010) Biosurface engineering through ink jet printing. Colloids and Surfaces B: Biointerfaces 75 (2):441-447

10. Martinez AW, Phillips ST, Carrilho E, Thomas Iii SW, Sindi H, Whitesides GM (2008) Simple telemedicine for developing regions: Camera phones and paper-based microfluidic devices for real-time, off-site diagnosis. Analytical Chemistry 80 (10):3699-3707

11. Abe K, Suzuki K, Citterio D (2008) Inkjet-printed microfluidic multianalyte chemical sensing paper. Analytical Chemistry 80 (18):6928-6934

12. Li X, Tian J, Nguyen T, Shen W (2008) Paper-based microfluidic devices by plasma treatment. Analytical Chemistry 80 (23):9131-9134

13. Fenton EM, Mascarenas MR, López GP, Sibbett SS (2009) Multiplex lateral-flow test strips fabricated by two-dimensional shaping. ACS Applied Materials and Interfaces 1 (1):124-129

14. Zhong ZW, Wang ZP, Huang GXD (2012) Investigation of wax and paper materials for the fabrication of paper-based microfluidic devices. Microsystem Technologies 18 (5):649-659

15. Olkkonen J, Lehtinen K, Erho T (2010) Flexographically printed fluidic structures in paper. Analytical Chemistry 82 (24):10246-10250

16. Dungchai W, Chailapakul O, Henry CS (2011) A low-cost, simple, and rapid fabrication method for paper-based microfluidics using wax screen-printing. Analyst 136 (1):77-82

17. Martinez AW, Phillips ST, Butte MJ, Whitesides GM (2007) Patterned paper as a platform for inexpensive, low-volume, portable bioassays. Angewandte Chemie - International Edition 46 (8):1318-1320

18. Li X, Ballerini DR, Shen W (2012) A perspective on paper-based microfluidics: Current status and future trends. Biomicrofluidics 6 (1)

19. Lu R, Shi W, Jiang L, Qin J, Lin B (2009) Rapid prototyping of paper-based microfluidics with wax for low-cost, portable bioassay. Electrophoresis 30 (9):1497-1500

20. Lu Y, Shi W, Qin J, Lin B (2010) Fabrication and characterization of paper-based microfluidics prepared in nitrocellulose membrane by Wax printing. Analytical Chemistry 82 (1):329-335

21. Wang W, Wu WY, Zhu JJ (2010) Tree-shaped paper strip for semiquantitative colorimetric detection of protein with self-calibration. Journal of Chromatography A 1217 (24):3896-3899

22. Dungchai W, Chailapakul O, Henry CS (2009) Electrochemical detection for paper-based microfluidics. Analytical Chemistry 81 (14):5821-5826

23. Nie Z, Deiss F, Liu X, Akbulut O, Whitesides GM (2010) Integration of paper-based microfluidic devices with commercial electrochemical readers. Lab on a Chip - Miniaturisation for Chemistry and Biology 10 (22):3163-3169

24. Nie Z, Nijhuis CA, Gong J, Chen X, Kumachev A, Martinez AW, Narovlyansky M, Whitesides GM (2010) Electrochemical sensing in paper-based microfluidic devices. Lab on a Chip - Miniaturisation for Chemistry and Biology 10 (4):477-483

25. Delaney JL, Hogan CF, Tian J, Shen W (2011) Electrogenerated chemiluminescence detection in paper-based microfluidic sensors. Analytical Chemistry 83 (4):1300-1306

26. Lee KS, Kim TH, Shin MC, Lee WY, Park JK (1999) Disposable liposome immunosensor for theophylline combining an immunochromatographic membrane and a thick-film electrode. Analytica Chimica Acta 380 (1):17-26

27. Yan M, Zang D, Ge S, Ge L, Yu J (2012) A disposable electrochemical immunosensor based on carbon screen-printed electrodes for the detection of prostate specific antigen. Biosensors and Bioelectronics 38 (1):355-361

28. Wang P, Ge L, Yan M, Song X, Ge S, Yu J (2012) Paper-based three-dimensional electrochemical immunodevice based on multi-walled carbon nanotubes functionalized paper for sensitive point-of-care testing. Biosensors and Bioelectronics 32 (1):238-243

29. Jagadeesan KK, Kumar S, Sumana G (2012) Application of conducting paper for selective detection of troponin. Electrochemistry Communications 20 (1):71-74

30. Liu H, Xiang Y, Lu Y, Crooks RM (2012) Aptamer-based origami paper analytical device for electrochemical detection of adenosine. Angewandte Chemie - International Edition 51 (28):6925-6928

31. Lu J, Ge S, Ge L, Yan M, Yu J (2012) Electrochemical DNA sensor based on three-dimensional folding paper device for specific and sensitive point-of-care testing. Electrochimica Acta 80:334-341

32. Shiroma LY, Santhiago M, Gobbi AL, Kubota LT (2012) Separation and electrochemical detection of paracetamol and 4-aminophenol in a paper-based microfluidic device. Analytica Chimica Acta 725:44-50

33. Rattanarat P, Dungchai W, Siangproh W, Chailapakul O, Henry CS (2012) Sodium dodecyl sulfate-modified electrochemical paper-based analytical device for determination of dopamine levels in biological samples. Analytica Chimica Acta 744:1-7

34. Ge S, Ge L, Yan M, Song X, Yu J, Huang J (2012) A disposable paper-based electrochemical sensor with an addressable electrode array for cancer screening. Chemical Communications 48 (75):9397-9399

35. epi-fluorescence with the microscopoe (cited 20.10.2013) Available: http://www.google.co.za/imgres?imgurl=http://web.uvic.ca/ail/techniques/Jablonski.jpg&imgrefurl=http://web.uvic.ca/ail/techniques/epi-fluorescence.html&h=331&w=504&sz=45&tbnid=6wWnr8sEt4wxIM:&tbnh=117&tbnw=178&zoom=1&usg=__38AvAVbwPJqmxK5yAvvUyDQr8RQ=&docid=CE5K5mGy6SPLOM&sa=X&ei=z4SUUvCGNqyQ7AbwvYCYDA&ved=0CDUQ9QEwBQ

36. Wang S, Ge L, Song X, Yu J, Ge S, Huang J, Zeng F (2012) Paper-based chemiluminescence ELISA: Lab-on-paper based on chitosan modified paper device and wax-screen-printing. Biosensors and Bioelectronics 31 (1):212-218

37. Yu J, Ge L, Huang J, Wang S, Ge S (2011) Microfluidic paper-based chemiluminescence biosensor for simultaneous determination of glucose and uric acid. Lab on a Chip - Miniaturisation for Chemistry and Biology 11 (7):1286-1291

38. Schroeder HR, Vogelhut PA, Carrico RJ, Boguslaski RC, Buckler RT (1976) Competitive protein binding assay for biotin monitored by chemiluminescence. Analytical Chemistry 48 (13):1933-1937

39. Van Weemen BK, Schuurs AHWM (1971) Immunoassay using antigen-enzyme conjugates. FEBS Letters 15 (3):232-236

40. Petti CA, Polage CR, Quinn TC, Ronald AR, Sande MA (2006) Laboratory medicine in Africa: A barrier to effective health care. Clinical Infectious Diseases 42 (3):377-382

41. Halas N (2005) Playing with plasmons: Tuning the optical resonant properties of metallic nanoshells. MRS Bulletin 30 (5):362-367

42. Klabunde K (2001) Nanoscale Materials in Chemistry

43. Moores A, Goettmann F (2006) The plasmon band in noble metal nanoparticles: An introduction to theory and applications. New Journal of Chemistry 30 (8):1121-1132

44. Liz-Marzán LM (2006) Tailoring surface plasmons through the morphology and assembly of metal nanoparticles. Langmuir 22 (1):32-41

45. Rathbone DL, Ge Y (2001) Selectivity of response in fluorescent polymers imprinted with N1-benzylidene pyridine-2-carboxamidrazones. Analytica Chimica Acta 435 (1):129-136

46. Omidfar K, Khorsand F, Darziani Azizi M (2013) New analytical applications of gold nanoparticles as label in antibody based sensors. Biosensors and Bioelectronics 43 (1):336-347

47. Liz-Marzán LM (2004) Nanometals: Formation and color. Materials Today 7 (2):26-31

48. Joshi SS, Patil SF, Iyer V, Mahumuni S (1998) Radiation induced synthesis and characterization of copper nanoparticles. Nanostructured Materials 10 (7):1135-1144

49. Lisiecki I, Filankembo A, Sack-Kongehl H, Weiss K, Pileni MP, Urban J (2000) Structural investigations of copper nanorods by high-resolution TEM. Physical Review B - Condensed Matter and Materials Physics 61 (7):4968-4974

50. Pileni MP, Ninham BW, Gulik-Krzywicki T, Tanori J, Lisiecki I, Filankembo A (1999) Direct relationship between shape and size of template and synthesis of copper metal particles. Advanced Materials 11 (16):1358-1362

51. Vijaya Kumar R, Mastai Y, Diamant Y, Gedanken A (2001) Sonochemical synthesis of amorphous Cu and nanocrystalline Cu2O embedded in a polyaniline matrix. Journal of Materials Chemistry 11 (4):1209-1213

52. Wu ML, Chen DH, Huang TC (2001) Synthesis of Au/Pd bimetallic nanoparticles in reverse micelles. Langmuir 17 (13):3877-3883

53. Dang CM, Trinh CD, Dang DMT, Fribourg-Blanc E (2013) Characteristics of colloidal copper particles prepared by using polyvinyl pyrrolidone and polyethylene glycol in chemical reduction method. International Journal of Nanotechnology 10 (3-4):296-303

54. Turkevich J (1985) Colloidal gold. Part I - Historical and preparative aspects, morphology and structure. Gold Bulletin 18 (3):86-91

55. Turkevich J, Stevenson PC, Hillier J (1951) A study of the nucleation and growth processes in the synthesis of colloidal gold. Discussions of the Faraday Society 11:55-75

56. Brust M, Walker M, Bethell D, Schiffrin DJ, Whyman R (1994) Synthesis of thiol-derivatised gold nanoparticles in a two-phase liquid-liquid system. Journal of the Chemical Society, Chemical Communications (7):801-802

57. Turkevich J, Kim G (1970) Palladium: Preparation and catalytic properties of particles of uniform size. Science 169 (3948):873-879

58. Bönnemann H, Richards RM (2001) Nanoscopic metal particles - Synthetic methods and potential applications. European Journal of Inorganic Chemistry (10):2455-2480

59. Frens G (1973) Controlled Nucleation for the Regulation of the Particle Size in Monodisperse Gold Suspensions. Physical Sciences 241 (241):20-22

60. Brust M, Fink J, Bethell D, Schiffrin DJ, Kiely C (1995) Synthesis and reactions of functionalised gold nanoparticles. Journal of the Chemical Society, Chemical Communications (16):1655-1656

61. Chen S, Murray RW (1999) Arenethiolate Monolayer-Protected Gold Clusters. Langmuir 15 (3):682-688

62. Wang Z, Tan B, Hussain I, Schaeffer N, Wyatt MF, Brust M, Cooper AI (2007) Design of polymeric stabilizers for size-controlled synthesis of monodisperse gold nanoparticles in water. Langmuir 23 (2):885-895

63. Han S, Sheela VP, Cao W, Balasubramanian R (2013) Brust-Schiffrin synthesis of catalytic bipodal PdPt nanoparticles with some mechanistic insights. RSC Advances 3 (22):8551-8558

64. Hussain I, Graham S, Wang Z, Tan B, Sherrington DC, Rannard SP, Cooper AI, Brust M (2005) Size-controlled synthesis of near-monodisperse gold nanoparticles in the 1-4 nm range using polymeric stabilizers. Journal of the American Chemical Society 127 (47):16398-16399

65. Kumar S, Gandhi KS, Kumar R (2007) Modeling of formation of gold nanoparticles by citrate method. Industrial and Engineering Chemistry Research 46 (10):3128-3136

66. Ji X, Song X, Li J, Bai Y, Yang W, Peng X (2007) Size control of gold nanocrystals in citrate reduction: The third role of citrate. Journal of the American Chemical Society 129 (45):13939-13948

67. Hu J, Zhang Y, Liu B, Liu J, Zhou H, Xu Y, Jiang Y, Yang Z, Tian ZQ (2004) Synthesis and properties tadpole-shaped gold nanoparticles. Journal of the American Chemical Society 126 (31):9470-9471

68. Kuo CH, Chiang TF, Chen LJ, Huang MH (2004) Synthesis of highly faceted pentagonal-And hexagonal-shaped gold nanoparticles with controlled sizes by sodium dodecyl sulfate. Langmuir 20 (18):7820-7824

69. Kuo CH, Huang MH (2005) Synthesis of branched gold nanocrystals by a seeding growth approach. Langmuir 21 (5):2012-2016

70. Kan C, Wang C, Zhu J, Li H (2010) Formation of gold and silver nanostructures within polyvinylpyrollidone (PVP) gel. Journal of Solid State Chemistry 183 (4):858-865

71. Gole A, Murphy CJ (2004) Seed-mediated synthesis of gold nanorods: Role of the size and nature of the seed. Chemistry of Materials 16 (19):3633-3640

72. Nadagouda MN, Varma RS (2007) A greener synthesis of core (Fe, Cu)-shell (Au, Pt, Pd, and Ag) nanocrystals using aqueous vitamin C. Crystal Growth and Design 7 (12):2582-2587

73. Shem PM, Sardar R, Shumaker-Parry JS (2009) One-step synthesis of phosphine-stabilized gold nanoparticles using the mild reducing agent 9-BBN. Langmuir 25 (23):13279-13283

74. Ding Y, Zhang X, Liu X, Guo R (2006) Adsorption characteristics of thionine on gold nanoparticles. Langmuir 22 (5):2292-2298

75. Aryal S, Remant BKC, Dharmaraj N, Bhattarai N, Kim CH, Kim HY (2006) Spectroscopic identification of SAu interaction in cysteine capped gold nanoparticles. Spectrochimica Acta - Part A: Molecular and Biomolecular Spectroscopy 63 (1):160-163

76. Grubbs RB (2007) Roles of polymer ligands in nanoparticle stabilization. Polymer Reviews 47 (2):197-215

77. Katz E, Willner I (2004) Integrated nanoparticle-biomolecule hybrid systems: Synthesis, properties, and applications. Angewandte Chemie - International Edition 43 (45):6042-6108

78. Ma Y-R, Niu H-Y, Zhang X-L, Cai Y-Q (2011) One-step synthesis of silver/dopamine nanoparticles and visual detection of melamine in raw milk. Analyst 136:4192-4196. doi:10.1039/c1an15327g

79. Vimala K, Samba Sivudu K, Murali Mohan Y, Sreedhar B, Mohana Raju K (2009) Controlled silver nanoparticles synthesis in semi-hydrogel networks of poly(acrylamide) and carbohydrates: A rational methodology for antibacterial application. Carbohydrate Polymers 75 (3):463-471

80. Khanna PK, Gokhale R, Subbarao VVVS, Vishwanath AK, Das BK, Satyanarayana CVV (2005) PVA stabilized gold nanoparticles by use of unexplored albeit conventional reducing agent. Materials Chemistry and Physics 92 (1):229-233

81. Tripathy P, Ram S, J.-Fecht H (2006) Gold nanoparticles from induced Au3+→Au0 reaction in polyvinyl alcohol molecules in presence of sucrose in hot water. Plasmonics 1 (2-4):121-127

82. Pérez-Juste J, Rodríguez-González B, Mulvaney P, Liz-Marzán LM (2005) Optical control and patterning of gold-nanorod-poly(vinyl alcohol) nanocomposite films. Advanced Functional Materials 15 (7):1065-1071

83. Hill HD, Mirkin CA (2006) The bio-barcode assay for the detection of protein and nucleic acid targets using DTT-induced ligand exchange. Nature Protocols 1 (1):324-336

84. Delmulle BS, De Saeger SMDG, Sibanda L, Barna-Vetro I, Van Peteghem CH (2005) Development of an immunoassay-based lateral flow dipstick for the rapid detection of aflatoxin B1 in pig feed. Journal of Agricultural and Food Chemistry 53 (9):3364-3368

85. Verheijen R, Stouten P, Cazemier G, Haasnoot W (1998) Development of a one step strip test for the detection of sulfadimidine residues. Analyst 123 (12):2437-2441

86. Gold nanoparticle: Worth their weight (Cited 10. 12. 2013) Available: http://biosensing.wordpress.com/2009/06/14/gold-nanoparticles-worth-its-weight-in-gold/

87. Uni Gold Recombigen *Hiv Test* (cited 3.11.13) Available: http://www.thebody.com/h/uni-gold-recombigen-hiv-test.html

88. Wang X, Li K, Shi D, Xiong N, Jin X, Yi J, Bi D (2007) Development of an immunochromatographic lateral-flow test strip for rapid detection of sulfonamides in eggs and chicken muscles. Journal of Agricultural and Food Chemistry 55 (6):2072-2078

89. Laitinen MPA, Vuento M (1996) Immunochromatographic assay for quantitation of milk progesterone. Acta Chemica Scandinavica 50 (2):141-145

90. Li D, Wei S, Yang H, Li Y, Deng A (2009) A sensitive immunochromatographic assay using colloidal gold-antibody probe for rapid detection of pharmaceutical indomethacin in water samples. Biosensors and Bioelectronics 24 (7):2277-2280

91. Zhang GP, Guo JQ, Wang XN, Yang JX, Yang YY, Li QM, Li XW, Deng RG, Xiao ZJ, Yang JF, Xing GX, Zhao D (2006) Development and evaluation of an immunochromatographic strip for trichinellosis detection. Veterinary Parasitology 137 (3-4):286-293

92. He Y, Zhang S, Zhang X, Baloda M, Gurung AS, Xu H, Liu G (2011) Ultrasensitive nucleic acid biosensor based on enzyme-gold nanoparticle dual label and lateral flow strip biosensor. Biosensors and Bioelectronics 26 (5):2018-2024

93. Luckham RE, Brennan JD (2010) Bioactive paper dipstick sensors for acetylcholinesterase inhibitors based on sol-gel/enzyme/gold nanoparticle composites. Analyst 135:2028-2035. doi:10.1039/c0an00283f

94. Ratnarathorn N, Chailapakul O, Henry CS, Dungchai W (2012) Simple silver nanoparticle colorimetric sensing for copper by paper-based devices. Talanta 99:552-557

95. Głowacki ED, Voss G, Leonat L, Irimia-Vladu M, Bauer S, Sariciftci NS (2012) Indigo and Tyrian purple - From ancient natural dyes to modern organic semiconductors. Israel Journal of Chemistry 52 (6):540-551

96. Berneth H (Methine Dyes and Pigments.) 2008. Ullmann's Encyclopedia of Industrial Chemistry

97. Wöhrle D, Schnurpfeil G, Makarov SG, Kazarin A, Suvorova ON (2012) Practical applications of phthalocyanines - from dyes and pigments to materials for optical, electronic and photo-electronic devices. Macroheterocycles 5 (3):191-202

98. E. Ross RN, W. Fischer, U. Jäschke, W.-D. Mayer, G. Wieland, E. J. Newman, C. M. Wilson,, (1989) "Indicator Reagents". Ullmann’s Encyclopedia of Industrial Chemistry, vol A14. VCH, Weinheim

99. E. Ross RN, W. Fischer, W.-D. Mayer, G. Wieland, E. J. Newman, C. M. Wilson (2002) "Indicator Reagents". in Ullmann’s Encyclopedia of In dustrial Chemistry. Wiley-VCH, Weinheim

100. Chemical Analysis of urine (cited 5.11.13) Available: http://www.google.co.za/url?sa=t&rct=j&q=&esrc=s&source=web&cd=1&ved=0CDQQFjAA&url=http%3A%2F%2Fedoqs.net%2Fdownload%2F9131bf050c0324c483aebf34b789cf7e&ei=bsxDU_b6Io2W0QX3i4HgDQ&usg=AFQjCNEP0RgvOfTHbF4Evu1w4Ui9TnPdIw&bvm=bv.64367178,d.d2k

101. Dungchai W, Chailapakul O, Henry CS (2010) Use of multiple colorimetric indicators for paper-based microfluidic devices. Analytica Chimica Acta 674 (2):227-233

102. Kalogianni DP, Goura S, Aletras AJ, Christopoulos TK, Chanos MG, Christofidou M, Skoutelis A, Ioannou PC, Panagiotopoulos E (2007) Dry reagent dipstick test combined with 23S rRNA PCR for molecular diagnosis of bacterial infection in arthroplasty. Analytical Biochemistry 361 (2):169-175

103. Abitbol CL, Chandar J, Onder AM, Nwobi O, Montané B, Zilleruelo G (2006) Profiling proteinuria in pediatric patients. Pediatric Nephrology 21 (7):995-1002

104. Snowden K, Hommel M (1991) Antigen detection immunoassay using dipsticks and colloidal dyes. Journal of Immunological Methods 140 (1):57-65

105. Zhu Y, He W, Liang Y, Xu M, Yu C, Hua W, Chao G (2002) Development of a rapid, simple dipstick dye immunoassay for schistosomiasis diagnosis. Journal of Immunological Methods 266 (1-2):1-5

106. Ornatska M, Sharpe E, Andreescu D, Andreescu S (2011) Paper bioassay based on ceria nanoparticles as colorimetric probes. Analytical Chemistry 83 (11):4273-4280

107. Pelton R (2009) Bioactive paper provides a low-cost platform for diagnostics. TrAC - Trends in Analytical Chemistry 28 (8):925-942

108 Millipore (cited 20.10.13) Available: http://www.millipore.com/publications.nsf/a73664f9f981af8c852569b9005b4eee/348ee7096d93729b85256bf40066a40d/$FILE/tb500en00.pdf

109. Tonkinson JL, Stillman BA (2002) Nitrocellulose: a tried and true polymer finds utility as a post-genomic substrate. Front Biosci 7:c1-12

110. Li X, Tian J, Garnier G, Shen W (2010) Fabrication of paper-based microfluidic sensors by printing. Colloids and Surfaces B: Biointerfaces 76 (2):564-570

111. Ellerbee AK, Phillips ST, Siegel AC, Mirica KA, Martinez AW, Striehl P, Jain N, Prentiss M, Whitesides GM (2009) Quantifying colorimetric assays in paper-based microfluidic devices by measuring the transmission of light through paper. Analytical Chemistry 81 (20):8447-8452

112. Ondarçuhu T, Joachim C (1998) Drawing a single nanofibre over hundreds of microns. Europhysics Letters 42 (2):215-220

113. Ikegame M, Tajima K, Aida T (2003) Template synthesis of polypyrrole nanofibers insulated within one-dimensional silicate channels: Hexagonal versus lamellar for recombination of polarons into bipolarons. Angewandte Chemie - International Edition 42 (19):2154-2157

114. Ma PX, Zhang R (1999) Synthetic nano-scale fibrous extracellular matrix. Journal of Biomedical Materials Research 46 (1):60-72

115. Hartgerink JD, Beniash E, Stupp SI (2001) Self-assembly and mineralization of peptide-amphiphile nanofibers. Science 294 (5547):1684-1688

116. Teo WE, Ramakrishna S (2006) A review on electrospinning design and nanofibre assemblies. Nanotechnology 17 (14):R89-R106

117. Doshi J, Reneker DH (1995) Electrospinning process and applications of electrospun fibers. Journal of Electrostatics 35 (2-3):151-160

118. Nakagawa H, Hara Y, Maeda S, Hasimoto S (2011) A pendulum-like motion of nanofiber gel actuator synchronized with external periodic pH oscillation. Polymers (Basel, Switz) 3:405-412. doi:10.3390/polym3010405

119. Mit-uppatham C, Nithitanakul M, Supaphol P (2004) Effects of solution concentration, emitting electrode polarity, solvent type, and salt addition on electrospun polyamide-6 fibers: A preliminary report. Macromol Symp 216:293-299. doi:10.1002/masy.200451227

120. Müller K, Quinn JF, Johnston APR, Becker M, Greiner A, Caruso F (2006) Polyelectrolyte functionalization of electrospun fibers. Chemistry of Materials 18 (9):2397-2403

121. Mit-Uppatham C, Nithitanakul M, Supaphol P Effects of solution concentration, emitting electrode polarity, solvent type, and salt addition on electrospun polyamide-6 fibers: A preliminary report. In, 2004. pp 293-299

122. Niu H, Lin T, Wang X (2009) Needleless electrospinning. I. A comparison of cylinder and disk nozzles. Journal of Applied Polymer Science 114 (6):3524-3530

123. Rujitanaroj PO, Pimpha N, Supaphol P (2010) Preparation, characterization, and antibacterial properties of electrospun polyacrylonitrile fibrous membranes containing silver nanoparticles. Journal of Applied Polymer Science 116 (4):1967-1976

124. Sill TJ, von Recum HA (2008) Electrospinning: Applications in drug delivery and tissue engineering. Biomaterials 29 (13):1989-2006

125. Deitzel JM, Kleinmeyer J, Harris D, Beck Tan NC (2001) The effect of processing variables on the morphology of electrospun nanofibers and textiles. Polymer 42 (1):261-272

126. Megelski S, Stephens JS, Bruce Chase D, Rabolt JF (2002) Micro- and nanostructured surface morphology on electrospun polymer fibers. Macromolecules 35 (22):8456-8466

127. Hohman MM, Shin M, Rutledge G, Brenner MP (2001) Electrospinning and electrically forced jets. II. Applications. Physics of Fluids 13 (8):2221-2236

128. Hohman MM, Shin M, Rutledge G, Brenner MP (2001) Electrospinning and electrically forced jets. I. Stability theory. Physics of Fluids 13 (8):2201-2220

129. Reneker DH, Yarin AL, Fong H, Koombhongse S (2000) Bending instability of electrically charged liquid jets of polymer solutions in electrospinning. Journal of Applied Physics 87 (9 I):4531-4547

130. Theron A, Zussman E, Yarin AL (2001) Electrostatic field-assisted alignment of electrospun nanofibres. Nanotechnology 12 (3):384-390

131. Bhattacharyya S, Kumbar SG, Khan YM, Nair LS, Singh A, Krogman NR, Brown PW, Allcock HR, Laurencin CT (2009) Biodegradable polyphosphazene-nanohydroxyapatite composite nanofibers: Scaffolds for bone tissue engineering. Journal of Biomedical Nanotechnology 5 (1):69-75

132. Choi JS, Yoo HS (2010) Nano-inspired fibrous matrix with bi-phasic release of proteins. Journal of Nanoscience and Nanotechnology 10 (5):3038-3045

133. Son YJ, Yoo HS (2012) PH-responsive microspheres encapsulated with iron oxide nanoaggregates for gastrointestinal delivery. Journal of Bioactive and Compatible Polymers 27 (1):54-66

134. Yoo HS, Kim TG, Park TG (2009) Surface-functionalized electrospun nanofibers for tissue engineering and drug delivery. Advanced Drug Delivery Reviews 61 (12):1033-1042

135. Katti DS, Robinson KW, Ko FK, Laurencin CT (2004) Bioresorbable nanofiber-based systems for wound healing and drug delivery: Optimization of fabrication parameters. Journal of Biomedical Materials Research - Part B Applied Biomaterials 70 (2):286-296

136. Dubský M, Kubinová Š, Širc J, Voska L, Zajíček R, Zajícová A, Lesný P, Jirkovská A, Michálek J, Munzarová M, Holáň V, Syková E (2012) Nanofibers prepared by needleless electrospinning technology as scaffolds for wound healing. Journal of Materials Science: Materials in Medicine 23 (4):931-941

137. Wang X, Si Y, Wang J, Ding B, Yu J, Al-Deyab SS (2012) A facile and highly sensitive colorimetric sensor for the detection of formaldehyde based on electro-spinning/netting nano-fiber/nets. Sensors and Actuators, B: Chemical 163 (1):186-193

138. Li Y, Si Y, Wang X, Ding B, Sun G, Zheng G, Luo W, Yu J (2013) Colorimetric sensor strips for lead (II) assay utilizing nanogold probes immobilized polyamide-6/nitrocellulose nano-fibers/nets. Biosensors and Bioelectronics 48:244-250

139. Boitumelo Mudabuka DO, Syvestre Degni, Sibulelo Vilakazi, Nelson Torto (2013) A colorimetric probe for ascorbic acid based on copper-gold nanoparticles in electrospun nylon. Microchimica Acta. doi:10.1007/s00604-013-1114-4

140. Wolfbeis OS (2004) Fiber-optic chemical sensors and biosensors. Analytical Chemistry 76 (12):3269-3284

141. Potyrailo RA, Hobbs SE, Hieftje GM (1998) Optical waveguide sensors in analytical chemistry: Today's instrumentation, applications and trends for future development. Fresenius' Journal of Analytical Chemistry 362 (4):349-373

142. Zourob M, Mohr S, Fielden PR, Goddard NJ (2005) An integrated disposable dye clad leaky waveguide sensor for μ-TAS applications. Lab on a Chip - Miniaturisation for Chemistry and Biology 5 (7):772-777

143. Yeo SY, Lee HJ, Jeong SH (2003) Preparation of nanocomposite fibers for permanent antibacterial effect. Journal of Materials Science 38 (10):2143-2147

144. Lee J, Sundar VC, Heine JR, Bawendi MG, Jensen KF (2000) Full color emission from II-VI semiconductor quantum dot-polymer composites. Advanced Materials 12 (15):1102-1105

145. Mayer ABR (1998) Formation of noble metal nanoparticles within a polymeric matrix: Nanoparticle features and overall morphologies. Materials Science and Engineering C 6 (2-3):155-166

146. Park SW, Bae HS, Xing ZC, Kwon OH, Huh MW, Kang IK (2009) Preparation and properties of silver-containing nylon 6 nanofibers formed by electrospinning. Journal of Applied Polymer Science 112 (4):2320-2326

147. Jin WJ, Lee HK, Jeong RH, Park WH, Youk JH (2005) Preparation of polymer nanofibers containing silver nanoparticles by using poly(N-vinylpyrrolidone). Macromolecular Rapid Communications 26 (24):1903-1907

148. Hamlett CAE, Jayasinghe SN, Preece JA (2008) Electrospinning nanosuspensions loaded with passivated Au nanoparticles. Tetrahedron 64 (36):8476-8483

149. Lee DY, Lee KH, Kim BY, Cho NI (2010) Silver nanoparticles dispersed in electrospun polyacrylonitrile nanofibers via chemical reduction. Journal of Sol-Gel Science and Technology 54 (1):63-68

150. Sichani GN, Morshed M, Amirnasr M, Abedi D (2010) In situ preparation, electrospinning, and characterization of polyacrylonitrile nanofibers containing silver nanoparticles. Journal of Applied Polymer Science 116 (2):1021-1029

151. Jin M, Zhang X, Nishimoto S, Liu Z, Tryk DA, Murakami T, Fujishima A (2007) Large-scale fabrication of Ag nanoparticles in PVP nanofibres and net-like silver nanofibre films by electrospinning. Nanotechnology 18 (7)

152. Fantini D, Costa L (2009) Dye, fluorophores and pigment coloration of nanofibers produced by electrospinning. Polymers for Advanced Technologies 20 (2):111-121

153. Camposeo A, Di Benedetto F, Stabile R, Cingolani R, Pisignano D (2007) Electrospun dye-doped polymer nanofibers emitting in the near infrared. Applied Physics Letters 90 (14)

154. Mohr GJ, Wolfbeis OS (1994) Optical sensors for a wide pH range based on azo dyes immobilized on a novel support. Analytica Chimica Acta 292 (1-2):41-48

155. Zhu Y, Gao C, Liu X, Shen J (2002) Surface modification of polycaprolactone membrane via aminolysis and biomacromolecule immobilization for promoting cytocompatibility of human endothelial cells. Biomacromolecules 3 (6):1312-1319

156. Arrigoni O, De Tullio MC (2002) Ascorbic acid: Much more than just an antioxidant. Biochimica et Biophysica Acta - General Subjects 1569 (1-3):1-9

157. Burns JJ (1959) Biosynthesis of l-ascorbic acid; basic defect in scurvy. The American Journal of Medicine 26 (5):740-748

158. Tolbert BM, Downing M, Carlson RW (1975) Chemistry and metabolism of ascorbic acid and ascorbate sulfate. Annals of the New York Academy of Sciences Vol. 258:48-69

159. Barnes MJ (1975) Function of ascorbic acid in collagen metabolism. Annals of the New York Academy of Sciences Vol. 258:264-277

160. Diliberto Jr EJ, Daniels AJ, Viveros OH (1991) Multicompartmental secretion of ascorbate and its dual role in dopamine β-hydroxylation. American Journal of Clinical Nutrition 54 (SUPPL. 6):1163S-1172S

161. Desole MS, Anania V, Esposito G, Carboni F, Senini A, Miele E (1987) Neurochemical and behavioural changes induced by ascorbic acid and d-amphetamine in the rat. Pharmacological Research Communications 19 (6):441-450

162. Shigenaga MK, Hagen TM, Ames BN (1994) Oxidative damage and mitochondrial decay in aging. Proceedings of the National Academy of Sciences of the United States of America 91 (23):10771-10778

163. Okiei W, Ogunlesi M, Azeez L, Obakachi V, Osunsanmi M, Nkenchor G (2009) The voltammetric and titrimetric determination of ascorbic acid levels in tropical fruit samples. International Journal Electrochemical Science 4 (Copyright (C) 2012 American Chemical Society (ACS). All Rights Reserved.):276-287

164. Jaber M, Robinson SW, Missale C, Caron MG (1996) Dopamine receptors and brain function. Neuropharmacology 35 (11):1503-1519

165. Lang AE, Lozano AM (1998) Parkinson's disease: Second of two parts. New England Journal of Medicine 339 (16):1130-1143

166. Lang AE, Lozano AM (1998) Parkinson's disease. New England Journal of Medicine 339 (15):1044-1053

167. Koob GF (1992) Drugs of abuse: Anatomy, pharmacology and function of reward pathways. Trends in Pharmacological Sciences 13 (5):177-184

168. Le Moal M, Simon H (1991) Mesocorticolimbic dopaminergic network: Functional and regulatory roles. Physiological Reviews 71 (1):155-234

169. Svehla G, Koltai L, Erdey L (1963) The use of 2,6-dichlorophenol-indophenol as indicator in iodometric titrations with ascorbic acid. Analytica Chimica Acta 29 (C):442-447

170. Ismail IA, Khalifa H, Zaky M (1984) Applications involving oxidation with ethanolic iodine. Rapid potentiometric method for some reductants. Microchemical Journal 30 (3):353-357

171. Zhang Y, Cai Y, Su S (2006) Determination of dopamine in the presence of ascorbic acid by poly(styrene sulfonic acid) sodium salt/single-wall carbon nanotube film modified glassy carbon electrode. Analytical Biochemistry 350 (2):285-291

172. Kim YR, Bong S, Kang YJ, Yang Y, Mahajan RK, Kim JS, Kim H (2010) Electrochemical detection of dopamine in the presence of ascorbic acid using graphene modified electrodes. Biosensors and Bioelectronics 25 (10):2366-2369

173. Oni J, Westbroek P, Nyokong T (2003) Electrochemical behavior and detection of dopamine and ascorbic acid at an iron(II)tetrasulfophthalocyanine modified carbon paste microelectrode. Electroanalysis 15 (10):847-854

174. Iwase H (2000) Use of an amino acid in the mobile phase for the determination of ascorbic acid in food by high-performance liquid chromatography with electrochemical detection. Journal of Chromatography A 881 (1-2):317-326

175. Dilgin Y, Nişli G (2005) Fluorimetric determination of ascorbic acid in vitamin C tablets using methylene blue. Chemical and Pharmaceutical Bulletin 53 (10):1251-1254

176. Pérez-Ruiz T, Martínez Lozano C, Tomás V, Ruiz E (2007) Flow injection fluorimetric determination of L-dopa and dopamine based on a photochemical inhibition process. Microchimica Acta 158 (3-4):299-305

177. Mamiński M, Olejniczak M, Chudy M, Dybko A, Brzózka Z (2005) Spectrophotometric determination of dopamine in microliter scale using microfluidic system based on polymeric technology. Analytica Chimica Acta 540 (1):153-157

178. Fujita Y, Mori I, Yamaguchi T, Hoshino M, Shigemura Y, Shimano M (2001) Spectrophotometric determination of ascorbic acid with iron(III) and p-carboxyphenylfluorone in a cationic surfactant micellar medium. Analytical Sciences 17 (7):853-857

179. Hossu A-M, Magearu V (2004) Determination of vitamin C in pharmaceutical products with physico-chemical and bioanalytical methods. Roum Biotechnol Lett 9:1497-1504

180. Dayton MA, Ewing AG (1980) Response of Microvoltammetric Electrodes to Homogeneous Catalytic and Slow Heterogeneous Charge-Transfer Reactions. Analytical Chemistry 52 (14):2392-2396

181. Hormozi Nezhad MR, Karimi MA, Shahheydari F (2010) A sensitive colorimetric detection of ascorbic acid in pharmaceutical products based on formation of anisotropic silver nanoparticles. Scientia Iranica 17 (2 F):148-153

182. Zhang Y, Li B, Xu C (2010) Visual detection of ascorbic acid via alkyne-azide click reaction using gold nanoparticles as a colorimetric probe. Analyst 135 (7):1579-1584

183. Zhang Y, Li B, Chen X (2010) Simple and sensitive detection of dopamine in the presence of high concentration of ascorbic acid using gold nanoparticles as colorimetric probes. Microchimica Acta 168 (1-2):107-113

184. Lee HC, Chen TH, Tseng WL, Lin CH (2012) Novel core etching technique of gold nanoparticles for colorimetric dopamine detection. Analyst 137 (22):5352-5357

185. Feng JJ, Guo H, Li YF, Wang YH, Chen WY, Wang AJ (2013) Single molecular functionalized gold nanoparticles for hydrogen-bonding recognition and colorimetric detection of dopamine with high sensitivity and selectivity. ACS Applied Materials and Interfaces 5 (4):1226-1231

186. Tao Y, Lin Y, Ren J, Qu X (2013) A dual fluorometric and colorimetric sensor for dopamine based on BSA-stabilized Au nanoclusters. Biosensors and Bioelectronics 42 (1):41-46

187. Schwank J (1983) Catalytic gold - Applications of elemental gold in heterogeneous catalysis. Gold Bulletin 16 (4):103-110

188. Harada M, Asakura K, Ueki Y, Toshima N (1992) Structure of polymer-protected palladium/platinum bimetallic clusters at the oxidized state. Extended X-ray absorption fine structure analysis. Journal of Physical Chemistry 96 (24):9730-9738

189. Link S, Wang ZL, El-Sayed MA (1999) Alloy formation of gold-silver nanoparticles and the dependence of the plasmon absorption on their composition. Journal of Physical Chemistry B 103 (18):3529-3533

190. Rockenbauer A, Korecz L (1996) Automatic computer simulations of ESR spectra. Applied Magnetic Resonance 10 (1-3):29-43

191. Gerber TIA HE, Mayer P, Tshentu Z. R Synthesis and characterization of rhenium(III) and (V) pyridylimidazole complexes. Journal Of Coordination Chemistry 59:243-253

192. Shi Q, Vitchuli N, Nowak J, Noar J, Caldwell JM, Breidt F, Bourham M, McCord M, Zhang X (2011) One-step synthesis of silver nanoparticle-filled nylon 6 nanofibers and their antibacterial properties. Journal of Materials Chemistry 21 (28):10330-10335

193. Scampicchio M, Arecchi A, Mannino S (2009) Optical nanoprobes based on gold nanoparticles for sugar sensing. Nanotechnology 20 (13)

194. Mallik K, Mandal M, Pradhan N, Pal T (2001) Seed Mediated Formation of Bimetallic Nanoparticles by UV Irradiation: A Photochemical Approach for the Preparation of "Core-Shell" Type Structures. Nano Letters 1 (6):319-322

195. Darroudi M, Ahmad MB, Abdullah AH, Ibrahim NA, Shameli K (2010) Effect of accelerator in green synthesis of silver nanoparticles. International Journal of Molecular Sciences 11 (10):3898-3905

196. Pal U, Sanchez Ramirez JF, Liu HB, Medina A, Ascencio JA (2004) Synthesis and structure determination of bimetallic Au/Cu nanoparticles. Applied Physics A: Materials Science and Processing 79 (1):79-84

197. Zhao W, Brook MA, Li Y (2008) Design of gold nanoparticle-based colorimetric biosensing assays. ChemBioChem 9 (15):2363-2371

198. Ventura MG, Parola AJ, De Matos AP (2011) Influence of heat treatment on the colour of Au and Ag glasses produced by the sol-gel pathway. Journal of Non-Crystalline Solids 357 (4):1342-1349

199. Li Z, Zhang J, Mu T, Du J, Liu Z, Han B, Chen J (2004) Preparation of polyvinylpyrrolidone-protected Prussian blue nanocomposites in microemulsion. Colloids and Surfaces A: Physicochemical and Engineering Aspects 243 (1-3):63-66

200. Lee SH, Huh YD (2012) Preferential evolution of Prussian blue's morphology from cube to hexapod. Bulletin of the Korean Chemical Society 33 (3):1078-1080

201. Krzyminiewski R, Kruczyński Z, Dobosz B, Zając A, Mackiewicz A, Leporowska E, Folwaczna S (2011) EPR Study of Iron Ion Complexes in Human Blood. Applied Magnetic Resonance 40 (3):321-330

202. Fujita Y, Tsuchiya K, Abe S, Takiguchi Y, Kubo SI, Sakurai H (2005) Estimation of the age of human bloodstains by electron paramagnetic resonance spectroscopy: Long-term controlled experiment on the effects of environmental factors. Forensic Science International 152 (1):39-43

203. Aasa R, Aisen P (1968) An electron paramagnetic resonance study of the iron and copper complexes of transferrin. Journal of Biological Chemistry 243 (9):2399-2404

204. Gamarra LF, Pontuschka WM, Amaro Jr E, Costa-Filho AJ, Brito GES, Vieira ED, Carneiro SM, Escriba DM, Falleiros AMF, Salvador VL (2008) Kinetics of elimination and distribution in blood and liver of biocompatible ferrofluids based on Fe3O4 nanoparticles: An EPR and XRF study. Materials Science and Engineering C 28 (4):519-525

205. Ślawska-Waniewska A, Mosiniewicz-Szablewska E, Nedelko N, Gałązka-Friedman J, Friedman A (2004) Magnetic studies of iron-entities in human tissues. Journal of Magnetism and Magnetic Materials 272-276 (III):2417-2419

206. Kelly KL, Coronado E, Zhao LL, Schatz GC (2003) The optical properties of metal nanoparticles: The influence of size, shape, and dielectric environment. Journal of Physical Chemistry B 107 (3):668-677